

ADA 083096

DDC FILE COPY

(12) LEVEL II

GALLIUM ARSENIDE ADVANCED CRYSTAL GROWTH AND BEAM PROCESSING

C.L. Anderson

Hughes Research Laboratories
3011 Malibu Canyon Road
Malibu, CA 90265

January 1980

Contract No. N00014-78-C-0337
Final Progress Report
1 May 1978 through 30 July 1979

Approved for public release, distribution unlimited.

Sponsored by
DEFENSE ADVANCED RESEARCH PROJECTS AGENCY
1400 Wilson Boulevard
Arlington, VA 22209

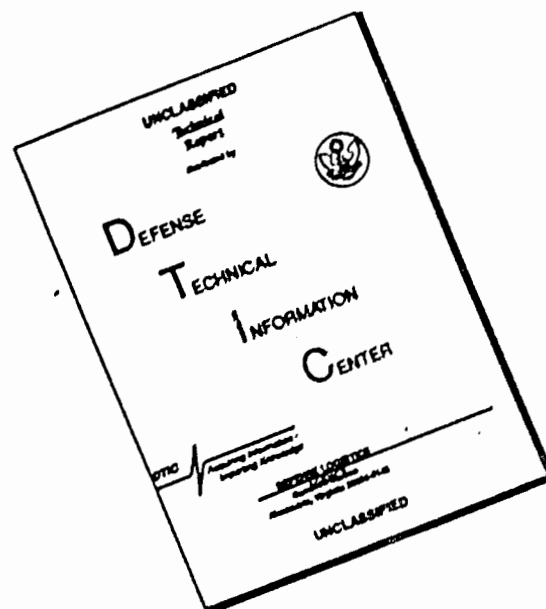
Monitored by
OFFICE OF NAVAL RESEARCH
Code 427
800 North Quincy Street
Arlington, VA 22217

DTIC
ELECTE
S APR 14 1980 D
A

The views and conclusions contained in this document are those of the authors and should not be interpreted as necessarily representing the official policies, either expressed or implied, of the Defense Armed Services Projects Agency or the U.S. Government.

80 4 14 032

DISCLAIMER NOTICE



THIS DOCUMENT IS BEST QUALITY AVAILABLE. THE COPY FURNISHED TO DTIC CONTAINED A SIGNIFICANT NUMBER OF PAGES WHICH DO NOT REPRODUCE LEGIBLY.

**BLANK PAGES
IN THIS
DOCUMENT
WERE NOT
FILMED**

ARPA ORDER Number:	3564
Project Element Number:	61101E
NR Number:	243-025
Contract Effective Date:	1 May 1978
Contract Expiration Date:	30 July 1979
Principal Investigator:	C.L. Anderson (213) 456-6411 Extension 176

UNCLASSIFIED

SECURITY CLASSIFICATION OF THIS PAGE (When Data Entered)

REPORT DOCUMENTATION PAGE		READ INSTRUCTIONS BEFORE COMPLETING FORM
1. REPORT NUMBER	2. GOVT ACCESSION NO.	3. RECIPIENT'S CATALOG NUMBER
4. TITLE (and Subtitle) GALLIUM ARSENIDE ADVANCED CRYSTAL GROWTH AND BEAM PROCESSING		5. TYPE OF REPORT & PERIOD COVERED Final Progress Report 1 May 1978 - 30 July 1979
7. AUTHOR(s) C.L. Anderson		6. PERFORMING ORG. REPORT NUMBER
9. PERFORMING ORGANIZATION NAME AND ADDRESS Hughes Research Laboratories 3011 Malibu Canyon Road Malibu, CA 90265		8. CONTRACT OR GRANT NUMBER(s) N00014-78-C-0337 DARPA DCT-3564
11. CONTROLLING OFFICE NAME AND ADDRESS DARPA 1400 Wilson Blvd. Arlington, Virginia 22209		10. PROGRAM ELEMENT, PROJECT, TASK AREA & WORK UNIT NUMBERS P.E. 61101E Order 3564 NR 243-025
14. MONITORING AGENCY NAME & ADDRESS (if different from Controlling Office) Office of Naval Research Code 427 800 North Quincy Street Arlington, Virginia 22217		12. REPORT DATE January 1980
16. DISTRIBUTION STATEMENT (of this Report) Approved for public release; distribution unlimited.		13. NUMBER OF PAGES 138
17. DISTRIBUTION STATEMENT (of the abstract entered in Block 20, if different from Report)		15. SECURITY CLASS (of this report) UNCLASSIFIED
18. SUPPLEMENTARY NOTES ONR Scientific Officer: Telephone: (202) 696-4218		15a. DECLASSIFICATION DOWNGRADING SCHEDULE
19. KEY WORDS (Continue on reverse side if necessary and identify by block number) GaAs Crystal Growth Laser Annealed Ion Implants Solution Growth of GaAs Laser Annealing of GaAs Laser Annealed Ohmic Contacts		
20. ABSTRACT (Continue on reverse side if necessary and identify by block number) This report describes the progress made during a fifteen-month program to study the feasibility of (a) growth of high-purity "epitaxial quality" bulk GaAs crystals from solution and (b) annealing of implanted layers and Ohmic contacts for device applications using laser and electron beams.		

DD FORM 1473

EDITION OF 1 NOV 65 IS OBSOLETE

UNCLASSIFIED

SECURITY CLASSIFICATION OF THIS PAGE (When Data Entered)

176.624

2 times 10 to the 15th power / cm cm.

UNCLASSIFIED

58 cm / 4 / 5

SECURITY CLASSIFICATION OF THIS PAGE(When Data Entered)

Millimeter-thick crystals have been grown by the low-temperature solution-growth process. Room-temperature n-type carrier concentrations of $(2 \times 10^{15} \text{ cm}^{-3})$ and liquid nitrogen mobilities of 30,000 $(\text{cm}^2 \text{ V}^{-1} \text{ s}^{-1})$ have been achieved. Theoretical studies of a variety of potential growth configurations were performed.

A detailed study of the laser annealing of implanted layers and Ohmic contacts was performed using several Q-switched and cw lasers. State-of-the-art results were achieved in both the implant-annealing and Ohmic-contact areas. Preliminary investigations of the annealing of implanted layers and Ohmic contacts using pulsed electron beams were also performed.

Approved For	
NTIS	NTIS
Excluded	Excluded
Unpublished	Unpublished
Justification	Justification
By	
Distribution	
Available For Release	
Dist	Available For Release
A	special

UNCLASSIFIED

SECURITY CLASSIFICATION OF THIS PAGE(When Data Entered)

TABLE OF CONTENTS

SECTION		PAGE
1	INTRODUCTION AND SUMMARY.	1
2	GALLIUM ARSENIDE ADVANCED CRYSTAL GROWTH	7
	A. HRL Bulk Solution Growth Apparatus	7
	B. Experimental and Theoretical Considerations	12
	C. Electrical Characteristics	26
	D. Summary	26
3	ANNEALING OF ION-IMPLANTED GaAs WITH LASER AND ELECTRON BEAMS	29
	A. Laser Annealed Si and Se Implants for GaAs Microwave Devices	31
	B. Application of Optical Techniques to Studies of Amorphous-Crystalline Transitions Induced by Laser Annealing	39
	C. Laser Annealing of Ion-Implanted Gallium Arsenide	51
	D. Pulsed Electron Beam Annealing of Ion- Implanted GaAs	65
	E. Annealing of Implanted Layers in Compound Semiconductors by Localized Beam Heating Techniques	77
4	ANNEALING OF OHMIC CONTACTS TO GaAs BY LASER AND ELECTRON BEAMS	89
	A. Laser-Annealed Ohmic Contacts for GaAs Microwave Devices	91
	B. GaAs Microwave Field Effect Transistors with Laser-Annealed Ohmic Contacts	99
	C. A Comparison of Chemical and Structural Characteristics of In-Au:Ge Ohmic Contacts Produced by Bulk Heating and Localized Laser Heating	103

SECTION	PAGE
D. Overview of Ohmic-Contact Formation on n-Type GaAs by Laser and Electron Beam Annealing	115
5 FOCUSED-BEAM ION IMPLANTATION	131
A. Rutherford Backscattering (RBS)	131
B. Hall Measurements	135

LIST OF ILLUSTRATIONS

FIGURE		PAGE
1	Micrograph showing cross section of 550- μ m-thick growth on 400 μ m Cr-doped substrate	8
2	Comparison of mobility range of commercial with HRL-grown GaAs	9
3	HRL bulk solution growth apparatus	10
4	HRL bulk solution growth apparatus	11
5	Summary of theoretical and experimental results concerning four candidate configurations	13
6	Ratio of compositional and thermal Rayleigh number (N_R^C/N_R^T) as a function of growth temperature	15
7	Micrograph of crystal cross section showing interface breakdown	16
8	Crucible width as a function of ΔT corresponding to a growth rate of 1 μ m/min; seed-at-the-side configuration	19
9	Cut-off time and cut-off growth distance as a function of distribution coefficient for infinite stirring	21
10	Solubility of GaAs in Ga	22
11	Growth volume/ $^{\circ}$ C drop in temperature	23
12	Competing growth mechanisms resulting from convective stirring	25
13	Free carrier concentration, N, as a function of reciprocal temperature	27
14	Hall mobility, μ , as a function of temperature	28
15	Submicrometer line doping - process step comparison	132
16	RBS analysis of Ga^+ ion implantation at 59 keV	134
17	Hall processing steps	136

FIGURE		PAGE
18	Focused Ga^+ beam implant and Al contacts for Hall measurement	137
19	Ga^+ implanted 5 to 10 $\Omega\text{-cm}$, n-type, $\langle 100 \rangle$ Si showing etched mesa, Al contacts, and registration marks	137

SECTION 1

INTRODUCTION AND SUMMARY

This report summarizes the results of a 15-month contract for the development of techniques for Gallium Arsenide Advanced Crystal Growth and Beam Processing. The long-term goal of this work is to develop a practical, high-yield, high-performance GaAs integrated-circuit technology based on direct implantation into "epitaxial-quality" substrates and transient annealing at low average substrate temperatures using direct energy beams (laser and electron beams). Preliminary evaluation of the use of focused ion beams for direct writing of device structures was also performed under partial funding from this contract and from contract N000123-78-C-0195, "Focused Ion Beam Technology," sponsored by the Defense Advanced Research Projects Agency and monitored by the Naval Ocean Systems Center (Dr. Isaac Lagnado).

The use of present commercial semi-insulating GaAs substrates for direct implantation for device applications is a troublesome procedure because of the highly variable properties of the material. Although several companies (notably Hughes Aircraft and Rockwell International) produce GaAs ICs by this procedure, exacting characterization of the material by a variety of qualification tests is required. Only a small fraction of GaAs ingots are acceptable for device applications. Furthermore, processing variables typically must be adjusted on an ingot-by-ingot basis. Because of these problems, epitaxial "buffer layers" are used by several firms to provide a more reliable host for direct implantation.

Under the present program, we have begun the development of techniques for low-temperature solution growth of "epitaxial quality" bulk GaAs that will be suitable for doping by ion implantation. The development of this technology will eliminate the need for epitaxial buffer layers and will represent a significant step toward a reproducible, high-yield GaAs IC process. Considerable progress was made in this area during this contract. 600- μ m-thick epitaxial layers with

carrier concentrations in the range of 1 to $3 \times 10^{15} \text{ cm}^{-3}$ and room-temperature mobilities of $7000 \text{ cm}^2 \text{ V}^{-1} \text{ sec}^{-1}$ have been grown. This work is discussed in Section 2.

Our efforts in the area of annealing of GaAs for device applications concentrated on two major topics: the annealing of ion-implanted layers and the alloying of Ohmic contacts. Substantial progress was made in both areas. The application of pulsed and cw laser annealing and pulsed electron-beam annealing to both of these technology areas was investigated. The results of our investigations of implant annealing are presented in Section 3. Ohmic contact alloying is discussed in Section 4.

During the present contract, four papers were published on the work performed on implant annealing and three were published on the formation of Ohmic contacts. These papers, in addition to two relevant published papers supported by Hughes internal funding, are listed in Table 1. Because these papers accurately summarize the status of our work in these areas, Sections 3 and 4 of this report consist primarily of reproductions of these published papers. Introductory remarks are provided to indicate the relevance of the contents of each paper to the general topic. In addition, an unpublished paper describing the performance of GaAs microwave field effect transistors having laser-annealed Ohmic contacts was presented at the Workshop on Compound Semiconductor Microwave Materials and Devices (Atlanta, Georgia, February 1979). The results of this study are included in Section 4. The Ohmic contact work was extended under Hughes internal funding after the termination of the present contract. A published paper describing these independent results is also included in Section 4.

Independent of the present program, a Hughes IR&D program investigated the application of optical techniques, principally photoacoustic spectroscopy, to the characterization of the annealing of semiconductors. The techniques developed were applied to the present program and the results obtained were included in one of our papers. A published paper describing these independently developed optical techniques is included in Section 3.

The application of submicrometer focused ion beams of very high current density (10^5 to 10^6 times that of typical ion-implantation systems) offers the promise of the direct writing of implanted regions in semiconductors. A variety of other applications, including deposition of contact metals, machining, trimming, and lithography, are also of interest. The application of this technology to the direct writing of implants promises to eliminate the need for implant masking and to permit rapid circuit modification because the implant "mask" exists only as a computer code which describes the scanning of the beam necessary to fabricate the implanted region. The combination of direct writing of implanted regions with transient annealing offers the promise of a complete in vacuo direct doping process.

During the present contract, we investigated the physical and electrical properties of implanted layers produced by the implantation of Ga^+ ions into Si by high-brightness tiny ion beams. One paper published on this work showed that the damage and the dopant distributions resulting from implantation of very high dose rates are comparable to those obtained by conventional implantation. Electrical measurements of thermally annealed samples implanted by this technique indicated that the electrical properties of the layers obtained were comparable to those of conventional implanted samples. These experiments are discussed in Section 5.

Because of the inclusion in this report of several published papers, each with its own set of references, references are provided on a section-by-section basis. Figure numbers in the reproductions of the papers are independent of those in the remainder of the text.

To ensure that the efforts of those responsible for a particular area of investigation are properly identified and acknowledged, we have provided a list of contributors to each section which does not include reproductions of papers.

Table 1. Publications and Presentations Supported by This
Contract and Relevant Related Works
Supported by Hughes

ANNEALING OF ION IMPLANTS INTO GaAs

1. LASER ANNEALED Si AND Se IMPLANTS FOR GaAs MICROWAVE DEVICES, presented at Materials Research Society Meeting, Boston, MA, November-December 1978. Published as AIP Conf. Proc. 50, 585 (1979). See Section 3.A.
2. LASER ANNEALING OF ION IMPLANTED GALLIUM ARSENIDE, presented at Electrochemical Society Meeting, Los Angeles, CA, October 1979. To be published in Proceedings of the Symposium on Laser and Electron Beam Processing of Electronic Materials, Electrochemical Society, 1980. See Section 3.C.
3. PULSED ELECTRON BEAM ANNEALING OF ION IMPLANTED GaAs, presented at Electrochemical Society Meeting, Los Angeles, CA, October 1979. To be published in Proceedings of the Symposium on Laser and Electron Beam Processing of Electronic Materials, Electrochemical Society, 1980. See Section 3.D.
4. ANNEALING OF IMPLANTED LAYERS IN COMPOUND SEMICONDUCTORS BY LOCALIZED BEAM HEATING TECHNIQUES, presented at Materials Research Society meeting, Cambridge, MA, November 1979. To be published in Laser-Solid Interactions and Laser Processing - 1979 (American Institute of Physics, 1980). See Section 3.E.

ANNEALING OF OHMIC CONTACTS TO GaAs

5. LASER-ANNEALED OHMIC CONTACTS FOR GaAs MICROWAVE DEVICES, presented at Materials Research Society Meeting, Boston, MA, November-December 1978. Published as AIP Conf. Proc. 50, 641 (1979). See Section 4.A.

Table 1. (Continued)

6. GaAs MICROWAVE FIELD EFFECT TRANSISTORS WITH LASER-ANNEALED OHMIC CONTACTS, presented at Workshop on Compound Semiconductor Microwave Materials and Devices, Atlanta, GA, February 1979. See Section 4.B.
7. A COMPARISON OF CHEMICAL AND STRUCTURAL CHARACTERISTICS OF In-Au:Ge OHMIC CONTACTS ON GaAs PRODUCED BY BULK HEATING AND LOCALIZED HEATING, presented at Electrochemical Society Meeting, Los Angeles, CA, October 1979. To be published in Proceedings of the Symposium on Laser and Electron Beam Processing of Electronic Materials, Electrochemical Society, 1980. See Section 4.C. Supported by Hughes.
8. OVERVIEW OF OHMIC-CONTACT FORMATION ON n-TYPE GaAs BY LASER AND ELECTRON-BEAM ANNEALING, Invited Paper presented at Materials Research Society Meeting, Cambridge, MA, November 1979. To be published in Laser-Solid Interactions and Laser Processing - 1979 (American Institute of Physics, 1980). See Section 4.D.

IMPLANTATION OF Si USING FOCUSED ION BEAMS

9. HIGH CURRENT DENSITY Ga^+ IMPLANTATIONS INTO Si, Appl. Phys. Lett. 35, 865 (1979).
10. Ga IMPLANTATION INTO Si AT ULTRA-HIGH DOSE RATES, presented at Device Research Conference, Boulder, CO, June 1979.

Table 1. (Continued)

OPTICAL DIAGNOSTICS OF DAMAGE AND ANNEALING

11. APPLICATION OF OPTICAL TECHNIQUES TO AMORPHOUS-CRYSTALLINE TRANSITIONS INDUCED BY LASER ANNEALING, presented at Electrochemical Society Meeting, Los Angeles, CA, October 1979. To be published in Proceedings of the Symposium on Laser and Electron Beam Processing of Electronic Materials, Electrochemical Society, 1980. See Section 3.B. Supported by Hughes.
12. DIAGNOSTICS OF LASER ANNEALED SEMICONDUCTOR MATERIALS USING PHOTOACOUSTIC, RELATED OPTICAL AND RUTHERFORD BACKSCATTERING TECHNIQUES, presented at Materials Research Society Meeting, Cambridge, MA, November 1979. To be published in Laser-Solid Interactions and Laser Processing - 1979 (American Institute of Physics, 1980). Supported by Hughes.
13. PHOTOACOUSTIC MEASUREMENTS OF ION IMPLANTED AND LASER ANNEALED GaAs, accepted by Appl. Phys. Lett. Supported by Hughes.

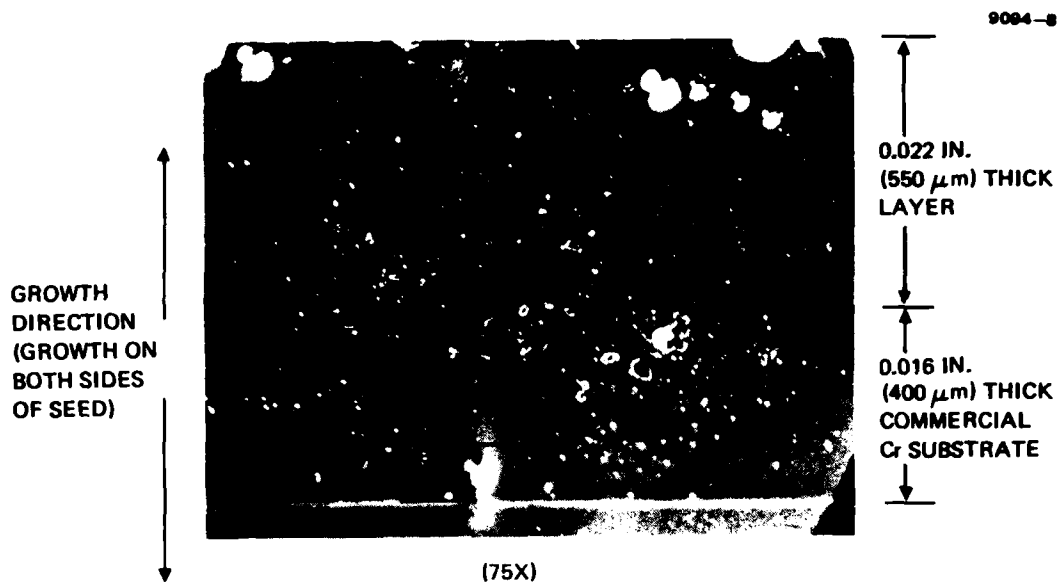
SECTION 2

GALLIUM ARSENIDE ADVANCED CRYSTAL GROWTH (D.E. Holmes, G.S. Kamath)

On the basis of an experimental and theoretical framework established at HRL for GaAs solution growth, we have grown millimeter-thick GaAs crystals (see Figure 1) from the new HRL solution growth system with room-temperature carrier concentrations in the 1 to $3 \times 10^{15} \text{ cm}^{-3}$ range and mobilities of $7000 \text{ cm}^2/\text{V-sec}$ (liquid nitrogen mobilities of $30,000 \text{ cm}^2/\text{V-sec}$). The quality of this material is significantly better than that presently available on a routine commercial basis, as illustrated in Figure 2. The equivalent of more than two substrates was grown over a 24-hr period, thereby demonstrating the feasibility of bulk, high-purity GaAs solution growth. Presently, our primary objectives are to (1) gain an additional factor-of-10 increase in crystal thickness while maintaining controlled conditions and (2) demonstrate the growth of high-resistivity material with Cr doping. Our program is discussed in more detail below.

A. HRL BULK SOLUTION GROWTH APPARATUS

The new HRL bulk solution growth apparatus, shown in Figure 3, is a flexible research tool for high-purity bulk solution growth development. The system is vertical and consists of a 52-in.-long, 6-in.-diameter quartz growth chamber. A concentric resistance-heated furnace provides operation up to 1100°C , and a dual-channel microprocessor controller provides flexible control of vertical temperature gradients. Adjoining the growth chamber at the top, and separated from it by a gate valve, is another vacuum-tight chamber, which allows seed crystals to be introduced into the growth chamber without contaminating the growth chamber. The solution is contained in a 4-3/4 in. diameter graphite crucible (Figure 4) positioned on a pedestal that extends from the base of the system. Ten thermocouples (five on each side) inserted in the outside crucible wall provide in situ, real-time



GROWTH TEMPERATURE 830°C

TECHNIQUE - SLOW COOLING

GROWTH TIME 26.75 HOURS

$N_D - N_A_{298^\circ\text{K}} = 1.8 \times 10^{15} \text{ CM}^{-3}$

$\mu_{298^\circ\text{K}} = 7000 \text{ CM}^2 \text{ V}^{-1} \text{ SEC}^{-1}$

$N_D - N_A_{77^\circ\text{K}} = 1.4 \times 10^{15} \text{ CM}^{-3}$

$\mu_{77^\circ\text{K}} = 30,000 \text{ CM}^2 \text{ V}^{-1} \text{ SEC}^{-1}$

Figure 1. Micrograph showing cross section of 550-nm-thick growth on 400 μm Cr-doped substrate. Growth occurred on both sides of the substrate. Growth parameters and electrical characteristics are given in the legend.

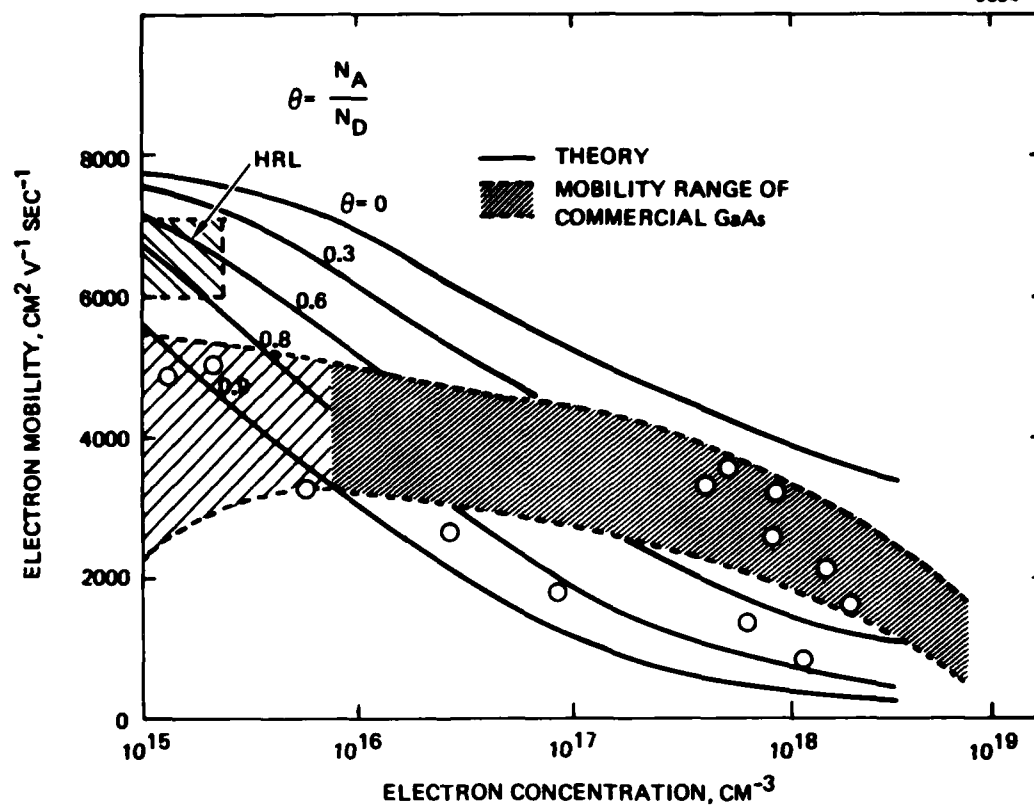


Figure 2. Comparison of mobility range of commercial with HRL-grown GaAs. The theoretical curves of mobility versus carrier concentration for various compensation ratios are also shown.

M12825



Figure 1. PbTe solution growth apparatus with the furnace in the crystal growth position.

M12845



Figure 4. BRL bulk solution growth apparatus with the furnace raised up to expose the crucible containing the solution.

monitoring of horizontal and vertical gradients. Internal thermal probing of the solution is also provided for. A cryogenic pumping station mounted on the base of the upper chamber produces pressures as low as 4×10^{-7} Torr in the growth chamber at 850°C to prebake furnace parts and remove volatile impurities from the Ga solution. Provision is also made for alternate heating and cooling schemes at the crucible to achieve more complex thermal configurations, the use of an AsH_3 gas as an arsenic source, and the introduction of current leads for electro-crystallization.

B. EXPERIMENTAL AND THEORETICAL CONSIDERATIONS

To establish fundamental guidelines for our solution growth experimentation and to evaluate the experimental results in terms of relevant growth parameters, theoretical modeling of four basic growth configurations, shown in Figure 5, was initiated. Emphasis was placed on the hydrodynamics of large solutions. Each configuration except No. 3 was studied experimentally. The advantages and disadvantages of each configuration and the important experimental results are summarized in the figure.

1. Seed-at-the-Top Configuration

The seed-at-the-top configuration is a constant-temperature process in which the upward transport of As from the source material to the seed is promoted by both thermal convection (hotter fluid is less dense and rises) and solutal convection (As-rich solution is less dense and rises). The degree of hydrodynamic instability is expressed in terms of the thermal and compositional Rayleigh numbers, N_R^T and N_R^C , which are given by

$$N_R^T = \frac{g\alpha}{\nu K} TH^3 \quad (1)$$

$$N_R^C = \frac{g\alpha'}{\nu D} CH^3, \quad (2)$$

where g = acceleration due to gravity, α = expansion coefficient with respect to temperature, α' = expansion coefficient with respect to As

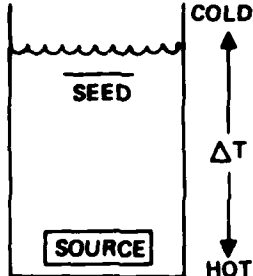
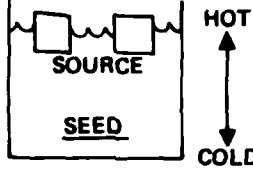
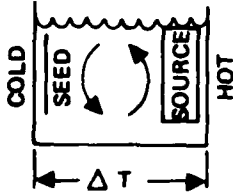
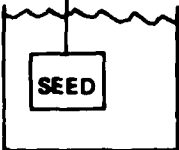
CONFIGURATION	ADVANTAGES	DISADVANTAGE	EXPERIMENTAL RESULTS
1. SEED-AT-THE-TOP 	<ul style="list-style-type: none"> ● COMBINATION OF THERMAL AND SOLUTAL CONVECTION PROVIDE FAST TRANSPORT ● POTENTIAL FOR CRYSTAL PULLING 	<ul style="list-style-type: none"> ● SPURIOUS NUCLEATION AT SOLUTION SURFACE ● TEMPERATURE AND A_s COMPOSITION ARE VARIABLE IN SPACE AND TIME 	<ol style="list-style-type: none"> 1. MAXIMUM CONTROLLED GROWTH-$800\mu\text{m}$ 2. MAXIMUM GROWTH EFFICIENCY-23% 3. MAXIMUM TIME FOR SUSTAINED AND CONTROLLED GROWTH OVER LARGE AREA -65 HOURS 4. SEED ROTATION ENHANCES GROWTH CONTROLLABILITY AND MORPHOLOGICAL STABILITY 5. SHOWED THE EXISTENCE AT "CRITICAL DEPTH" BELOW WHICH SEEDS ETCH
2. SEED-AT-THE-BOTTOM 	<ul style="list-style-type: none"> ● SEED AWAY FROM SOLUTION SURFACE 	<ul style="list-style-type: none"> ● SLOW-DIFFUSION-CONTROLLED PROCESS IN THE ABSENCE OF HORIZONTAL THERMAL GRADIENTS 	<ul style="list-style-type: none"> ● (SEE DISCUSSION OF SLOW COOLING IN TEXT)
3. SEED-AT-THE-SIDE 	<ul style="list-style-type: none"> ● CONVECTION MORE CONTROLLABLE AND PREDICTABLE 	<ul style="list-style-type: none"> ● UNKNOWN SOLUTAL EFFECT 	<ul style="list-style-type: none"> ● (SEE DISCUSSION OF SLOW COOLING IN TEXT)
4. SLOW COOLING 	<ul style="list-style-type: none"> ● STRAIGHT FORWARD 	<ul style="list-style-type: none"> ● SPURIOUS NUCLEATION 	<ol style="list-style-type: none"> 1. MAXIMUM CONTROLLED THICKNESS - $800\mu\text{m}$ 2. MAXIMUM GROWTH EFFICIENCY 100%

Figure 5. Summary of theoretical and experimental results concerning four candidate configurations.

composition, v = kinematic viscosity, K = thermal diffusivity, D = As mass diffusivity, T = temperature difference between the source and seed, C = difference in As composition in the liquid at the source and the seed, and H = vertical separation of the source and seed. A comparison of the calculated values of N_R^C and N_R^T over the range of growth temperatures from 600 to 900°C, shown in Figure 6, indicates that transport is dominated by solutal convection.

The seed at the top configuration was investigated experimentally by varying the growth parameters over the wide range indicated in Table 2. Growth could be maintained within about 1 cm from the top surface of the solution when a single piece of source material was used; seeds positioned at deeper levels etched away. This "critical growth depth" was increased to about 3 cm when the source consisted of 8 parallel GaAs plates extending vertically from the bottom of the solution. This indicates that the cool descending fluid requires a finite interaction time in contact with the source material to saturate more completely; ascending As-rich fluid apparently forms a stagnant layer at the solution surface.

The best result obtained by the technique was the growth of 600 μm on the B side of a horizontal (111) seed with a growth efficiency* of 23%. However, growth could not be controlled beyond a period of a few days because of spurious nucleation. Spurious nucleation is the formation in the solution of unwanted crystals that grow at the expense of the seed and result in low growth efficiencies. The presence of many small crystals in the vicinity of the seed also results in morphological breakdown of the growth front (i.e., the transition from controlled growth with a smooth interface to uncontrolled growth with a grossly irregular interface, as shown in Figure 7). One possible approach to obtaining more uniform transport of GaAs to the seed would be to move the seed away from the spurious crystals to reduce their mutual interaction and simultaneously increase the surface area of the source to enhance the total amount of GaAs transported. In practice, however, such an arrangement seems to increase the transport of the solute to the spurious crystals rather than the seed.

* Growth efficiency = $\frac{\text{GaAs deposited on the substrate}}{\text{GaAs rejected by the solution}}$

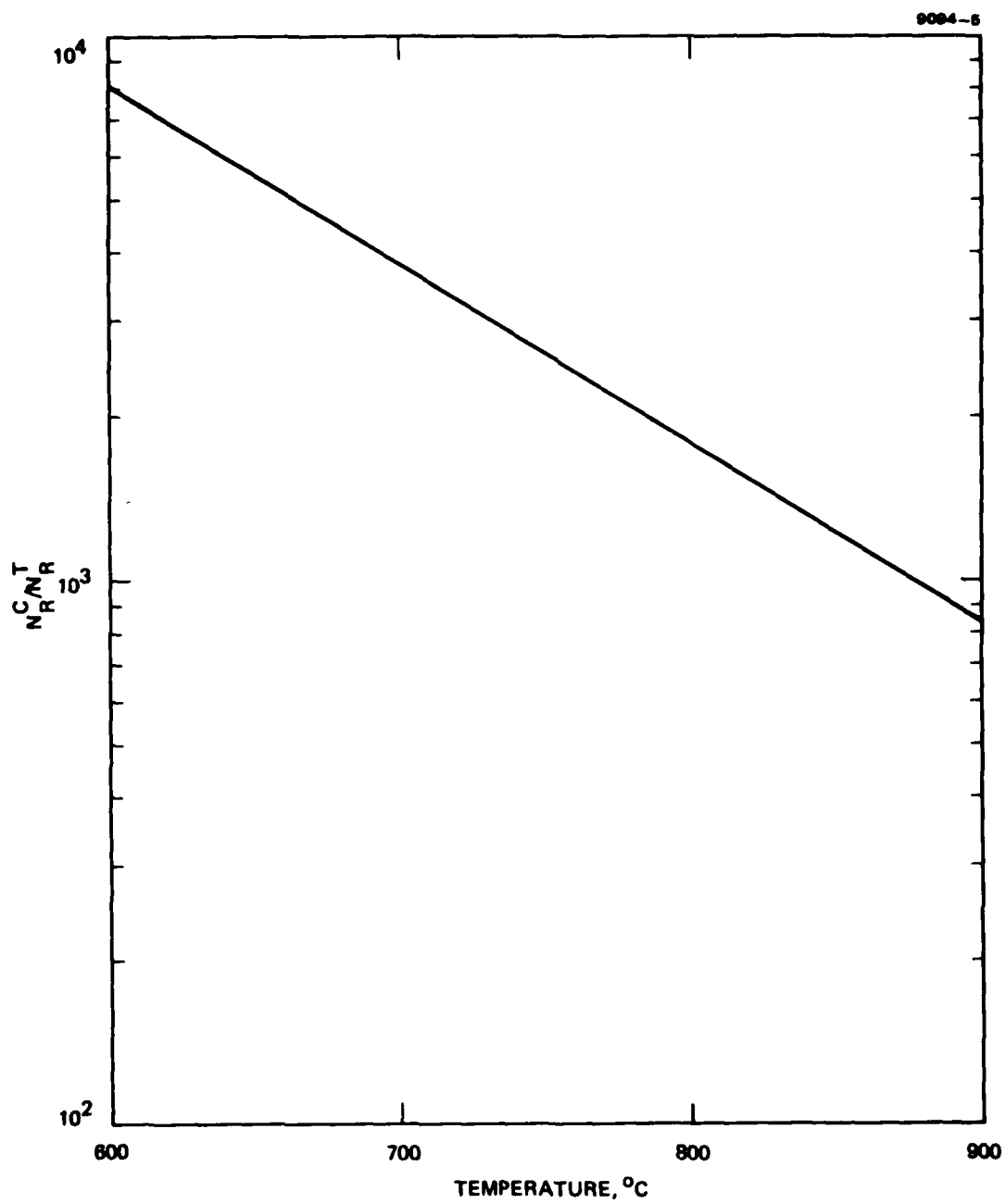


Figure 6. Ratio of compositional and thermal Rayleigh numbers (N_R^C/N_R^T) as a function of growth temperature.



Figure 7. Micrograph of crystal cross section showing interface breakdown.

Table 2. Range of Growth Parameters Used to Investigate the Seed-at-the-Top Configuration

Growth temperatures	750 to 840°C
Seed orientation	(100), (111)B
Temperature difference between the source and seed, ΔT	1 to 10°C
Solution height, H	3.5 in.
Solution diameter	1.5 in.
Orientation of seed axis	Horizontal and vertical

2. Seed-at-the-Side Configuration

The seed-at-the-side configuration is a constant-temperature process in which a unicellular flow pattern driven by a horizontal gradient controls the transport of the source (hot side) to the seed (cold side). The dependence of growth rate on other growth parameters was investigated theoretically by establishing an effective boundary layer thickness, outside of which transport is controlled by convection and inside of which it is controlled by diffusion. Assuming that growth is controlled by As diffusion through the boundary layer, the growth rate, R, is given by

$$R = \frac{D(T)\Omega\Delta}{m(T)\delta}, \quad (3)$$

where $D(T)$ and $m(T)$ are, respectively, the temperature-dependent As diffusion coefficient and the liquidus slope of the phase diagram; Ω is the volume per As atom; and δ is the boundary layer thickness. The boundary layer thickness is given by

$$\delta = 3(v/D)^{-1/3} \left(\frac{vx}{\mu_{\infty}(T)} \right)^{1/2}, \quad (4)$$

where μ_{∞} is the fluid flow velocity at the edge of the momentum boundary layer for laminar flow over a flat plate at a distance x from the leading

edge. μ_{∞} is coupled to ΔT because convection and growth depend on the temperature difference. The functional relationship, obtained from the stream function for unicellular flow, is given by

$$\mu_D = \frac{2}{3} \frac{\kappa}{L} N_R^T x^2 (1-x)^2 y (1-y) (1-2y) , \quad (5)$$

where x and y are dimensionless units of vertical and horizontal distance. ΔT is contained in N_R^T (see Eq. 1).

These calculations yield a set of curves, shown in Figure 8, showing the relationship between temperature difference and crucible width required to maintain a growth rate of 1 $\mu\text{m}/\text{min}$. A growth rate of 1 $\mu\text{m}/\text{min}$ is considered to be a lower limit for a candidate large-scale process. The results indicate that this rate can be achieved at temperatures near 700°C with reasonable crucible dimensions and a controllable ΔT . It is important to note that these temperatures are as much as 500°C below the operating temperature used in conventional bulk growth techniques. Further, control is expected to be more difficult at temperatures above 850°C because the magnitude of ΔT would decrease to less than 1°C for practical crucible dimensions. The presence of appropriately spaced baffles within the solution would therefore enhance controllability in the regime by reducing the flow velocity.

Another parameter that must be maximized for an economical, large-scale process is the quantity of GaAs produced per unit volume of Ga solution. Common impurities in the source material such as Si with segregation coefficients less than 1 gradually accumulate in the solution as growth proceeds. Therefore, at some point in time, the background impurity concentration in the regrown material rises to a level where the repurification of the Ga solution becomes necessary. We shall refer to the total growth time up to this point as the cutoff time, and the corresponding crystallization thickness as the cut-off thickness. A throughput model was developed describing the accumulation of impurities over time as crystallization proceeds. On the basis of this model, we analyzed the cut-off time and cut-off thickness as a function of the segregation coefficient of impurities (see Figure 9). We assumed growth conditions that are representative of our experiment.

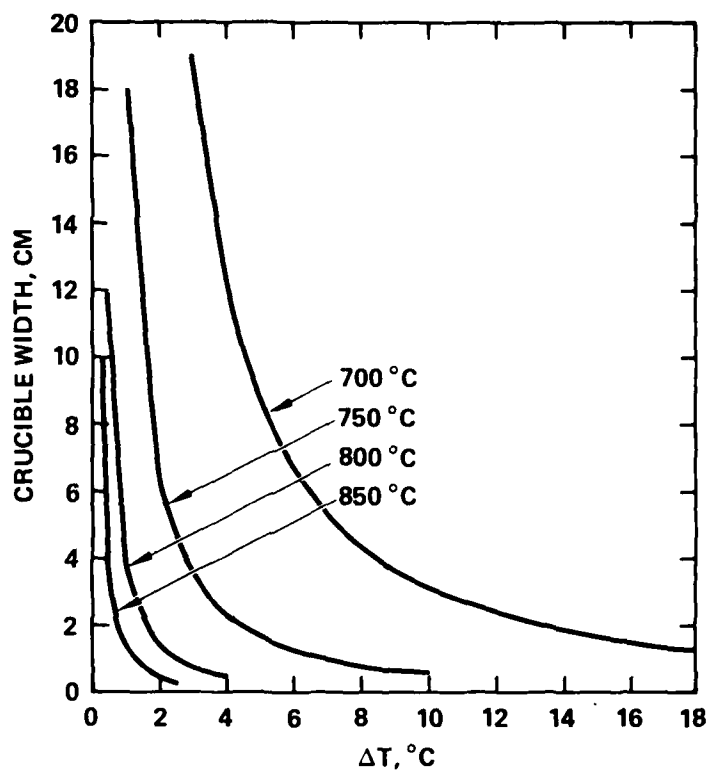


Figure 8. Crucible width as a function of ΔT corresponding to a growth rate of $1 \mu\text{m}/\text{min}$; seed-at-the-side configuration.

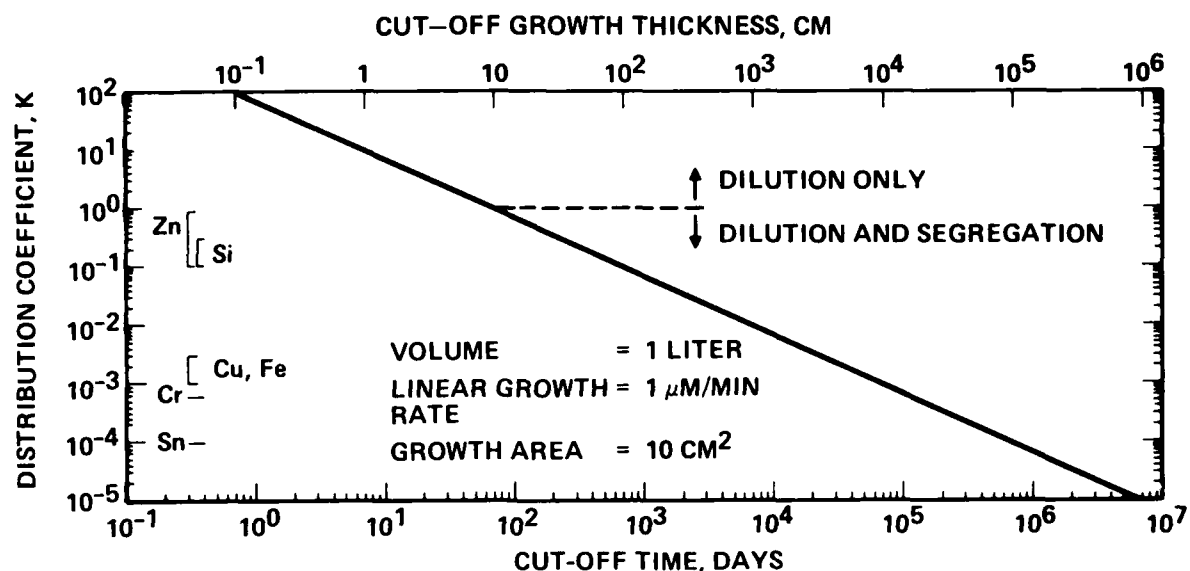


Figure 9. Cut-off time and cut-off growth thickness as a function of distribution coefficient for infinite stirring.

As seen in Figure 9, both the cut-off thickness and time generally increase as the segregation coefficient decreases. In practical terms, this means that the yield of regrown material with the desired level of purification is governed by the impurity with the highest distribution coefficient. Of the common electrically active impurities known to exist in commercially available GaAs, Si occurs in relatively high concentration and has a large distribution coefficient (see Figure 9). Therefore, Si is expected to be one of the impurities that will limit the quantity of GaAs produced per unit volume of Ga solution.

3. Seed-at-the-Bottom Configuration

The theoretical results pertaining to the seed-at-the-side configuration can be shown to be generally applicable to the seed-at-the-bottom configuration since the governing convective transport process for the solute is the same in the two cases.

4. Slow Cooling

The slow cooling technique is a straightforward extension of the established HRL infinite solution LPE process, which is based on the decrease in GaAs solubility with decreasing temperature. The solubility of GaAs in Ga and the volume of grown material obtained per 1°C drop in temperature, shown by the curves in Figures 10 and 11, are substantial although somewhat low at operating temperatures of 900°C . For example, up to 525 g of GaAs can be obtained from a 5300-g solution by dropping from 900°C to 700°C .

A major experimental problem initially encountered with this technique was spurious nucleation. The problem was overcome by growing on a rotating vertical seed (0.5 rpm) positioned in the center of the solution. The vertical gradient was uniform, with the bottom of the crucible colder than the top by no more than about 2°C , and the cooling rate was 0.3°C/hr . Millimeter-thick crystals were grown by the technique. An example is shown in Figure 1.

Once 100% efficient growth could be controlled over a period of about 30 hr, the limiting factor to growth for longer periods of time was interface breakdown (see Figure 7). When we attempted to eliminate breakdown by further reducing the cooling rate, we observed that seeds

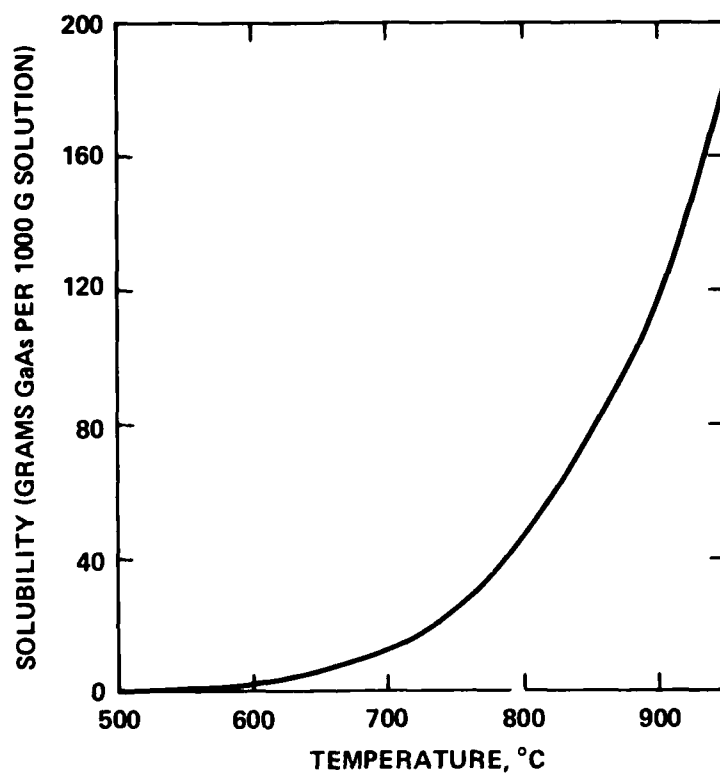


Figure 10. Solubility of GaAs in Ga.

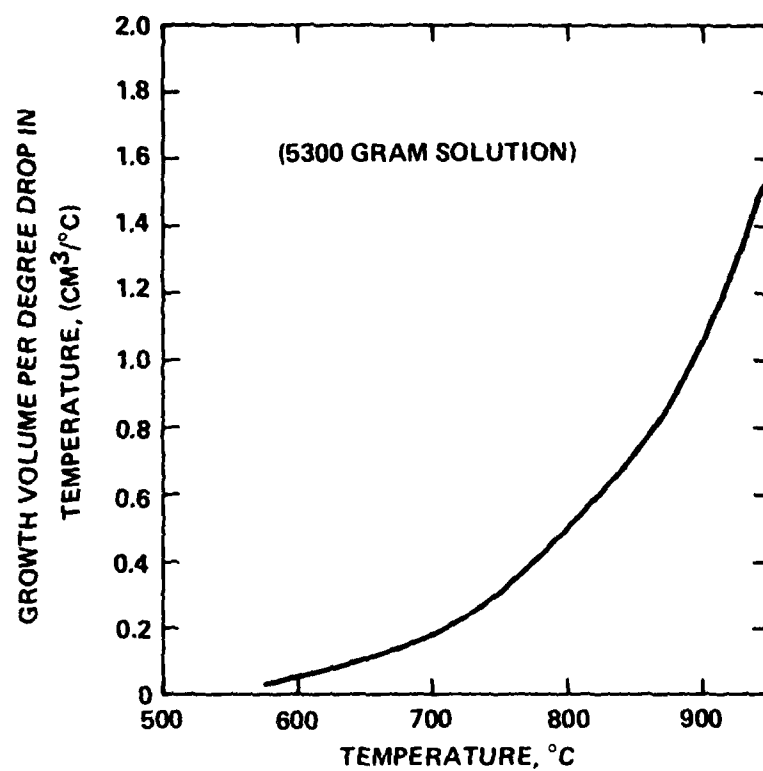


Figure 11. Growth volume/°C drop in temperature.

began to etch away. This behavior is similar to the etching characteristics observed in the seed-at-the-top experiments. In later experiments, we verified that spurious nucleation occurred on the graphite wall at the bottom of the crucible. Since the vertical gradient was stabilizing (slightly hotter at the top), we concluded that unavoidable horizontal gradients caused significant convective flow, which in turn resulted in transport of GaAs to the coldest region of the solution.

The confirmation of horizontal-gradient-driven convective transport is significant because it is now apparent that the natural flow in the large solution can be exploited as a constant-temperature growth process. In fact, it effectively combines the advantages of the seed-at-the-top and seed-at-the-side configurations: source material is held at the solution surface, spurious nucleation at the solution surface does not interfere with the process, and convection is more controllable and more predictable.

The observation of spontaneous heterogeneous nucleation on the dense, high-purity graphite crucible wall was unexpected because Ga does not wet graphite. Therefore, the seed-at-the-bottom configuration may require the use of new crucible materials.

The results above have also provided insight into crystal growth from large solutions. A model is now evolving. As depicted in Figure 12, at high cooling rates (on the order of $0.1^{\circ}\text{C}/\text{min}$), the normal growth process takes place (path 1). At very slow cooling rates (less than about $0.3^{\circ}\text{C}/\text{hr}$), convection processes driven by destabilizing horizontal or vertical gradients result in transport from the seed to the coldest region of the solution (path 2 or 2' in Figure 12). The two processes are competitive: if the cooling rate is too slow, the seed etches away and normal growth takes place at the spurious crystals (path 3 to 3' in Figure 12). The critical cooling rate is about $0.3^{\circ}\text{C}/\text{hr}$ and appears to depend on whether or not the seed is rotated.

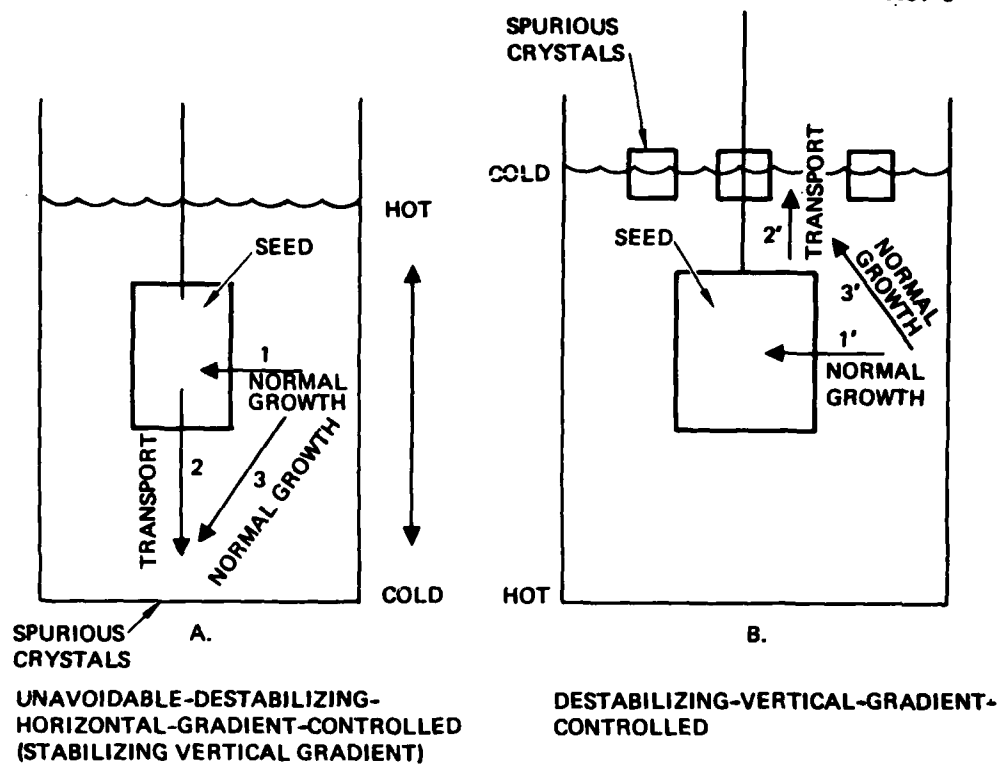


Figure 12. Competing growth mechanisms resulting from convective stirring.

C. ELECTRICAL CHARACTERISTICS

The free carrier concentration and electron mobility were measured as a function of temperature by the van der Pauw Hall technique. Representative curves are shown in Figures 13 and 14. The mobility maxima, of up to $30,000 \text{ cm}^2 \text{ V}^{-1} \text{ sec}^{-1}$, occurred at $\sim 77^\circ\text{K}$ (liquid nitrogen temperature), and the corresponding carrier concentration ranged from 1 to $4 \times 10^{15} \text{ cm}^{-3}$. The compensation ratio (N_A/N_D) consistent with these data ranges from 0.65 to 0.83. A computer curve fit of carrier concentration versus inverse temperature based on a single-donor-single-acceptor model indicates that the background donor level is very shallow with an activation energy of about 0.015 eV. We are attempting to determine the chemical identity of this shallow level.

D. SUMMARY

The growth of millimeter-thick crystals with considerably improved background impurity levels compared with commercially available melt-grown GaAs brings the growth of centimeter-thick crystals within reach. Systematic experimental and theoretical investigations of candidate growth configurations has provided a necessary understanding of production limits, optimal design and growth parameters, particular advantages that can be exploited, and disadvantages that must be dealt with. This experience will aid in achieving our next goal - an order-of-magnitude increase in crystal thickness. The relatively low background impurity levels represent a first-order improvement gained by low-temperature processing. As we continue to learn to exploit this crystal growth environment, uniquely available in our low-temperature system, we expect to improve the reproducible control of purity in the bulk material grown. This is a necessary first step to achieving semi-insulating characteristics in the grown GaAs by adding Cr or other deep-level dopants to the solution.

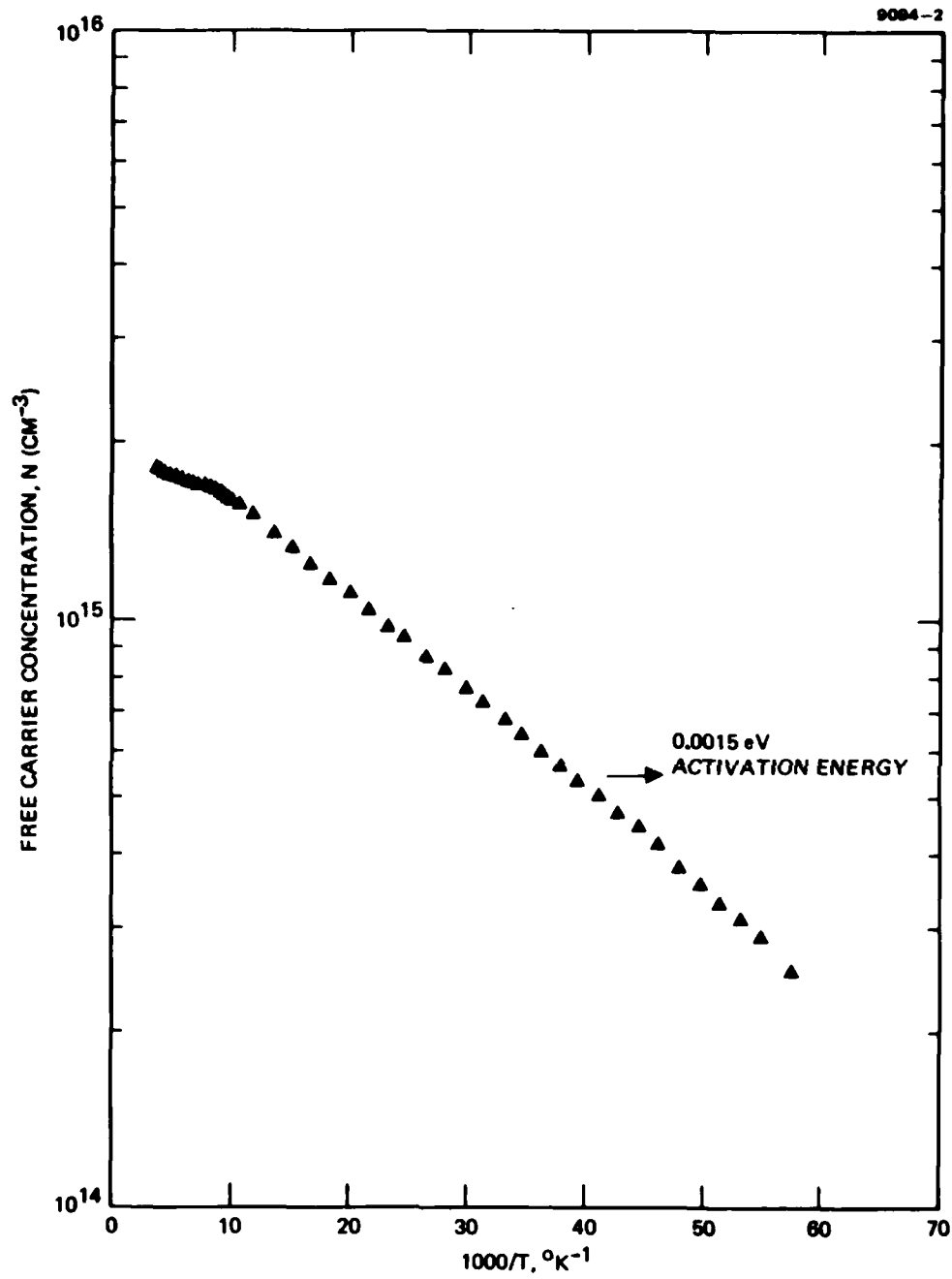


Figure 13. Free carrier concentration, N , as a function of reciprocal temperature.

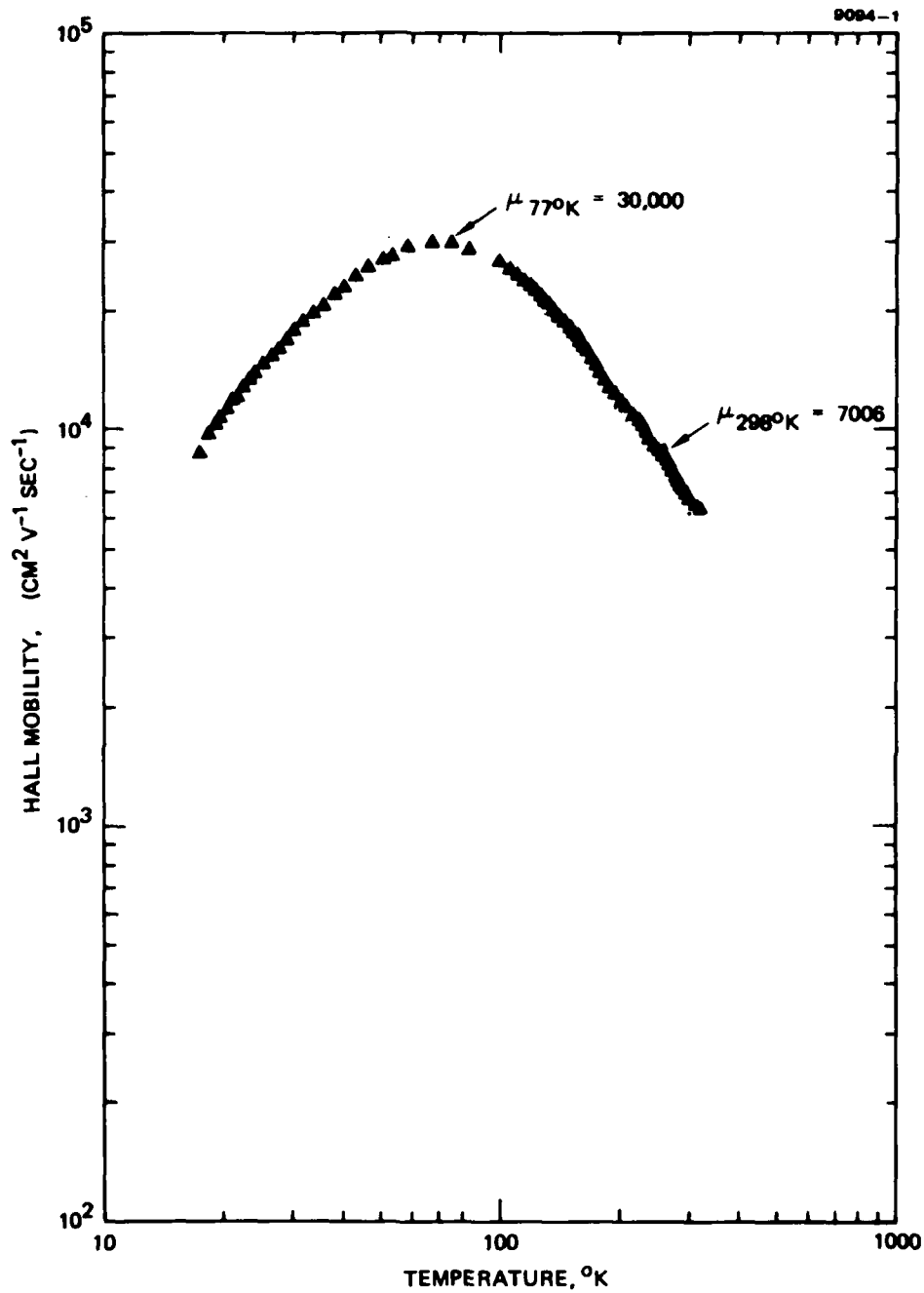


Figure 14. Hall mobility, μ , as a function of temperature.
Sample thickness = 100 μm .

SECTION 3

ANNEALING OF ION-IMPLANTED GaAs WITH LASER AND ELECTRON BEAMS

During this program, we systematically investigated the annealing of ion-implanted GaAs using pulsed (Q-switched as opposed to free-running) lasers, cw lasers, and pulsed electron beams.

Our initial investigations were aimed at determining appropriate laser-annealing conditions for GaAs and at determining the "window" in the annealing parameters within which satisfactory annealing could be achieved. To do this, we developed the diagnostic technique of channeling yield topography (CYT) to profile the damage level across annealed wafers. The use of this technique provided clear evidence that the annealing "window" in GaAs is quite narrow and that control of the uniformity of energy deposition is critical if uniform annealing is to be achieved. These results were assembled in a published paper, reproduced as Section 3.A.

A second class of diagnostic techniques applicable to the characterization of laser annealing of implantation damage is based on the increase in optical absorption associated with lattice damage. The equipment and procedures needed for applying these techniques were developed under Hughes internal funding. The basic procedures involved and the application of the techniques to laser-annealed GaAs were described in three published papers, one of which is reproduced as Section 3.B.

Our later work on laser annealing of GaAs concentrated on the optimization of the electrical properties of the implanted layers. Our results in this area represent or are highly comparable to the state of the art for both pulsed and cw laser annealing. These results are summarized in a published paper reproduced as Section 3.C.

A preliminary investigation of the use of pulsed-electron-beam annealing of GaAs was performed in the later stages of the contract. The results of this study were published in a paper reproduced as Section 3.D.

A paper summarizing all our laser and electron-beam annealing results was presented at the Materials Research Society meeting, Boston, MA, November 1979. This paper compares the results obtained by cw laser annealing, pulsed laser annealing, and pulsed electron beam annealing. It also relates our results to the state of the art. This paper, submitted for publication and reproduced in Section 3.E, provides an excellent summary of the results obtained under the present contract.

SECTION 3.A

LASER ANNEALED Si AND Se IMPLANTS FOR GaAs MICROWAVE DEVICES

(C. L. Anderson, H. L. Dunlap, L. D. Hess,
and K. V. Vaidyanathan)

Presented at Materials Research Society
Meeting, Boston, MA, November-December 1978.

Published in Laser-Solid Interactions and
Laser Processing - 1978.
(AIP Conf. Proc. 50, 585 (1979)).

GaAs - Implanted

LASER-ANNEALED Si AND Se IMPLANTS FOR GaAs MICROWAVE DEVICES*

C. L. Anderson, H. L. Dunlap, L. D. Hess,
and K. V. Vaidyanathan
Hughes Research Laboratories, Malibu, CA 90265

ABSTRACT

We have studied the room temperature annealing of Si- and Se-implanted GaAs, using pulsed Nd:YAG (1.06 μm), pulsed KrF excimer (0.25 μm), and scanned cw Ar (0.488, 0.514 μm) lasers as energy sources. Low-fluence (10^{13}cm^{-2}) implants similar to those used for microwave FET channel formation and high-fluence ($3\text{-}5 \times 10^{14}\text{cm}^{-2}$) implants typical of ohmic contact formation applications were annealed. The primary evaluation technique used has been channeling yield topography (CYT), the Rutherford backscattering equivalent of X-ray mapping in an SEM. Using our apparatus, the lowest channeling yield obtainable is about 0.05 of the random equivalent signal level. Yields below 0.1 of random have been obtained with all three lasers. The best result to date has been obtained with the KrF laser, which produced a yield of 0.057 of random.

INTRODUCTION

We have been performing a systematic study of the laser annealing of Si and Se implants into GaAs for microwave device applications. To date we have been concentrating on lasers and annealing conditions which are readily compatible with uniform annealing of large areas of material for device applications. Our primary emphasis, therefore, has been on room temperature annealing with (1) pulsed lasers which exhibit large beams and high pulse rates and (2) scanned cw lasers. The lasers which we have employed are pulsed Nd:YAG (1.06 μm), pulsed KrF excimer (0.25 μm) and scanned cw Ar (0.488, 0.514 μm). Although some promising results have been obtained with pulsed ruby lasers¹⁻³, the small beam diameter and low pulse repetition rate of single mode oscillator configurations for ruby lasers are serious drawbacks to their use in practical device applications. Fan and co-workers⁴ have reported promising results using a scanned cw Nd:YAG laser to anneal implanted layers in GaAs and InP. Best results were obtained when the GaAs samples were heated to about 500°C to increase the optical absorption of the material at 1.06 μm . All studies reported here were performed with the substrate held at room temperature. We have emphasized Si and Se implants because of the practical importance of these n-type dopants in microwave device technology.

EXPERIMENTAL PROCEDURES AND RESULTS

Because reordering of the crystal lattice is a necessary first

*This work was supported in part by the Defense Advanced Research Projects Agency (DARPA Order 3564) and monitored by the Office of Naval Research under contract N00014-78-C-0337.

ISSN:0094-243X/79/500585-05\$1.50 Copyright 1979 American Institute of Physics

step to obtaining electrical activation of ion implanted dopants in GaAs, we have concentrated on determining annealing parameters which result in optimum crystallinity of the laser-annealed surface region. In these studies we have made extensive use of the technique of channeling yield topography (CYT).

The basic concept of CYT is readily illustrated with reference to Figure 1, which shows the aligned and random-equivalent Rutherford backscattering (RBS) spectra obtained from a sample of GaAs subjected to a high-fluence Se implant and annealed in air with a pulsed multi-mode Nd:YAG laser. In a typical crystalline sample, the ratio of the random equivalent backscattering yield to the aligned yield (the "channeling dip") is greatest in a small number of analyzer channels. The signal in these channels arises from a region of the crystal near the surface but below the disordered region which causes the "surface peak" typically observed in aligned spectra. Since a heavily damaged or amorphous layer will produce an aligned spectrum very similar to the random spectrum in Figure 1, an assessment of the spatial variations in the degree of annealing of the sample can be obtained by scanning a small ion beam aligned with a channeling axis across the sample surface while monitoring the count rate in those analyzer channels which exhibit the maximum channeling dip. This technique, which we call channeling yield topography or "CYT" is analogous to the mapping of X-ray count rates in an SEM. In all spectra presented here, the probe beam was a 140 keV H^+ beam 125 μm in diameter. The energy regions of interest used in Figures 2-5 are shown in Figure 1. The selenium implanted GaAs sample number (3,3), Se 106, is the sample used to derive the spectra of Figures 1 and 2. Observation of the full RBS spectrum of this sample indicated that the small spectral region which was monitored while scanning the analyzing beam included a substantial fraction of the surface peak. Accordingly, the CYT scans for Figures 3 through 5 were obtained with the more suitable spectral region of interest shown in Figure 1.

The CYT scan obtained from sample (3,3), Se 106 is shown in Figure 2. Because of the highly non-uniform distribution of laser power incident on the sample surface as a consequence of the multimode character of the laser, a wide variation of degree of annealing is seen. The area to the left of Figure 2 is essentially unannealed, while substantial annealing with a channeling dip of about 10 to 1 is evident near the right of the figure. The regions in which the maximum degree of annealing occurred - from about 0.2 to 0.25 cm and from about 0.35 to 0.40 cm on the horizontal scale - were separated by a region in which the sample was visibly damaged. This would appear to indicate that the annealing threshold of GaAs at this wavelength (1.06 μm) is very close to the damage threshold. However, there are other factors to consider simultaneously. First, this particular multimode laser tends to have a "hot spot" near the center of its beam. Thus there may have been very rapid power gradients near the damaged spot. Second, the photon energy of this laser is below the GaAs bandgap. However, the amorphous region produced by the Se implant will exhibit significant absorption at 1.06 μm . As the GaAs is heated by the absorption in the amor-

phous region, the bandgap in the heated region decreases, thereby increasing the intrinsic absorption of the GaAs at $1.06 \mu\text{m}$. Thus it is possible that some form of thermal runaway may occur during $1.06 \mu\text{m}$ irradiation of GaAs. Such an effect would be less pronounced with visible lasers.

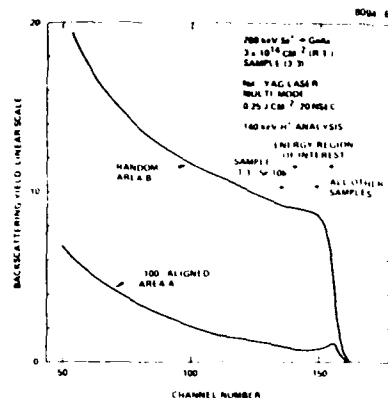


Fig. 1. Rutherford backscattering spectra of a laser-annealed GaAs sample, showing energy regions of interest used for the channeling yield topography (CYT) scans in Figs. 2-5.

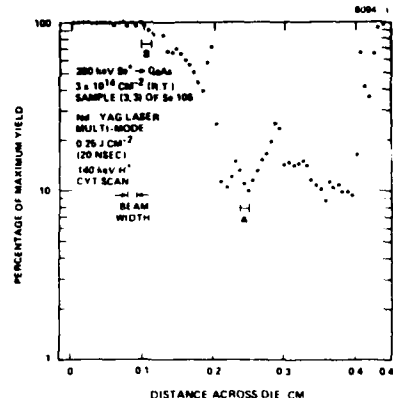


Fig. 2. CYT scan of a GaAs sample given a high-dose Se implant and annealed in air with a pulsed multimode Nd:YAG laser.

A corresponding CYT scan obtained from a sample given a high-dose Se implant and annealed with a pulsed KrF excimer laser operating at $0.25 \mu\text{m}$ is shown in Figure 3. This laser exhibits a relatively large ($3 \text{ mm} \times 15 \text{ mm}$) beam with slow spatial variations in intensity. However, the spatial inhomogeneity of this laser was sufficient to produce some localized damage at several points on the sample. A very good channeling dip is observed near the middle of the sample. Analysis of a complete RBS spectrum from the best annealed area on this sample indicated that the lowest channeling yield was 0.057 of random. With our apparatus, the lowest yield attainable with single crystal GaAs is 0.05 of random. Thus this region of the implanted sample has been restored to an excellent degree of crystallinity. It is apparent, however, that this region of excellent annealing is very close to a damaged region, indicating that the damage threshold of GaAs is quite close to the threshold for annealing of high-dose Se implants at this wavelength. It is interesting and encouraging to note that short pulse ultraviolet radiation which should be absorbed in a layer only a fraction of the amorphous layer thickness (about $0.2 \mu\text{m}$) is nevertheless very effective in restoring the crystallinity of this layer.

CYT scans obtained from samples implanted with two different fluences of Si ions and annealed in flowing forming gas with a

scanned cw Ar laser are presented in Figures 4 and 5. These scans were taken along paths which traversed numerous lines annealed by the raster-scanned laser beam. As expected, the scanned laser

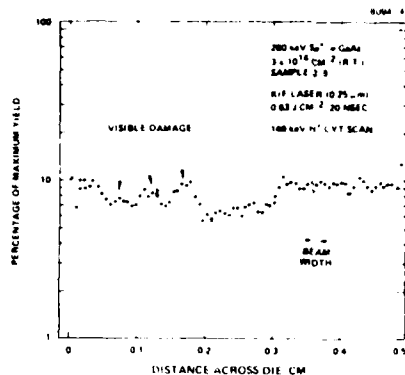


Fig. 3. CYT scan of a GaAs sample given a high-dose Se implant and annealed in air with a pulsed KrF excimer laser.

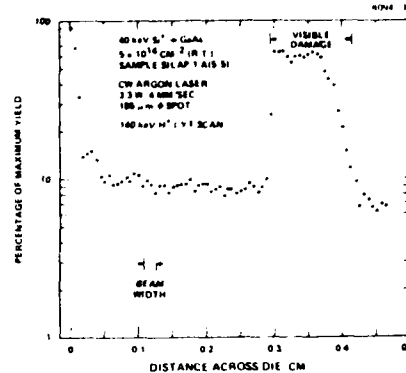


Fig. 4. CYT scan of a GaAs sample given a high-dose Si implant and annealed in forming gas with a scanned cw Ar laser.

produces relatively uniform annealing. The presence of the visibly damaged region in Figure 4 is probably the result of a surface defect or a dirty area on the sample surface prior to annealing.

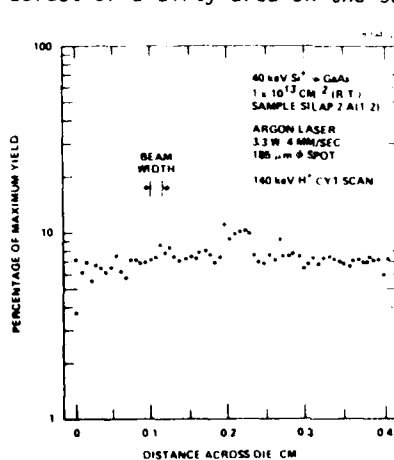


Fig. 5. CYT scan of a GaAs sample given a low-dose Si implant and annealed in forming gas with a scanned cw Ar laser.

Small damaged regions were observed quite frequently in the samples annealed with the cw laser. In particular, we observed that the Ar laser could not be scanned over cleaved edges of the GaAs samples without damaging the sample surface in nearby areas. Therefore, we typically adjusted the raster size and position to lie within the perimeter of the sample. It is interesting to note that the best channeling yield from the sample of Figure 4 (about 15 to 1) was obtained near the edge of the scanned field, a region where the laser beam scan rate typically slows somewhat. We expect that somewhat better results may be obtained in the center of the sample at a lower scan rate.

In the case of the low-dose Si implant, the channeling dip is roughly 15 to 1 across the entire sample. The low implant fluence used in this sample would not be expected to produce an amorphous layer. Therefore, even the unannealed sample exhibits a sizable channeling dip. It is encouraging to note that except for a small area near the center of the sample the laser treatment was not detrimental to the crystallinity of the sample surface.

Our attempts to produce layers of good electrical quality have concentrated on the use of the scanned cw laser system. To date we have obtained primarily disappointing results. Although several samples have exhibited very good apparent electrical activation of the dopant species (up to 90% for low 10^{13} cm⁻² implants), the observed mobilities have generally been very low. Optical examination of the sample surfaces reveals the presence of subtle lines which may indicate slippage or other crystallographic problems. These lines may result in part from the very high thermal gradients at the edges of the region being annealed. One way to reduce the size of these gradients is simply to heat the substrate and reduce the laser power accordingly. We will be investigating this approach in the near future.

CONCLUSIONS

We have obtained good restoration of crystallinity following laser annealing of amorphous layers produced by high-dose Si and Se implants into GaAs. Pulsed Nd:YAG and KrF excimer lasers have been used to anneal samples damaged by ion implantation to a depth of about 0.2 μ m. A scanned cw Ar laser has been used to anneal layers about 0.1 μ m in thickness. In all cases the samples were easily damaged by the laser beam, and the regions of best crystallinity typically were very close to damaged regions. Inert or reducing ambients appear to be important for cw annealing of GaAs. Electrical and optical evaluations of samples annealed with the scanned laser indicate that good carrier activation is occurring, but that crystallographic problems are probably preventing free transport of the charge carriers.

REFERENCES

1. W. L. Brown, J. A. Golovchenko, K. A. Jackson, L. C. Kimerling, H. J. Leamy, G. L. Miller, J. M. Poate, J. W. Rodgers, G. A. Rozgonyi, T. T. Sheng, and T. N. C. Venkatesan, in Proceedings of the Conference on Rapid Solidification Processing - Principles and Applications, November 13-16, 1977, Claitors Publishing Division, Baton Rouge (1978), pp. 123-128.
2. J. A. Golovchenko and T. N. C. Venkatesan, *Appl. Phys. Lett.* **32**, 147 (1978).
3. J. M. Woodcock and H. Butler, talk presented at the International Conference on Ion Beam Modification of Materials, Budapest, Hungary, 1978 (to appear in conference proceedings).
4. J. C. Fan, J. P. Donnelly, C. O. Bozler, and R. L. Chapman, talk presented at the International Symposium on GaAs and Related Compounds, Clayton, Missouri, September 24-27, 1978 (to appear in symposium proceedings).

SECTION 3.B

APPLICATION OF OPTICAL TECHNIQUES TO STUDIES
OF AMORPHOUS-CRYSTALLINE TRANSITIONS INDUCED
BY LASER ANNEALING

(R. A. McFarlane, L. D. Hess, and G. L. Olson)

Presented at Electrochemical Society Meeting,
Los Angeles, CA, October, 1979.

To be published in Proceedings of the Symposium
on Laser and Electron Beam Processing of
Semiconductor Materials, Electrochemical Society,
1980.

APPLICATION OF OPTICAL TECHNIQUES TO
STUDIES OF AMORPHOUS - CRYSTALLINE TRANSITIONS
INDUCED BY LASER ANNEALING

R. A. McFarlane, L. D. Hess and G. L. Olson
Hughes Research Laboratories
3011 Malibu Canyon Road
Malibu, CA 90265

Photoacoustic techniques have been developed for use as a rapid and sensitive diagnostic of crystalline disorder produced by ion implantation in GaAs. Optical transmission measurements on implanted samples using both laser and filtered white light sources indicate that useful amounts of absorption take place in the damaged surface layer and this absorption can be sensed both in transmission and by photoacoustic determination of absorbed energy. With a fluence of 150 keV silicon ions as low as 10^{12} cm^{-2} a measurable photoacoustic signal was observed and the magnitude of this signal showed the expected saturation as dose levels were increased beyond 10^{14} cm^{-2} to 10^{16} cm^{-2} . Recrystallization of ion implanted gallium arsenide by laser annealing is evidenced by an increase in optical transmission and a reduction of the photoacoustic signal to a level characteristic of single crystal material.

Introduction

Optical studies are being performed on ion implanted semiconductor materials to evaluate the transition from amorphous to crystalline surface layer structure brought about by laser annealing. The objective of this work is to characterize ion implanted, amorphous surface layers by measuring the optical absorption and photoacoustic response of the material using an interrogating laser beam. Changes in the optical characteristics of the sample due to laser annealing are being investigated as a rapid diagnostic of the degree of recrystallization achieved.

For silicon and gallium arsenide it is possible to select interrogating wavelengths longer than the band edge where single crystal material is substantially transparent and where the amorphous layer caused by implantation damage has an optical extinction coefficient of 10^3 - 10^4 cm^{-1} . To determine the magnitude of the expected absorption in the implanted layer it is necessary to estimate the thickness of this layer. For the present work we will confine our discussion to GaAs and for a given implant energy of silicon ions, we will use the LSS model to estimate the distribution of the impurity ion density as a function of distance. As a first

approximation we assume that the defect distribution in the implanted layer has a width that is related to the width of the distribution of the implanted ion density. The impurity density is distributed in a Gaussian function of distance with a peak at the projected range R_p and with a standard deviation ΔR_p . Since the density falls to 50 percent of its peak value at $R_p \pm 1.2 \Delta R_p$ we will use $2.4\Delta R_p$ as an estimate of the layer thickness in which a substantial defect density is present. We assume the implant dose is sufficient to produce a completely amorphous layer. For our studies of GaAs, the 1.06 μm output from a cw Nd:YAG laser was used as the excitation source for our photoacoustic experiments. An amorphous layer in GaAs was estimated to have an optical absorption coefficient of 10^4 cm^{-1} at this wavelength (1). Table I shows the results of the calculation for silicon implants in GaAs.

Table I
Estimate of Absorption due to Amorphous Layers
 $\text{Si}^+ \rightarrow \text{GaAs (100)}$

<u>Implant Energy, keV</u>	<u>$2.4\Delta R_p^0$ (Å)</u>	<u>Calculated Absorption, %</u>
40	511	5.0
60	706	6.8
100	1061	10.1
150	1457	13.5

The calculated absorptions are amenable to experimental determination and as we will see below, actually underestimate the absorptions realized in the laboratory.

Photoacoustic Detector System

The photoacoustic effect has recently been developed into a very useful technique for spectroscopic investigations of solids. A rather complete theory to describe it has been presented by Rosencwaig and others (2,3,4). In its simplest form, the technique involves placing the sample to be studied inside a closed cell containing a gas, such as air, and a sensitive microphone. The sample is then illuminated with chopped monochromatic light; if the sample absorbs light, heating occurs due to nonradiative deexcitation. The heat flows from the sample into the surrounding transparent gas causing a pressure change, which is sensed by the microphone. Because the light beam is chopped, the pressure is

modulated at the chopping frequency and the signal from the microphone is measured with a lock-in amplifier using a signal derived from the chopper as a reference. The apparatus is shown schematically in Figure 1. The sample under study, typically a 400 μm thick, 5 mm by 5 mm wafer, sits on a transparent plug of fused silica, and any light transmitted through the sample exits from the lower window. Not shown in the figure is a sensor placed below the cell to measure the power of the transmitted beam.

The details of the photoacoustic cell are shown in Figure 2. The cell is designed to have minimum internal volume with large, clear input and exit windows, and no direct light path to the microphone from the input window or sample. The acoustic detector, a B&K Type 4165 condenser microphone, is integrally mounted to a unity gain preamplifier, the signal from which drives the lock-in amplifier. Because of chopper speed limitations, all PAS data reported here were taken at 84 Hz; this frequency is slightly less than the optimum value since we found that the S/N ratio was still increasing with frequency at that chopping speed.

For experiments on ion-implanted GaAs, we used a 300 mW cw Nd:YAG laser with multimode output at 1.06 μm . The laser beam was directed at a turning mirror and focusing lens mounted on a common motor-driven micrometer stage, thereby permitting the 40 μm diameter focal spot to be scanned along a line across the sample. In this way it was possible to observe changes in the crystallinity of the sample as a function of position and identify where any amorphous regions remained following laser annealing of implanted material. By operating at 1.06 μm , the dominant absorption, and therefore the PAS signal, originated only in the amorphous layer with little or no contribution from the substrate crystal.

Photoacoustic Measurement Results

Initial observations were made of the photoacoustic signal from the implanted layer of 150 keV Si^+ ions into semi-insulating GaAs with a total fluence of $5 \times 10^{14} \text{ cm}^{-2}$. As shown below, this dose is adequate to render the layer totally amorphous. Figure 3 shows the sample transmission and photoacoustic signal that resulted from scanning the 40 μm focused laser spot across this GaAs sample. At 1.06 μm , the refractive index for GaAs is $n = 3.479$ (5), resulting in a two-surface transmission:

$$T = \left\{ \frac{4n}{(1+n)^2} \right\}^2 = 0.481$$

We can compare this to a measured reflectivity near the laser wave-

length (6) $R = 0.289$, which gives a two-surface transmission

$$T = (1 - 0.289)^2 = 0.506 .$$

Differences due to minor variations in surface preparation were apparent on our measured samples, and we have assumed a value of $T = 0.5$ for instances where no reference level was available against which to measure absorption due to a damaged layer. For a fluence of $5 \times 10^{14} \text{ cm}^{-2} \text{ Si}^+$ ions in GaAs, there is a very significant absorption resulting in an overall transmission well below the Fresnel level.

In all cases, the photoacoustic signal increased significantly (typically a factor of two) when the beam was at the sample edge. It can be argued that, when the focused laser spot is at the edge of the sample, the deposited energy can diffuse thermally only into a half-plane, whereas, when the beam is positioned well away from an edge, the thermal diffusion can occur into the whole plane. We believe that small differences from the factor of two may appear due to the effects of the scribe marks that remain after larger wafers have been diced. This "thermal wing" effect should become apparent when the beam is placed within a "thermal diffusion length" of the sample edge:

$$\text{Thermal Diffusion Length} = \sqrt{\frac{\alpha_{TD}}{\pi f}} ,$$

where α_{TD} is the thermal diffusivity, and f is the chopping frequency. For GaAs the thermal diffusivity is $\alpha_{TD} = 0.44 \text{ cm}^2/\text{sec}$, which for $f = 84 \text{ Hz}$ gives a thermal diffusion length of 0.41 mm . This is an order of magnitude larger than our beam spot size and is consistent with the observed width of the thermal wings.

The origin of the periodic structure in the photoacoustic signal as the beam scans across the center of the crystal has not been identified. As shown below, effects due to interference between reflections from the top and bottom surfaces of the sample affect the measurements of samples with less opaque damaged layers, but we believe this cannot explain the observation. We are examining effects due to any nonuniformity in the mechanical drive system and also some optical gradients in the transparent silica plug in the PAS cell, but we have not yet reached any specific conclusions. The signal level produced by single-crystal material is shown as a reference baseline. Again small variations in this level have been found from one sample to another. The level is larger than would be expected for the optical absorption characteristic of crystalline material.

To permit comparing the photoacoustic measurements with other methods of characterizing the structure of the implanted layer, a series of measurements were made on samples of GaAs implanted with 150 keV Si^+ ions with dose levels from 10^{12} cm^{-2} to 10^{16} cm^{-2} . The variation of signal (above the single-crystal level) is shown in Figure 4. It has the same form as measurements of Rutherford back-scattering of He ions that characterize the degree of displacement of atoms from positions in a regular crystal lattice. In both cases, there is a saturation of signal with implant dose which is interpreted to result from a totally amorphous structure in the implanted region, and in both cases this occurs at implant dose levels near 10^{14} cm^{-2} . It is generally agreed that the result of a high-energy ion being introduced into a crystalline substrate is to produce a disordered region around the path of the ion with a diameter on the order of several tens of angstroms (1). At high dose levels, the cross sections of individual regions overlap, which leads to a saturation of the damage inferred from any measurement at a flux value over 10^{14} cm^{-2} . The photoacoustic technique is capable of producing signals at dose levels as low as 10^{12} cm^{-2} , a task that is very difficult for RBS. Reducing the single-crystal signal level should improve the capability further for the photoacoustic method.

An advantage of the photoacoustic determination is the speed with which the spatial variation of the structural properties of the damaged layer can be measured. Figure 5 shows the photoacoustic signal from a sample of GaAs that has been implanted with 40 keV Si^+ ions with a fluence of $5 \times 10^{14} \text{ cm}^{-2}$ and the transmitted intensity of the laser as it is scanned across the sample. The photoacoustic signal is somewhat less for the 40 keV Si^+ than for the 150 keV Si^+ ion, which is to be expected from the smaller range and damage layer thickness. When a similar sample is irradiated with a ruby laser with an energy density of 0.74 J/cm^2 , the implanted layer is restored to crystalline form and the photoacoustic signal returns to very close to that from a single crystal for most of the sample width. The transmitted signal increases to a level identified with Fresnel loss alone, which again is consistent with restoration of the amorphous layer to single-crystal structure. Notice that the edges of the sample were not annealed, which caused transmission at the sample edges to be lower (i.e., absorption to be higher) and the photoacoustic signal to be substantially higher than would be expected from "thermal wing" effects from single-crystal material.

Optical Transmission - Xenon Arc Source

The transmission characteristics of the several implant layers were measured simultaneously with the dose dependence of the photoacoustic signal. At low dose levels particularly, the effects of interference between reflections from the front and back surface give rise to etalon effects, which must be accounted for in any

determination of an effective absorption coefficient. To eliminate these effects, the laser source was replaced with a 150 W xenon arc lamp. The arc was imaged onto an aperture of variable diameter, and this aperture was imaged by a 1:1 optical system onto the sample under study. To characterize only amorphous GaAs, a long-pass filter consisting of a single crystal silicon window was placed in the beam to pass radiation at 1.13 μm and beyond. A 14 mm long sample with three 2 mm wide implanted stripes separated by 2 mm single-crystal stripes was scanned by a 500 μm focused spot. Figure 6 shows the data for three different implant dose levels of 150 keV Si^+ ions in GaAs. The 50% Fresnel loss is apparent as the beam is scanned onto the sample, and the absorption of the damaged regions can be measured with respect to that level. All the absorption data are summarized in Figure 7. It is apparent that an implant dose of 10^{12} cm^{-2} is readily detectable, and again the onset of saturation occurs at fluences in excess of 10^{14} cm^{-2} . Two remarks should be made concerning such measurements. It is to be expected that the reflectivity of the surface will be altered by the implantation process, and this needs to be accurately measured before we can accurately characterize the optical properties of the amorphous layer. Note also from Figure 7 that since there are wavelengths in the xenon source that are longer than the wavelength of the 1.06 μm laser and have lower extinction coefficients, the xenon lamp data saturate at a higher level of transmission than do the laser data.

The extension of these white light transmission measurements to samples which have been laser annealed is currently underway with efforts to improve the spatial resolution of the above results.

Conclusion

We have demonstrated that photoacoustic techniques are advantageous for detecting the presence of an amorphous layer produced at the surface of a semiconductor by ion implantation. The photoacoustic method provides a complementary diagnostic technique which is rapid and sensitive; dose levels as low as 10^{12} cm^{-2} are readily detectable. Because of these characteristics—speed, sensitivity, and spatial resolution, photoacoustic and optical transmission measurements are particularly useful for the analysis of recrystallization by laser annealing. Because the photoacoustic measurement provides a signal against an ideally zero background from crystalline material it may be a more satisfactory method for characterizing departure from single crystal conditions than a determination of small changes in a large signal as occurs in measurements of optical transmission.

Acknowledgments: The authors are grateful to L. M. Lewis, J. Popson and A. Pepitone for skillful technical assistance.

REFERENCES

1. N. F. Mott and E. A. Davis, *Electronic Processes in Non-crystalline Materials*, Clarendon Press, Oxford 1971.
2. A. Rosencwaig and A. Gersho, *J. Appl. Phys.* 47 (1) 64 (1976).
3. A. Rosencwaig, *Rev. Sci. Instrum.* 48 (9) 1133 (1977).
4. J. F. McClelland and R. N. Knisely, *Appl. Optics* 15 (11) 2658 (1976).
5. S. T. F. Markle, *J. Appl. Phys.* 35, 1241 (1964).
6. B. Piriou and F. Cabannes, *Compt. Rend.* 255, 2932 (1962).

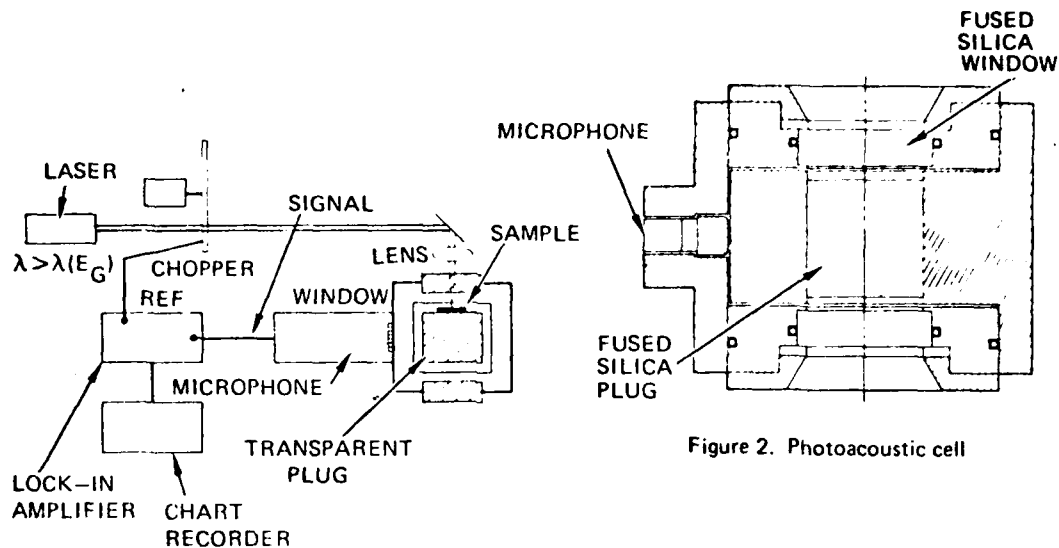


Figure 1. Photoacoustic detection of amorphous films.

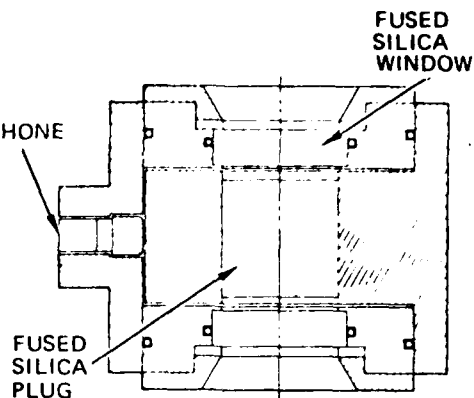


Figure 2. Photoacoustic cell

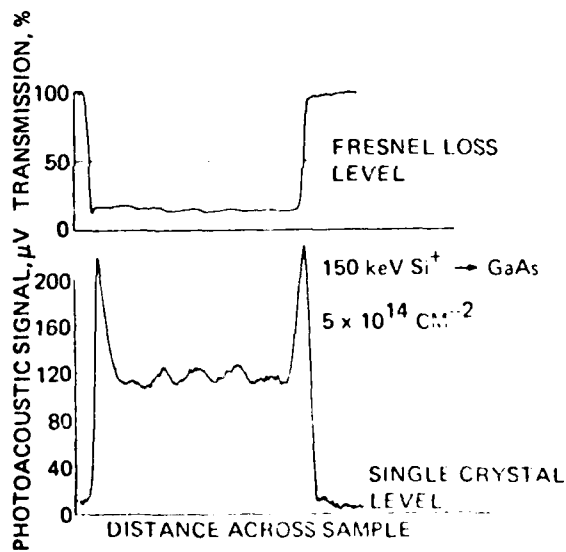


Figure 3. Optical transmission and photoacoustic signal as 1.06 μm laser is scanned across sample.

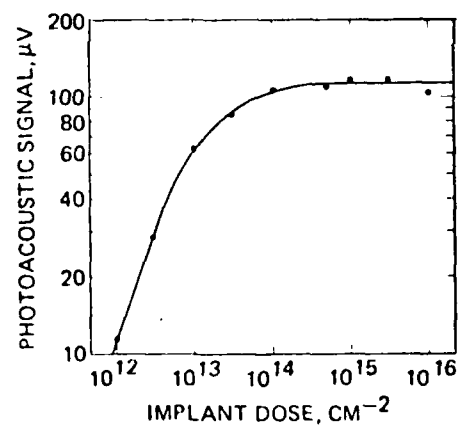


Figure 4. Photoacoustic signal from damaged layer produced by 150 keV Si⁺ in GaAs.

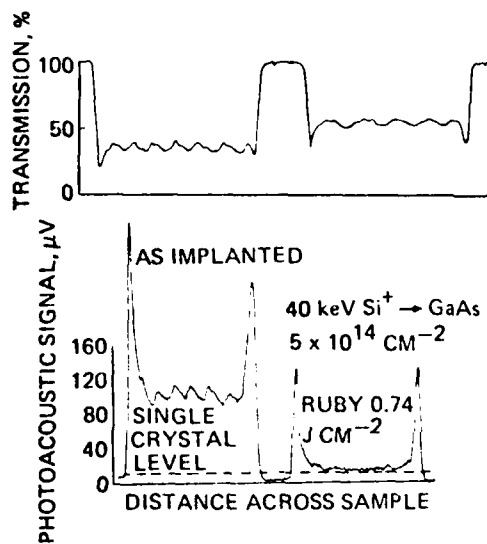


Figure 5. Optical transmission and photoacoustic signal as 1.06 μm laser is scanned across implanted sample and implanted and laser annealed sample.

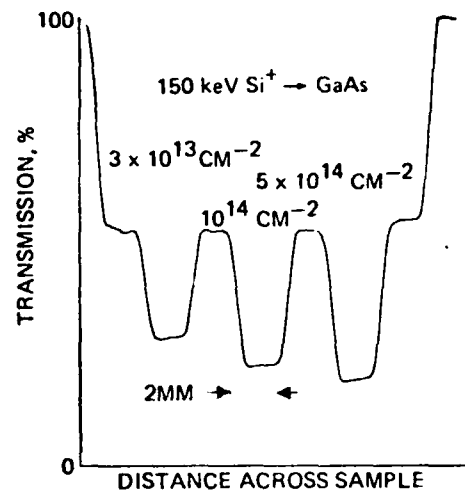


Figure 6. Optical transmission for three implanted regions with the indicated dose. Xenon arc source and silicon long pass filter.

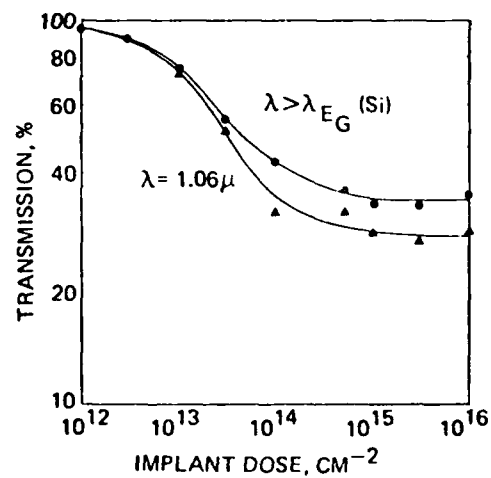


Figure 7. Optical transmission of damaged layer produced by 150 keV Si⁺ in GaAs.

SECTION 3.C

LASER ANNEALING OF ION-IMPLANTED GALLIUM ARSENIDE

(G. L. Olson, C. L. Anderson, H. L. Dunlap, L. D. Hess,
R. A. McFarlane, and K. V. Vaidyanathan)

Presented at Electrochemical Society Meeting, Los
Angeles, CA, October 1979.

To be published in Proceedings of the Symposium on
Laser and Electron Beam Processing of Electronic
Materials, Electrochemical Society, 1980.

LASER ANNEALING OF ION-IMPLANTED GALLIUM ARSENIDE

G. L. Olson, C. L. Anderson, H. L. Dunlap, L. D. Hess
R. A. McFarlane, and K. V. Vaidyanathan
Hughes Research Laboratories
3011 Malibu Canyon Road
Malibu, CA 90265

The effects of laser radiation on the electrical properties of ion-implanted GaAs were investigated using pulsed laser radiation at .249 μm , .532 μm , .6943 μm , and 1.064 μm and cw laser radiation at 0.51 μm and 1.064 μm . Laser energy density, scan rate, and substrate temperature were varied and both high dose ($5 \times 10^{14} \text{ cm}^{-2}$) and low dose ($1 \times 10^{13} \text{ cm}^{-2}$) shallow implants of Si and Se in GaAs were studied. Apparent electrical activation $\leq 8\%$ and electron mobilities $< 350 \text{ cm}^2/\text{V-sec}$ were obtained for high dose implants which were annealed by the pulsed laser sources. High mobilities ($\sim 2000 \text{ cm}^2/\text{V-sec}$) and low apparent activations ($\leq 1.2\%$) were obtained when the cw sources were used to anneal the high dose implants at elevated substrate temperatures. Electrical activation was not obtained for low dose implants (amorphous or crystalline) irradiated by either pulsed or cw lasers. The difference in mobilities between samples annealed by cw and pulsed radiation is discussed in terms of effects due to spatial nonuniformities in laser pulse intensity, and generation of defects by nonstoichiometric regrowth.

Introduction

Laser annealing of ion implantation damage in semiconductors is being intensively studied as a method for restoring sample crystallinity without introducing defects or impurities into the crystal lattice. Although most of the work to date has been directed toward electrical characterization and determination of annealing mechanisms in silicon, there has been an increasing interest in laser-induced recrystallization and electrical activation of ion-implanted compound semiconductors, most notably GaAs (1-12). Although previous work on laser annealing of ion-implanted layers in GaAs has

*This work was supported in part by the Defense Advanced Research Projects Agency and monitored by the Office of Naval Research under contract N00014-78-C-0337.

concentrated primarily on pulsed laser annealing of both encapsulated (2,5) and unencapsulated GaAs (3,9,10-12), excellent activation ($\sim 30\%$) and high mobilities ($> 2000 \text{ cm}^2/\text{V-sec}$) have been reported (7) for cw Nd:YAG laser annealing of GaAs implanted with Se (400 keV, $1 \times 10^{14} \text{ cm}^{-2}$). The high mobilities obtained in the cw experiments were attributed to reduction in the thermal stress by the cw technique relative to the pulsed approach. The lower thermal stress condition results in a reduced density of planar defects. In the present study we compare the effects of laser radiation on the electrical properties of amorphous and crystalline, thin ($\sim 1000 \text{ \AA}$) films of ion-implanted GaAs (low dose and high dose Se and Si implants). We are conducting a laser annealing study of these shallow implants using both pulsed and cw laser systems operating in the uv to near-ir spectral region. A survey of the preliminary results obtained from these investigations is presented, and differences in the electrical properties of the GaAs samples annealed by these sources are discussed in this paper.

A number of GaAs sample and laser parameters were systematically varied in this study. These parameters are summarized below. Additional details are presented in the next section.

(a) Sample parameters - high dose ($5 \times 10^{14} \text{ cm}^{-2}$) and low dose ($1 \times 10^{13} \text{ cm}^{-2}$) selenium and silicon implants with and without high dose co-implants of Ga and As (to ensure the creation of an amorphous region) were employed, and hot (250°C) and room temperature implants were studied.

(b) Laser parameters and irradiation conditions - Pulsed laser radiation at wavelengths of .249 μm , .532 μm , .6943 μm and 1.064 μm , and cw laser radiation at wavelengths of .51 μm and 1.064 μm were used. Laser energy and power density were varied, and selected scan rates were employed for the cw experiments. Exposure of the ion-implanted region to 1.064 μm (cw and pulsed) radiation from the implanted side directly (frontside illumination) or following transmission through the single crystal substrate (backside illumination) was also conducted to assess the relative merits of initial heating at the crystal/amorphous interface.

Since we are primarily interested in the electronic properties of large area laser annealed materials the samples were evaluated by Van der Pauw/Hall effect measurements of 5mm x 5mm dice. Restoration of sample crystallinity in selected samples was determined by photo-acoustic spectroscopic techniques (13).

Experimental

The sample utilized in the present study consisted of semi-insulating Cr doped, GaAs (100) wafers which were implanted at 25°C or 250°C with either Si or Se. Both low dose ($1 \times 10^{13} \text{ Si/cm}^2$, 40 keV), ($1 \times 10^{13} \text{ Se/cm}^2$, 110 keV) and high dose ($5 \times 10^{14} \text{ Si/cm}^2$, 40 keV), ($5 \times 10^{14} \text{ Se/cm}^2$, 110 keV) single ion implants were prepared (all

25°C implants were high dose). In addition, samples made amorphous by co-implantation with Ga [$5 \times 10^{14} \text{ cm}^{-2}$, 100 keV (when co-implanted with Se), 85 keV (when co-implanted with Si)], and As [$5 \times 10^{14} \text{ cm}^{-2}$, 110 keV (when co-implanted with Se), 90 keV (when co-implanted with Si)] were also prepared. To facilitate the formation of ohmic contacts for electrical measurements, the low dose implanted samples also received contact implants of $5 \times 10^{14} \text{ cm}^{-2}$ Si or Se at the corners of the samples. The implanted GaAs wafers were then cleaved into 5mm x 5mm sample dice. The samples were not encapsulated.

A KrF excimer laser (.249 μm , 70 mJ/pulse, 25 nsec FWHM) was used for the uv laser annealing experiments. Samples from each implant group were irradiated at energy densities of 0.5, 0.7 and 0.9 J/cm² using ~40% spatial overlap of sequential pulses for complete coverage of the samples. Pulsed laser annealing at .6943 μm was conducted with an actively Q-switched, multimode ruby laser (pulsewidth: 20 nsec FWHM) with energy densities from 0.5 to 1.4 J/cm². The influence of substrate temperature on the electrical properties of the laser annealed samples was examined by irradiating high dose implants at 25°C, 250°C and 500°C.

A passively Q-switched Nd:YAG laser (1.064 μm , 15 nsec FWHM, TEM₀₀) permitted pulsed annealing at a wavelength for which the single crystal is transparent but the amorphous layer is absorbing. Two amplifier stages were employed to increase the output pulse energy to ~500 mJ. Although the annealing experiments were performed in the far field of the oscillator, spatial nonuniformity due to diffraction in the second amplifier persisted. It was necessary to spatially overlap pulses by 50% or more to alleviate this problem. Energy densities from ~.5 J/cm² to ~1 J/cm² were employed. In addition to irradiation of samples from the front (implanted) side, we examined the effect of irradiating the ion-implanted region from the backside (through the single crystal substrate). All samples were irradiated at room temperature. We also utilized 0.532 μm laser radiation in the present study. Radiation at this wavelength was generated by frequency doubling the Nd:YAG fundamental in a KD*P crystal. For some samples, a ground glass plate placed approximately 5mm from the sample was used to decrease spatial nonuniformities in the sample plane.

CW laser annealing experiments were performed at 0.51 μm and 1.064 μm with argon and Nd:YAG lasers respectively. The argon laser (TEM₀₀) operated on all visible lines with the primary output at 0.51 μm and 0.49 μm . The beam was mildly focused to ~1 mm diameter in the sample plane by a plano-convex lens, and the beam was scanned across the sample by galvanometer driven mirrors. The sample was mounted on a resistively heated vacuum chuck in a stream of forming gas.

The cw Nd:YAG laser used in the present experiments was a high average power, multimode (35 λ/d) source. The 160W output was attenuated to ~ 7 W by partially transmitting dielectric reflectors and focused by a cylindrical lens to a spot size of $\sim 6\mu\text{m} \times \sim 200\mu\text{m}$ in the sample plane. The sample was mounted on a resistively heated vacuum chuck which was scanned through the beam at a constant rate by means of a dc torque motor. As in the cw argon experiments, a forming gas atmosphere was employed during annealing.

Van der Pauw/Hall effect measurements were performed on samples following laser irradiation. For these preliminary studies electrical measurements were conducted on 5mm x 5mm x 0.5mm dice. An In-Ag-Ge alloy was used to make electrical contact at the ion-implanted contact pads located at the corners of the samples. Photoacoustic measurements were employed to determine the extent of sample recrystallization after annealing (13).

Results and Discussion

Electrical data for the pulsed and cw annealing experiments described above are summarized in Tables I and II for high dose ($5 \times 10^{14} \text{ cm}^{-2}$) Si and Se implants and co-implants of these ions with Ga and As. Results for only high dose implants are given because no apparent electrical activation was obtained for any of the low dose ($1 \times 10^{13} \text{ cm}^{-2}$) samples (crystalline or amorphous) which were irradiated with either the pulsed or cw lasers used in the present work.

As shown in Table I, apparent dopant activation after pulsed laser irradiation was $\leq 8\%$ for these samples. At the implant concentrations utilized in these experiments (peak $\sim 10^{20} \text{ cm}^{-3}$) degeneracy effects will limit the apparent activation to a few percent (unless substantial dopant redistribution occurs) when sheet carrier concentration measurements are used for determination of activated ion concentrations (14). The Hall electron mobility was consistently less than 400 $\text{cm}^2/\text{V-sec}$ for all samples annealed by the pulsed laser sources used in this study. Electron mobilities obtained for samples irradiated at 1.064 μm and .6943 μm are plotted as a function of energy density in Fig. 1. Although there is scatter in the data, improved annealing occurs as the laser energy density increases until the energy density exceeds $\sim 1 \text{ J/cm}^2$. Insufficient data were available for .249 μm or 0.532 μm irradiated samples to allow a photon flux dependence to be determined for those wavelengths. Other results and observations include: (a) there was not a marked dependence of electrical properties on substrate temperature utilized during pulsed ruby laser annealing; (b) very high sheet resistivities ($> 10^4 \Omega/\square$) were measured for all samples annealed with .249 μm radiation at power densities greater than 0.5 J/cm^2 , and spatial nonuniformities present in the 0.532 μm pulse precluded reproducible annealing at that wavelength; (c) exposure to

pulsed, 1.064 μm radiation from the back (single crystal) side was shown to be effective for activation of the high dose implants; (d) samples containing amorphous layers, created either by room temperature, high dose implantation of Si or Se or by co-implantation of hot implants of these ions with Ga and As, generally gave more reproducible electrical results after pulsed annealing than did samples which were not amorphous prior to annealing.

The restoration of crystallinity in amorphous samples which were annealed by pulsed laser radiation is evidenced by the photoacoustic measurements shown in Fig. 2. By using a probe laser at a wavelength which is absorbed by the amorphous layer but transmitted by the crystalline region (e.g. 1.064 μm), it is possible to monitor the effects of pulsed laser radiation on the sample by measuring the photoacoustic response of the sample before and after laser annealing. Figure 2 shows the result obtained when a Si-implanted ($5 \times 10^{14} \text{ cm}^{-2}$) GaAs sample is probed before and after ruby laser irradiation (.74 J/cm²). The change in the amplitude of the photoacoustic signal from the amorphous level to the single crystal level indicates that crystallinity has been restored by the pulsed laser radiation.

Best pulsed annealing results are obtained in GaAs for a narrow range of laser power densities, with optimum annealing occurring at power densities slightly less than the surface damage threshold (see Fig. 1). This result is contrasted by those obtained in ion-implanted silicon in which a wide range of power densities may be used for effective annealing. In order to access this narrow intensity "window" it is important to utilize a laser pulse which does not possess large intensity fluctuations across its spatial profile. The effect of intensity fluctuations on annealing characteristics is illustrated schematically in Fig. 3 for Si and GaAs. For pulsed laser annealing of ion-implanted Si the annealing range is sufficiently large to accommodate spatial variations in laser intensity, and relatively high electron mobilities over large areas may therefore be obtained. For GaAs, however, the effective annealing window is not large enough to accommodate the large intensity fluctuations, and damaged areas as well as unannealed areas are present after annealing. The presence of these regions will of course have a deleterious effect on the electrical properties of the implanted layers (11,12).

In addition to effects arising from spatial intensity variations, it is also possible that the low mobilities observed in pulsed laser annealed GaAs may be a direct consequence of the recrystallization mechanism operative in compound semiconductors. Creation of a transient molten region by rapid deposition of pulsed laser radiation may be accompanied by the evolution of arsenic from the sample (10). Subsequent crystallization with localized nonstoichiometric concentrations of Ga and As occurs in the lattice will generate vacancies which will adversely affect the electron mobility. It may be possible to overcome this arsenic deficiency problem by co-implantation

with excess arsenic prior to annealing.

The electrical characteristics of the samples annealed by cw argon and Nd:YAG laser radiation (see Table II) are significantly different from those obtained from the pulsed laser annealed samples. In particular, the Hall electron mobilities are much greater for the cw laser annealed samples. For example, for cw laser annealed samples containing Si implants, mobilities of $\sim 2000 \text{ cm}^2/\text{V-sec}$ have been obtained. In contrast, similar samples after pulsed laser annealing had mobilities $\leq 320 \text{ cm}^2/\text{V-sec}$. This increase in mobility by cw annealing is contrasted by a decrease in apparent dopant activation relative to the samples irradiated by the pulsed laser sources. A variety of cw laser power densities, sample scan rates, and substrate temperatures were employed in this study. As discussed in Refs. 7 and 11, slip lines and defect planes could be readily produced by the cw laser radiation. These, of course, have a detrimental effect upon the mobility, and conditions which would promote annealing of the ion-implanted layer without forming these irregularities were sought. The creation of large thermal gradients in the substrate was minimized by elevating the substrate temperature to $\sim 500^\circ\text{C}$ and subsequently performing the laser annealing experiments with low scan rates ($\sim 0.5 \text{ mm/sec}$) and relatively low power densities ($\leq 500 \text{ W/cm}^2$). At higher scan rates and concomitant higher power densities required for annealing, surface damage due to thermally induced stress was produced in the sample. Best results were obtained for power levels and scan rates slightly below those required for production of slip lines. As shown in the Table, these values were 0.5 mm/sec and $\sim 400 \text{ W/cm}^2$ at $0.51 \mu\text{m}$ and $250\text{--}500 \text{ W/cm}^2$ at $1.064 \mu\text{m}$ at a substrate temperature of $\sim 500^\circ\text{C}$. High mobilities were obtained by cw annealing of hot implants made amorphous by Ga and As implantation as well as single, hot implants in which the crystallinity of the implanted layer was retained. Unlike the pulsed laser results, backside irradiation of the samples with cw $1.064 \mu\text{m}$ radiation (0.5 mm/sec , 500 W/cm^2) was not effective for electrical activation and achievement of high mobilities. This may be due to the fact that at the substrate temperatures employed for these experiments the bandgap shifts significantly and may preclude the $1.064 \mu\text{m}$ radiation from penetrating sufficiently to the implanted layer.

Summary

We have examined the effects of pulsed and cw laser radiation on a variety of GaAs samples containing shallow implants ($\sim 1000\text{\AA}$) of low dose and high dose Si and Se ions. The dependence of electrical characteristics on parameters such as laser wavelength, power density, substrate temperature, and degree of crystallinity of the implanted layers were examined. The major results are listed below.

Pulsed laser: Apparent activation $\leq 8\%$ and Hall electron mobility $< 350 \text{ cm}^2/\text{V-sec}$ were obtained for high dose ($5 \times 10^{14} \text{ cm}^{-2}$) implants. No activation of low dose ($1 \times 10^{13} \text{ cm}^{-2}$) implants was observed. There was not a marked dependence of annealing (at $.5943 \mu\text{m}$) on substrate temperature. Both back and front side illumination at $1.064 \mu\text{m}$ was effective for electrical activation of high dose implants. Restoration of crystallinity in the implanted layers was quite good as measured by photoacoustic techniques.

cw laser: Mobilities of approximately $2000 \text{ cm}^2/\text{V-sec}$ were obtained for samples annealed by argon and Nd:YAG laser radiation. Scan rates of $\sim .5 \text{ mm/sec}$ and power densities $\leq 500 \text{ W/cm}^2$ were most effective for annealing both Si and Se high dose implants. Apparent activation was low ($\leq 1.2\%$) for high dose implants and was not obtained for low dose implants. High mobilities were obtained for both amorphous and crystalline implanted layers. An elevated substrate temperature ($\sim 500^\circ\text{C}$) was used to minimize the production of large thermal gradients during annealing.

The low mobilities obtained for the pulsed laser-annealed samples are interpreted in terms of nonuniform annealing due to spatial variations in the laser pulse intensity distribution, and generation of vacancies by nonstoichiometric regrowth following irradiation.

Acknowledgements

The authors gratefully acknowledge the assistance of B. A. Ambriz and B. M. Barrett with the electrical measurements and the cooperation of E. I. Moses and H. D. Stovall, who made available the cw Nd:YAG laser used in these experiments.

REFERENCES

1. V. V. Bolotov, N. B. Pridachin, and L. S. Smirnov, Sov. Phys. Semicond. 10, 338 (1976).
2. G. A. Kachurin, N. B. Pridachin, and L. S. Smirnov, Sov. Phys. Semicond. 9, 946 (1976).
3. J. A. Golovchenko and T. N. C. Venkatesan, Appl. Phys. Lett. 32, 147 (1978).
4. S. S. Kular, B. J. Sealy, K. G. Stephens, D. R. Chick, Q. V. Davis and J. Edwards, Electron. Lett. 14, 85 (1978).
5. B. J. Sealy, S. S. Kular, K. G. Stephens, R. Croft and A. Palmer, Electron. Lett. 14, 721 (1978).
6. R. Tsu, J. E. Baglin, G. J. Lasher, and J. C. Tsang, Appl. Phys Lett. 34, 153 (1979).
7. J. C. Fan, J. P. Donnelly, C. O. Bozler and R. L. Chapman, Inst. Phys. Conf. Ser. No. 45: ch. 6, 472, 1978).
8. E. Rimini, P. Baeri, and G. Foti, Phys. Lett. 65A, 153 (1978).
9. S. U. Campisano, I. Catalano, G. Foti, E. Rimini, F. Eisen and M. A. Nicolet, Sol. State Electron. 21, 485 (1978).
10. T. N. C. Venkatesan, D. H. Auston, J. A. Golovchenko and C. M. Surko, Appl. Phys. Lett. 35, 88 (1979).
11. C. L. Anderson, H. L. Dunlap, L. D. Hess and K. V. Vaidyanathan, AIP Conf. Proc. 50, 585 (1979).
12. J. L. Tandon, M. A. Nicolet, W. F. Tseng, F. H. Eisen, S. U. Campisano, G. Foti and E. Rimini, Appl. Phys. Lett, 34, 597 (1979).
13. R. A. McFarlane and L. D. Hess, submitted to Appl. Phys. Lett.
14. J. F. Gibbons and R. E. Tremaine, Jr., Appl. Phys. Lett. 20, 199 (1975).

TABLE I. Electrical characteristics of pulsed laser annealed GaAs. Implant ion: Si ($5 \times 10^{14} \text{ cm}^{-2}$, 40 keV), Se ($5 \times 10^{14} \text{ cm}^{-2}$, 110 keV) at 25°C and 250°C, no encapsulant, substrate temperature 25°C except where noted.

Laser	$\lambda (\mu\text{m})$	Energy Density (J/cm^2)/Substrate Temperature	Implant/ Implant Temperature	Sheet Resistivity (Ω/\square)	Hall Electron Mobility ($\text{cm}^2/\text{V-s}$)	Sheet Electron Concentration (cm^{-2})	Apparent Dopant Activation (%)
KrF	.249	0.5	Si+Ga+As (250°C)	1263	229	2.2×10^{13}	4.4
		0.5	Se+Ga+As (250°C)	5155	55	2.2×10^{13}	4.4
		0.5	Se (250°C)	6596	27	3.3×10^{13}	6.6
2x Nd:YAG	.532	0.60	Se+Ga+As (250°C)	4449	81	1.7×10^{13}	3.4
Ruby	.6943	0.8	Si (250°C)	727	271	3.2×10^{13}	6.4
		1.0	Si (25°C)	995	283	2.2×10^{13}	4.4
		1.4	Si (25°C)	6327	36	2.7×10^{13}	5.4
		0.9	Se (25°C)	1126	220	2.5×10^{13}	5.0
		0.7 (500°C)	Se (25°C)	1177	154	3.4×10^{13}	6.8
		0.9 (500°C)	Se (250°C)	866	292	2.5×10^{13}	5.0
		1.0 (250°C)	Se (250°C)	741	345	2.4×10^{13}	4.8
		0.5	Se+Ga+As (250°C)	1594	102	3.8×10^{13}	7.6
		0.7	Se+Ga+As (250°C)	1403	159	2.8×10^{13}	5.6
Nd:YAG	1.064	0.9	Si+Ga+As (250°C)	629	322	3.1×10^{13}	6.2
		0.7	Si+Ga+As (250°C)	1088	259	2.2×10^{13}	4.4
		0.5	Si+Ga+As (250°C)	3062	102	2.0×10^{13}	4.0
		0.7 (backside)	Si+Ga+As (250°C)	731	233	3.7×10^{13}	7.4
		0.5 (backside)	Se (25°C)	696	266	3.4×10^{13}	6.8

TABLE II. Electrical Characteristics of cw laser annealed GaAs Implant ion:
 Si ($5 \times 10^{14} \text{ cm}^{-2}$ 40 keV), Se ($5 \times 10^{14} \text{ cm}^{-2}$ 110 keV) at 250°C, no
 encapsulant, substrate temperature: 500°C, scan rate: 0.5 mm/sec

Laser	$\lambda (\mu\text{m})$	Power Density (W/cm ²)	Implant	Sheet Resistivity (Ω/\square)	Hall Electron Mobility (cm ² /V-sec)	Sheet Electron Concentration (cm ⁻²)	Apparent Dopant Activation (%)
Argon	0.51	390	Si	1012	2204	2.8×10^{12}	0.6
	0.51	430	Se	1284	1212	4.0×10^{12}	0.8
Nd:YAG	1.064	500	Se	623	1651	6.1×10^{12}	1.2
	1.064	500	Si	877	2081	3.4×10^{12}	0.7
	1.064	250	Si+Ga+As	1000	1910	3.3×10^{12}	0.7

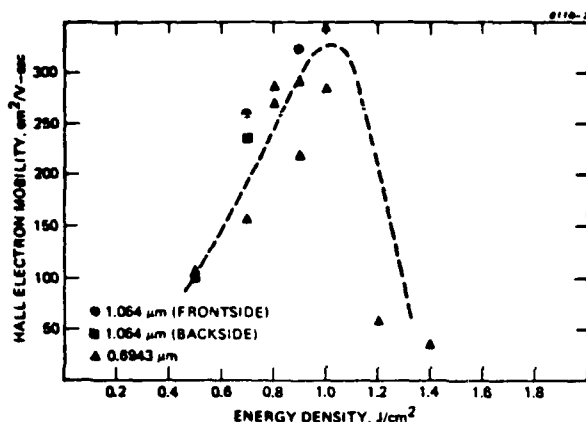


Figure 1.
Dependence of Hall electron mobility on laser energy density. All samples contained high dose ($5 \times 10^{14} \text{ cm}^{-2}$) Si or Se implants ($\sim 1000 \text{ \AA}$ depth). Sample damage occurred at $\sim 1.2 \text{ J/cm}^2$.

Figure 2.
Photoacoustic signals generated in silicon-implanted GaAs (40 keV, $5 \times 10^{14} \text{ cm}^{-2}$) before and after pulsed laser irradiation. The amplitude of the photoacoustic signal before laser irradiation indicates the amorphous nature of the implanted layer. The signal obtained after irradiation indicates that crystallinity has been achieved.

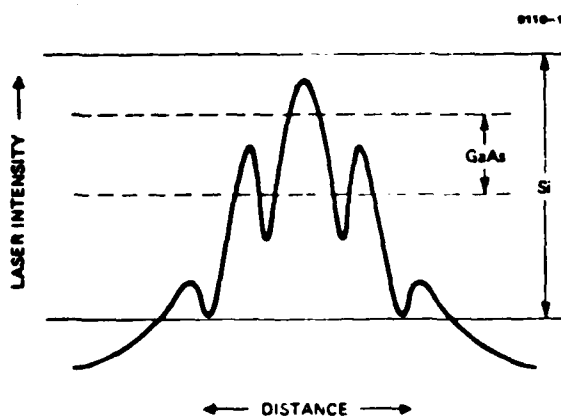
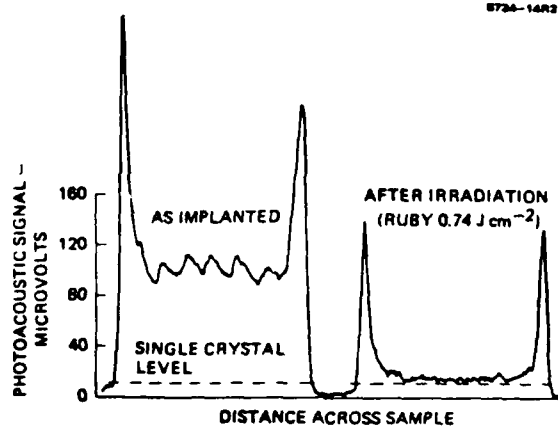


Figure 3.
Effect of spatial variations in laser intensity upon annealing of ion-implanted Si and GaAs. The large intensity window for effective annealing in Si is contrasted by the narrow window observed for GaAs. At laser intensities greater than those indicated by the upper limits for Si and GaAs, surface damage occurs. At intensities below the lower limits, the pulse does not anneal the sample.

SECTION 3.D

PULSED ELECTRON BEAM ANNEALING OF ION-IMPLANTED GaAs

(K. V. Vaidyanathan, C. L. Anderson, B. M. Barrett,
H. L. Dunlap, and L. D. Hess)

Presented at Electrochemical Society Meeting,
Los Angeles, CA, October 1979.

To be published in Proceedings of the Symposium
on Laser and Electron Beam Processing of Electronic
Materials, Electrochemical Society, 1980.

PULSED ELECTRON BEAM ANNEALING OF ION IMPLANTED GaAs

K. V. Vaidyanathan, C. L. Anderson, B. M. Barrett,
H. L. Dunlap and L. D. Hess
Hughes Research Laboratories
3011 Malibu Canyon Road
Malibu, CA 90265

The electrical properties of Si- Se- and Be-ion implanted GaAs layers annealed by a pulsed electron beam are reported. The presence of an amorphous layer formed by Ga and As co-implantation results in increased activation of low fluence ($1 \times 10^{13} \text{ cm}^{-2}$) Si and Se implanted GaAs. The electron mobility, however, is very low ($\sim 400 \text{ cm}^2\text{-V}^{-1}\text{-s}^{-1}$). High electrical activation is achieved in high fluence implanted layers which remain amorphous after implantation.

Introduction

Ion implantation followed by high temperature annealing has been widely used to form doped layers in GaAs device fabrication (1,2). To avoid surface dissociation of GaAs during the high temperature annealing, it is customary to encapsulate the samples with a dielectric layer (3). Problems with the adhesion of the dielectric to the surface of GaAs as well as in- and out-diffusion of the components of the dielectric and GaAs at the anneal temperatures can result in irreproducible activation of the implanted impurities (4,5). Localized heating of the implanted layers for short periods of time using intense laser and electron beams is potentially capable of overcoming some of the processing problems.

In this paper, we discuss the electrical properties of Se-, Si- and Be-implanted GaAs layers which have been subjected to pulsed electron beam annealing. The influence of the presence of an amorphous layer in the as implanted wafer on the electrical activation of implanted impurities is investigated. In this work such amorphous layers were introduced by co-implantation of Ga and As. The influence of the implantation temperature was also investigated.

*This work was supported in part by the Defense Advanced Research Projects Agency and monitored by the Office of Naval Research under contract N00014-78-C-0337.

Experimental

Samples from (100) Cr-doped semi-insulating GaAs ingots were implanted with either 260 keV Se, 100 keV Si or 35 keV Be. The samples were implanted to doses ranging from $1 \times 10^{13} \text{ cm}^{-2}$ to $1 \times 10^{15} \text{ cm}^{-2}$. To investigate the influence of an amorphous layer on pulsed electron beam annealing, some of the samples also received 250 keV As and 230 keV Ga implants to fluences of $5 \times 10^{14} \text{ cm}^{-2}$. In the case of high fluence ($1 \times 10^{15} \text{ cm}^{-2}$) Se^+ implants, the effect of implant temperature was investigated by performing the implants at $\sim 250^\circ\text{C}$ and $\sim 250^\circ\text{C}$. All other implants were performed at $\sim 25^\circ\text{C}$. In all cases, the samples were tilted at $\sim 7^\circ$ relative to the incident ion beam to avoid channeling effects. Square ($\sim 4 \text{ mm} \times 4 \text{ mm}$) Hall specimens from the implanted and annealed wafers were prepared by making ohmic contacts at the corners using an In:Ag:Ge alloy.

Pulsed electron beam annealing of the samples was accomplished using the SPI-PULSE 6000 system at Spire Corporation. The average electron energy of the beam was 12 keV. Because of the small geometry of the samples used, edge effects play a strong role and affect the incident energy density. Accurate determination of the incident energy fluence was therefore precluded. The charging voltage applied to the cylindrical capacitor was used instead as a monitor of the energy fluence. The anode-cathode geometry used in these experiments produces a beam referred to by the personnel at SPIRE Corporation as beam 3a. The approximate energy fluence delivered by the uniform region of the beam into a large sample is given in Table I as a function of charging voltage.

Results and Discussion

For many GaAs device applications, it is necessary to be able to activate low fluence implants ($1 \times 10^{13} \text{ cm}^{-2}$ or less). Also, the electron mobility in the implanted layers should be high. Previous studies have indicated that with both laser and pulsed electron beam annealing, low influence implants cannot be activated. However, high fluence implants have been pulse electron beam annealed with high apparent electrical activation. The presence of the amorphous layer is generally believed to enhance coupling of the incident energy to the lattice (6). To test this hypothesis, some samples were co-implanted with Ga and As to a total fluence of $1 \times 10^{15} \text{ cm}^{-2}$. The electrical properties of low fluence implanted and annealed samples are summarized in Table II.

As can be seen from Table 2, no electrical activation was obtained from samples implanted to low fluences without co-implants. In the case of samples co-implanted with Ga and As and made amorphous, however, apparent activation of $\sim 35\%$ and $\sim 54\%$ were obtained from Se- and Si-implanted samples, respectively. The

measured mobilities, however, were extremely poor, indicating that the layers were heavily compensated.

The electrical properties of samples implanted with Se and electron beam annealed are shown in Figures 1, 2 and 3. In the case of samples implanted to a fluence of $1 \times 10^{14} \text{ cm}^{-2}$, an apparent activation of $\sim 20\%$ with mobility of $\sim 1,000 \text{ cm}^2 \text{ V}^{-1} \text{ s}^{-1}$ was obtained in the range of the e-beam energy densities studied. At high energy densities, both the activation and mobility dropped rapidly. In the case of $5 \times 10^{14} \text{ cm}^{-2}$ and $1 \times 10^{15} \text{ cm}^{-2}$ implanted samples, electrical activation of $\sim 35\%$ and $\sim 25\%$ with mobilities of $\sim 900 \text{ cm}^2 \text{ V}^{-1} \text{ s}^{-1}$ and $\sim 400 \text{ cm}^2 \text{ V}^{-1} \text{ s}^{-1}$, respectively, were obtained. In all these cases, no increased activation was observed in samples which also received the co-implants. This result is not entirely surprising since even at the lowest fluence used ($1 \times 10^{14} \text{ cm}^{-2}$), Se causes sufficient damage to form an amorphous layer at the surface. The extremely high activation observed in $5 \times 10^{14} \text{ cm}^{-2}$ and $1 \times 10^{15} \text{ cm}^{-2}$ is worth noting. Such high activation is generally not attainable with conventional thermal annealing. The data in Figure 3 indicate that implanting at 250°C results in lower activation and lower mobility compared to room temperature implants. This evidence further substantiates the idea that the presence of an amorphous layer results in increased electrical activation by pulsed electron beam annealing (PEBA).

The results from Si implanted and annealed GaAs layers are shown in Figures 4 and 5. In the case of samples implanted to a fluence of $1 \times 10^{15} \text{ cm}^{-2}$, a sheet carrier concentration of $\sim 5 \times 10^{12} \text{ cm}^{-2}$ was obtained following annealing at a charging voltage of $\sim 160 \text{ keV}$. In samples which were co-implanted with Ga and As, however, sheet carrier concentrations of $2.5 \times 10^{13} \text{ cm}^{-2}$ and mobilities of $\sim 1000 \text{ cm}^2 \text{ V}^{-1} \text{ s}^{-1}$ were measured. This dramatic increase in activation further substantiates our earlier conclusion that the presence of an amorphous layer results in increased activation following PEBA. In the case of samples implanted to a fluence of $5 \times 10^{14} \text{ cm}^{-2}$, sheet carrier concentrations of $\sim 1 \times 10^{14} \text{ cm}^{-2}$ and mobilities of $1000 \text{ cm}^2 \text{ V}^{-1} \text{ s}^{-1}$ were obtained. A slight increase in activation was observed in co-implanted samples. Sheet carrier concentrations of $\sim 1.6 \times 10^{14} \text{ cm}^{-2}$ and mobilities of $\sim 320 \text{ cm}^2 \text{ V}^{-1} \text{ s}^{-1}$ were measured in samples implanted to a fluence of $1 \times 10^{15} \text{ cm}^{-2}$ and electron beam annealed. At this fluence, no significant differences between the Si implanted and co-implanted samples were observed.

Figure 6 shows the results from samples implanted with Ga, As and $1 \times 10^{15} \text{ cm}^{-2}$ Be and electron beam annealed. Sheet hole concentrations of $\sim 4 \times 10^{14} \text{ cm}^{-2}$ and hole mobilities $\sim 50 \text{ cm}^2 \text{ V}^{-1} \text{ s}^{-1}$ were obtained. Extremely poor activation was observed from low fluence ($1 \times 10^{13} \text{ cm}^{-2}$) Be-implanted samples.

Conclusions

The following conclusions can be drawn from this study.

- (1) There is a narrow range of pulsed electron energy fluence over which effective annealing can occur. In our case, this range was found to occur between charging voltages of 140 and 160 keV (See Table 1).
- (2) The presence of an amorphous layer helps in increasing the apparent electrical activation of low fluence implants in GaAs. The mobility in the implanted layers, however, is poor.
- (3) Very high activation and reasonable carrier mobilities can be obtained in high fluence implanted samples following electron beam annealing.

REFERENCES

1. R. G. Hunsperger and N. Hirsch, Solid State Electronics 18, 349 (1975).
2. J. A. Higgins, B. M. Welch, F. H. Eisen and G. D. Robinson, Electronic Letters 12, 18 (1976).
3. J. P. Donnelly, Inst. Phys. Conf. Ser. No. 33(b) 167 (1977) and references therein.
4. J. Gyulai, J. W. Mayer, I. V. Mitchell and V. Rodriguez, Appl. Phys. Lett., 17, 332 (1970).
5. K. V. Vaidyanathan, M. J. Helix, D. J. Welford, B. G. Streetman, R. J. Blattner and C. A. Evans, Jr., J. Electrochem. Soc. 124, 1783 (1977).
6. J. L. Tandon and F. H. Eisen, AIP Conf. Proc. 50, 616 (1979).

TABLE I. Approximate Energy Fluence Delivered by
SPI-PULSE 6000 Beam 3a into
Large Area Sample*

Charging Voltage (kV)	Fluence per Pulse (J-cm ⁻²)
140	no data
145	no data
150	.33
155	.36
160	.39
165	.43
170	.47

*Prepared from Graphical data furnished by SPIRE
Corporation

TABLE II. Electrical Properties of Low Fluence Implanted and Electron Beam Annealed GaAs

Implanted Impurity	Dose (cm ⁻²)	Charging Voltage (kV)	Sheet Resistivity Ω/\square	Electron Mobility cm ² V ⁻¹ s ⁻¹	Sheet Electron Concentration (cm ⁻²)
Se	1 x 10 ¹³	155	2.11 x 10 ⁹	30	9.5 x 10 ⁷
Se	1 x 10 ¹³				
+Ga	5 x 10 ¹⁴	155	4500	400	3.45 x 10 ¹²
+As	5 x 10 ¹⁴				
Si	1 x 10 ¹³	160	2.85 x 10 ⁹	1300	1.7 x 10 ⁶
Si	1 x 10 ¹³				
+Ga	5 x 10 ¹⁴	155	1990	590	5.4 x 10 ¹²
+As	5 x 10 ¹⁴				

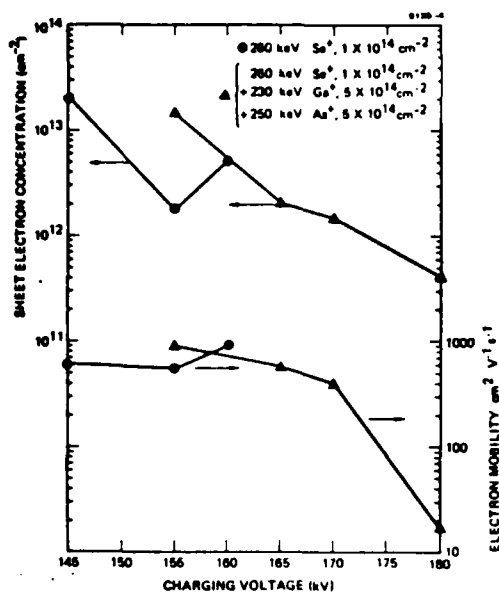


Figure 1.
Sheet electron concentration and mobility as a function of charging voltage in electron beam annealed Se-implanted GaAs.

Figure 2.
Variation of sheet electron concentration and mobility as a function of the charging voltage in e-beam annealed GaAs:Se.

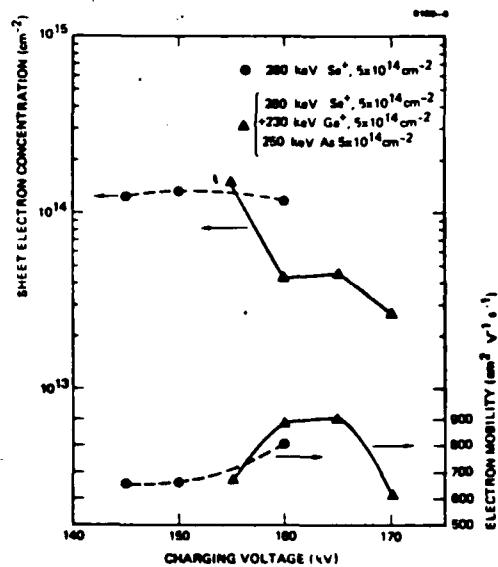
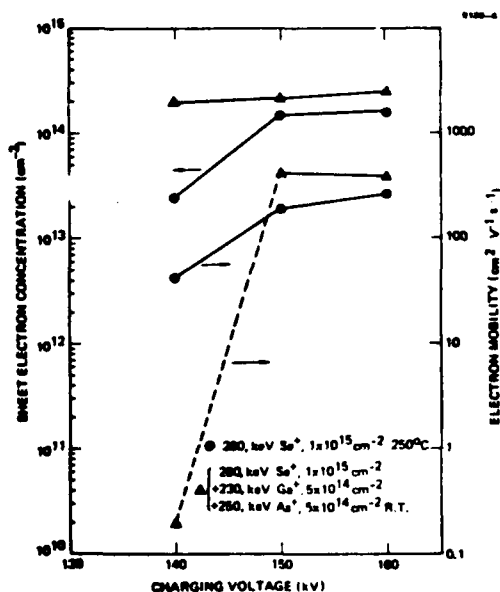


Figure 3.
Sheet electron concentration and mobility as a function of charging voltage in electron beam annealed Se-implanted GaAs.

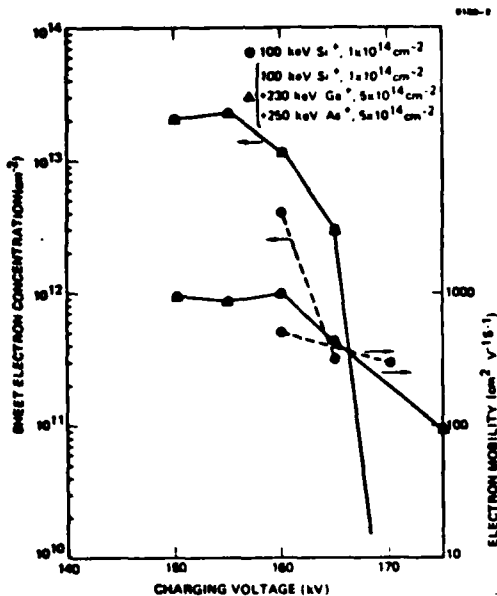


Figure 5. Sheet electron concentration and mobility as a function of charging voltage e-beam annealed, Si-implanted GaAs.

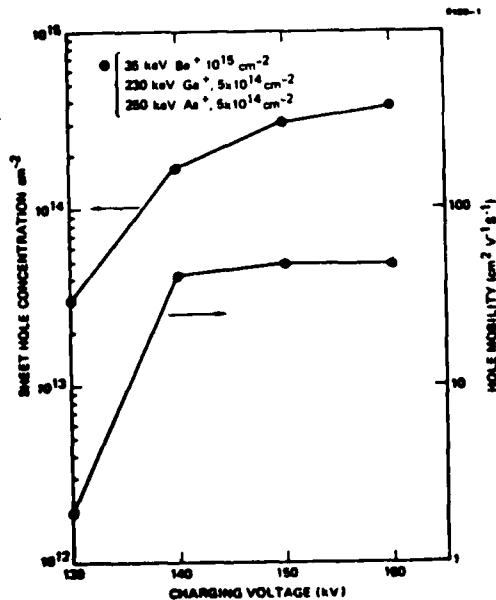


Figure 4. Variation of sheet electron concentration and mobility as a function of charging voltage in electron beam annealed Si-implanted GaAs.

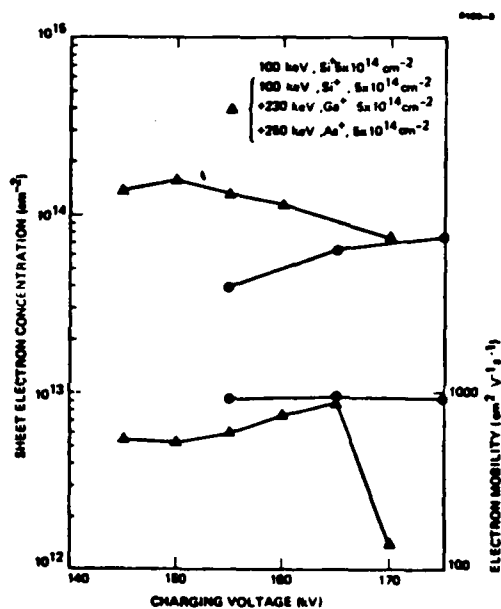


Figure 6. Sheet hole concentration and mobility as a function of charging voltage in Be-implanted, pulsed electron beam annealed GaAs.

SECTION 3.E

ANNEALING OF IMPLANTED LAYERS IN COMPOUND
SEMICONDUCTORS BY LOCALIZED BEAM HEATING
TECHNIQUES

(C. L. Anderson, H. L. Dunlap, L. D. Hess,
G. L. Olson, and K. V. Vaidyanathan)

Presented at the Materials Research Society
Meeting, Cambridge, MA, November-December 1979

To be published in Laser-Solid Interactions
and Laser Processing - 1979, American Institute
of Physics, 1980.

ANNEALING OF IMPLANTED LAYERS
IN COMPOUND SEMICONDUCTORS BY LOCALIZED
BEAM HEATING TECHNIQUES

C. Lawrence Anderson, H. L. Dunlap, L. D. Hess,
G. L. Olson and K. V. Vaidyanathan
Hughes Research Laboratories
Malibu, California

A comparative study of the transient annealing of Si- and Se-implanted GaAs has been performed using pulsed and CW lasers and pulsed electron beams. Both low (10^{13} cm^{-2}) and high ($5 \times 10^{14} \text{ cm}^{-2}$) implant fluences were studied. Activation of low fluence implants was achieved only in electron beam annealed samples co-implanted with Ga and As. Pulsed laser annealing yielded layers with low electron mobilities ($< 350 \text{ cm}^2 \text{ V}^{-1} \text{ s}^{-1}$) and apparent dopant activation of 4 to 7%. Much higher mobilities ($\sim 2000 \text{ cm}^2 \text{ V}^{-1} \text{ s}^{-1}$) and lower activation were observed in cw laser annealed samples. Pulsed electron beam annealing produced the highest apparent dopant activation (20-35%) and intermediate mobilities ($900\text{-}1000 \text{ cm}^2 \text{ V}^{-1} \text{ s}^{-1}$). Some possible explanations for the differences observed between the various types of annealing are discussed.

I. INTRODUCTION

High temperature annealing using dielectric encapsulants is widely used for the annealing of ion implantation damage in GaAs. Problems such as poor adhesion of the encapsulant and in- and out-diffusion of the components of the dielectric and the substrate (1,2) have resulted in the development of a variety of encapsulant-free thermal annealing techniques (3-6). Recently, there has been considerable interest in the transient annealing of GaAs using localized beam heating techniques such as laser (7-19) and electron beam annealing (20-21). We have been performing a systematic study of laser annealing of ion implanted GaAs using six different lasers. We have recently reported the results of a preliminary investigation of pulsed electron beam annealing (PEBA) of implanted GaAs (20). In this paper we present a comparison of the results obtained at our laboratory from comparable samples annealed using three principal transient annealing techniques: pulsed laser annealing (PLA), cw laser annealing (CWLA), and pulsed electron beam annealing (PEBA). This paper represents the first direct comparison of the three types of annealing as applied to ion implanted GaAs.

II. EXPERIMENTAL

Samples of Cr-doped (100) oriented semi-insulating GaAs were implanted at 250°C or 250°C with either Si or Se. Implant energies of 40 and 110 keV were used for Si and Se, respectively, for samples to be annealed by PLA or CWLA. These energies placed essentially all the dopant atoms within one optical absorption length of the surface for the visible lasers employed. Samples for PEBA annealing were implanted with 110 keV Si or 260 keV Se at 25°C. To investigate the influence of a very heavily damaged layer on annealing behavior, some samples were co-implanted with $5 \times 10^{14} \text{ cm}^{-2}$ As at energies at which the projected range of the Ga and As implants matched that of the dopant implants. PLA was performed at four wavelengths. A KrF excimer laser (0.249 μm , 70 mJ/pulse, 25 ns FWHM) was used for the uv laser annealing experiments. PLA at 0.6943 μm was conducted with an actively Q-switched, multimode ruby laser (20 ns FWHM). The influence of substrate temperature on the electrical properties of the laser annealed samples was examined by irradiating high dose implants at 25°C, 250°C and 500°C.

A passively Q-switched Nd:YAG laser with two amplifier stages (1.064 μm , 15 ns FWHM, TEM_{00}) permitted PLA at a wavelength at which crystalline GaAs is transparent but heavily damaged GaAs is absorbing. Both front side and backside illumination were used at this wavelength. Fifty percent pulse overlap was employed to alleviate problems due to spatial nonuniformities in the laser output. We also evaluated annealing using 0.532 μm radiation by frequency doubling the output of this laser.

CWLA experiments were performed at 0.51 μm and 1.064 μm with argon and Nd:YAG lasers, respectively. The argon laser (TEM_{00}) operated on all visible lines with the primary output at 0.51 μm and 0.49 μm . The beam was mildly focused to 1 mm diameter by a plano-convex lens, and the beam was scanned across the sample by galvanometer driven mirrors. The sample was mounted on a resistively heated vacuum chuck in a stream of forming gas.

The cw Nd:YAG laser used in the present experiment was a 160 W, multimode (35 λ/d) source, attenuated to ~ 7 W by partially transmitting dielectric reflectors and focused by a cylindrical lens to a spot size of 6 μm x 200 μm . The sample was mounted in a forming gas atmosphere on a resistively heated vacuum chuck which was scanned through the beam at a constant rate by means of a dc torque motor.

III. RESULTS AND DISCUSSIONS

The best electrical data obtained from the pulsed and CW laser annealing experiments described above are summarized in Table I for high dose ($5 \times 10^{14} \text{ cm}^{-2}$) Si and Se implants and co-implants of these ions with Ga and As. No apparent electrical activation was obtained for any of the laser annealed low dose ($1 \times 10^{13} \text{ cm}^{-2}$) samples.

Table I. Best Results Obtained from Laser Annealing of Ion Implanted GaAs

Implant Fluence: $5 \times 10^{14} \text{ cm}^{-2}$ of each ion (energies in text)

Implant Temperature: 250°C unless noted

Substrate Temperature During Anneal: 25°C unless noted (PLA), 500°C (CWLA)

Wavelengths: Argon ($0.51 \mu\text{m}$), Ruby ($0.6943 \mu\text{m}$), Nd:YAG ($1.064 \mu\text{m}$)

Implant	Laser	Pulsed/cw	Energy or Power Density ^a (Substrate Temperature)	Sheet Electron Concentration (10^{13} cm^{-2})	Hall Electron Mobility ($\text{cm}^2 \text{ V}^{-1} \text{ s}^{-1}$)
Si	Ruby	Pulsed	0.9	3.2	271
Si(250°C)		"	1.0	2.2	283
Si+Ga+As	Nd:YAG	"	0.9	3.1	322
		"	0.7 ^b	3.7	233
Se	Ruby	"	0.9 (500°C)	2.5	292
		"	0.7 (250°C)	2.4	345
Se(250°C)	Nd:YAG	"	0.5 ^b	3.4	266
Si	Argon	cw	390	0.28	2204
	Nd:YAG	"	500	0.34	2081
Si+Ga+As	Nd:YAG	"	250	0.33	1910
Se	Argon	"	430	0.40	1212
	Nd:YAG	"	500	0.61	1651

^a J cm^{-2} for pulsed lasers; W cm^{-2} for cw lasers

^b Backside illumination

As shown in Table I, apparent dopant activation after PLA was <8%. At the implant concentration utilized in these experiments, degeneracy effects will limit the apparent activation to a few percent (unless substantial dopant redistribution occurs) when sheet carrier concentration measurements are used for determination of activation (22). The Hall electron mobility was less than 400 cm²/V-s for all PLA samples. Electron mobilities obtained for samples irradiated at 1.064 μ m and 0.6943 μ m are plotted as a function of energy density in Figure 1. Although there is scatter in the data, improved annealing occurs as the laser energy density increases until the energy density exceeds 1 J/cm².

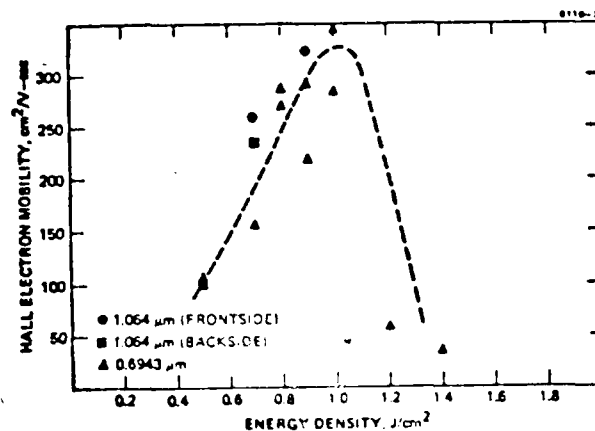


FIGURE 1. Dependence of Hall electron mobility on laser energy density. All samples contained high dose (5×10^{14} cm⁻²) Si or Se implants (~ 1000 Å depth). Sample damage occurred at ~ 1.2 J/cm².

It is apparent that the best PLA results are obtained for a narrow range of laser power densities, with optimum annealing occurring at power densities slightly below the surface damage threshold. In order to exploit this narrow intensity "window," it is important to utilize a laser pulse which does not possess large intensity fluctuations across its spatial profile.

The Hall electron mobilities are much greater for the CWLA samples. In our experiments this increase in mobility by CWLA is contrasted by a decrease in apparent dopant activation relative to the PLA samples. As discussed in References 13 and 17, slip lines and defect planes could be readily produced by the CW laser radiation. Laser-induced thermal gradients in the substrate were minimized by elevating the substrate temperature to 500°C and performing the laser annealing

experiments with low scan rates (0.5 mm/s) and relatively low power densities ($<500 \text{ W/cm}^2$). Best results were obtained for power levels and scan rates slightly below those required for production of slip lines.

Pulsed electron beam annealing (PEBA) was performed using the SPI-PULSE 6000 system at Spire Corporation, Bedford, MA. The anode-cathode geometry used produces a beam referred to by Spire personnel as beam 3a. It exhibits a small region (about 2 cm diameter) of very good uniformity. The pulse length is about 100 ns, and the average electron energy is about 12 keV. Because small samples were used, edge effects play a strong role and affect the incident energy density. The energy fluence delivered by the uniform area of the beam into a large sample can be approximated by $[0.33 + 0.007 (V_c - 150)] \text{ J cm}^{-2}$ where V_c is the charging voltage in kV.

In the case of low fluence implants, PEBA resulted in apparent activation of 35% and 54% of the implanted Se and Si, respectively, when the dopants were co-implanted with Ga and As. The corresponding mobilities were 400 and $590 \text{ cm}^2 \text{ V}^{-1} \text{ s}^{-1}$. Comparable samples prepared without co-implants exhibited sheet resistivities in excess of 10^9 ohms per square.

The electrical properties of high-fluence implants are presented in Figures 2 and 3. In the case of Se implants, the best results were obtained from samples without co-implants. The purpose of the co-implant is to produce a heavily damaged layer, which improves the coupling of the annealing pulse to the crystal lattice (21). The Se ion is sufficiently massive that at this implant fluence a very heavily damaged layer is produced by the dopant implant itself. Apparent electrical activities as high as 35% and mobilities as high as $900 \text{ cm}^2 \text{ V}^{-1} \text{ s}^{-1}$ were achieved. Somewhat higher activations with lower mobilities have been recently reported by Inada and coworkers (23). Such high activation is generally not achievable by thermal annealing at this fluence.

In the case of Si-implanted high fluence samples, apparent electrical activities of ~20% and mobilities of $1000 \text{ cm}^2 \text{ V}^{-1} \text{ s}^{-1}$ were achieved. Co-implantation significantly improved the electrical activation of the impurities. Co-implantation has more dramatic effects at lower fluences and little or no effect at fluences of 10^{15} cm^{-2} (20).

Although this paper has concentrated on the n-type dopants Si and Se, it is worth noting that 40% apparent activation of the p-type dopant Be and hole mobilities of $50 \text{ cm}^2 \text{ V}^{-1} \text{ s}^{-1}$ can be obtained by PEBA of samples co-implanted with Ga and As (20).

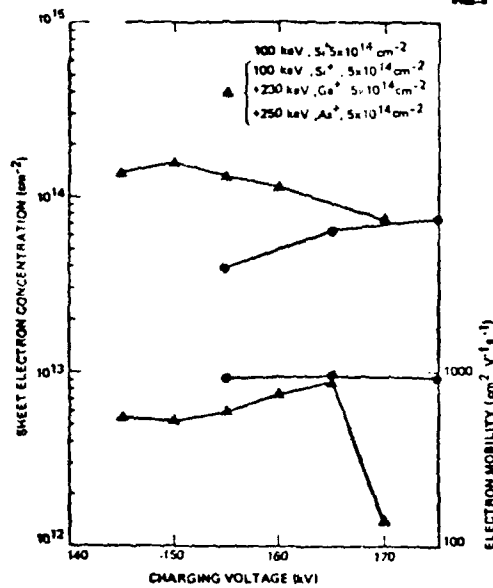
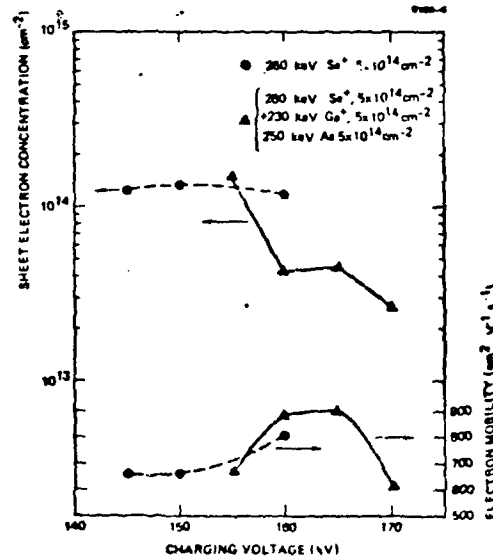


FIGURE 2. Variation of sheet electron concentration and mobility as a function of the charging voltage in e-beam annealed GaAs:Se.

FIGURE 3. Sheet electron concentration and mobility as a function of charging voltage e-beam annealed, Si-implanted GaAs.



Both PLA and PEBA resulted in layers with electron mobilities substantially below those achieved by CWLA. This may be a consequence of high spatial intensity fluctuations and acoustic shock effects. It is also possible that the low mobilities observed in pulse annealed GaAs may be a direct consequence of the recrystallization mechanism operative in compound semiconductors. Creation of a transient molten region by rapid deposition of pulsed laser radiation may be accompanied by evolution of arsenic from the sample (16, 24). Subsequent crystallization with localized nonstoichiometric regions in the lattice will generate defects which adversely affect the electron mobility. It may be possible to overcome this arsenic deficiency problem by co-implantation of As alone. Even if gross stoichiometry is maintained, however, the rapid solidification of molten GaAs resulting from pulse annealing may still produce considerable concentrations of antistructural defects (e.g., Ga_{As} and As_{Ga}) and regions of local nonstoichiometry, which cannot occur in elemental materials.

The most promising results presented here are those resulting from CWLA, in which high mobilities have been achieved. It is interesting to speculate why we have observed such low electrical activations, when Fan and coworkers have reported activations of 30% for 400 keV, 10^{14} cm^{-2} Se implants using a Nd:YAG laser focused through a cylindrical lens (13). One factor may be the higher implant energy used in their work. Because the $1.064 \mu\text{m}$ radiation is preferentially absorbed in the damaged region, the wider, deeper damaged region in their samples probably produces lower thermal gradients for comparable annealing conditions. Additionally, the characteristics of the Nd:YAG laser used in their work may have been a factor in achieving high activation. We are optimistic over the prospects for localized annealing of implanted GaAs by cw laser methods. Continuous electron beam annealing may also offer a similar promise, since both techniques allow slower, steady state regrowth during annealing which may be critical in achieving stoichiometric regrowth of compound semiconductors.

ACKNOWLEDGEMENT

The authors gratefully acknowledge the assistance of B. A. Ambriz and B. M. Barrett with the electrical measurements, the technical assistance of L. M. Lewis, and the cooperation of E. I. Moses and H. D. Stovall, who made available the cw Nd:YAG laser used in these experiments.

This work was supported in part by the Defense Advanced Research Projects Agency and monitored by the office of Naval Research under contract N00014-78-0-0337.

REFERENCES

1. J. Gyulai, J. W. Mayer, I. V. Mitchell and V. Rodriguez, Appl. Phys. Lett., 17, 332 (1970).
2. K. V. Vaidyanathan, M. J. Helix, D. J. Wolfrod, B. G. Streetman, R. J. Blattner and C. A. Evans, Jr., J. Electrochem. Soc. 124, 1783 (1977).
3. R. M. Malbon, D. H. Lee and J. M. Whelan, J. Electrochem. Soc. 123, 1413 (1976).
4. A. A. Immorlica and F. H. Eisen, Appl. Phys. Letts. 29, 94 (1976).
5. C. L. Anderson, K. V. Vaidyanathan, H. L. Dunlap and G. S. Kamath, to be published in J. Electrochem. Soc.
6. J. Kasahara, M. Arai and N. Watanabe, J. Electrochem. Soc., 126, 1997 (1979).
7. V. V. Bolotov, N. B. Pridachin and L. S. Smirnov, Sov. Phys. Semicond. 10, 338 (1976).
8. G. A. Kachurin, N. B. Pridachin and L. S. Smirnov, Sov. Phys. Semicond. 9, 946 (1976).
9. J. A. Golovchenko and T. N. C. Venkatesan, Appl. Phys. Lett. 32, 147 (1978).
10. S. S. Kular, B. J. Sealy, K. G. Stephens, D. R. Chick, Q. V. Davis and J. Edwards, Electron. Lett. 14, 85 (1978).
11. B. J. Sealy, S. S. Kular, K. G. Stephens, R. Croft and A. Palmer, Electron. Lett. 14, 721 (1978).
12. R. Tsu, J. E. Baglin, G. J. Lasher and J. C. Tsang, Appl. Phys. Lett. 34, 153 (1979).
13. J. C. Fan, J. P. Donnelly, C. O. Bozler and R. L. Chapman, Inst. Phys. Conf. Ser. No. 45: ch. 6, 427, (1978).
14. E. Rimini, P. Baeri and G. Foti, Phys. Lett. 65A, 153 (1978).
15. S. U. Campisano, I. Catalano, G. Foti, E. Rimini, F. Eisen and M. A. Nic, Sol. St. Electron. 21, 485 (1978).
16. T. N. C Venkatesan, D. H. Auston, J. A. Golovchenko and C. M. Surio, Appl. Phys. Lett. 35, 88 (1979).
17. C. L. Anderson, H. L. Dunlap, L. D. Hess and K. V. Vaidyanathan, AIP Conf. Proc. 50, 585 (1979).
18. J. L. Tandon, M. A. Nicolet, W. F. Tseng, F. H. Eisen, S. U. Campisano, G. Foti and E. Rimini, Appl. Phys. Lett., 34, 597 (1979).
19. G. L. Olson, C. L. Anderson, H. L. Dunlap, L. D. Hess and R. A. McFarlane, "Laser Annealing of Ion-Implanted Gallium Arsenide," in Proceedings of the Symposium on Laser and Electron Beam Processing of Electronic Materials,

- C. L. Anderson, G. K. Celler and G. A. Rozgoni, eds., Los Angeles, 1979, to be published by the Electrochemical Society.
20. K. V. Vaidyanathan, C. L. Anderson, B. M. Barrett, H. L. Dunlap and L. D. Hess, "Pulsed Electron Beam Annealing of Ion Implanted GaAs," in C. L. Anderson, G. K. Celler and G. A. Rozgoni, eds., op cit.
 21. J. L. Tandon and F. H. Eisen, AIP Conf. Proc. 50, 616 (1979).
 22. J. F. Gibbons and R. E. Tremaine, Jr., Appl. Phys. Lett. 20, 199 (1974).
 23. R. Tsu, J. E. Baglin, G. J. Lasker and J. C. Tsang, AIP Conf. Proc. 50, 623 (1979).
 24. T. Inada, K. Tokunaga and S. Taka, Appl. Phys. Letts. 35, 546 (1979).

SECTION 4

ANNEALING OF OHMIC CONTACTS TO GaAs BY LASER AND ELECTRON BEAMS

During this program, we systematically investigated the transient annealing of Au:Ge-based Ohmic contacts to GaAs. These studies demonstrated the potential superiority of laser-annealed Ohmic contacts relative to thermally annealed contacts from the point of view of contact resistance, edge definition, and metallurgical properties. GaAs microwave transistors using laser-annealed Ohmic contacts were fabricated in our preliminary studies and found to compare favorably in microwave performance to devices fabricated conventionally.

Our initial investigations emphasized a qualitative evaluation of the results obtained by annealing Au-Ge-based contacts with a variety of lasers. A published paper summarizing these results is reproduced as Section 4.A.

Microwave transistor fabrication employing laser-annealed contacts was performed using the knowledge gained from these studies. The results obtained from these first-generation laser-annealed transistors are presented in Section 4.B.

After the completion of the contract period, our investigations were continued under Hughes internal funding. Highly promising results were obtained using In-Au:Ge contacts. A published paper summarizing these results is presented as Section 4.C.

An overview of our results in the area of transient annealing of Ohmic contacts to GaAs, including some internally funded work on pulsed-electron-beam annealing, was presented as an invited talk at the Materials Research Society Meeting, Boston, MA, November 1979. This paper, submitted for publication, is reproduced as Section 4.D and provides an excellent summary of our work and its relationship to the state of the art.

SECTION 4.A

LASER-ANNEALED OHMIC CONTACTS FOR GaAs MICROWAVE
DEVICES

(G. Eckhardt, C. L. Anderson, L. D. Hess, and
(C. F. Krumm)

Presented at Materials Research Society Meeting,
Boston, MA, November 1978.

Published in Laser-Solid Interactions and
Laser Processing - 1978 (AIP Conf. Proc. 50,
641 (1979)).

LASER-ANNEALED OHMIC CONTACTS FOR GaAs MICROWAVE DEVICES*

G. Eckhardt, C. L. Anderson, L. D. Hess, and C. F. Krumm
Hughes Research Laboratories, Malibu, CA 90265

ABSTRACT

We have produced ohmic contacts of excellent electrical and morphological quality on GaAs by means of laser-induced annealing. A systematic investigation was conducted of the effects of different metal combinations, substrates and laser parameters on the quality of ohmic contacts formed by the laser technique. Using a scanning cw argon laser we have successfully annealed contacts for a number of 1- μ m gate microwave FETs. The I-V characteristics of the contacts, as well as the dc performance of the finished devices, compare very favorably with thermally annealed control samples. It is noteworthy that the surface morphology of the laser-annealed contacts is far superior to those formed by conventional techniques.

INTRODUCTION

The performance of almost all GaAs devices (e.g., lasers, solar cells, IMPATT diodes and FETs) is critically dependent on the quality and reliability of their ohmic contacts. For example, microwave FETs require the lowest possible contact resistance to achieve minimum noise figure and maximum gain. Reliability of ohmic contacts for GaAs devices is also a subject of continuing concern because recent reliability investigations^{1,2} have shown that degradation of ohmic contacts can cause failure of GaAs FETs.

Many of the problems associated with conventional contact formation result from the requirement of subjecting the entire device to the alloying temperature of the metallization systems. The technique of laser-annealing for contact formation, which was introduced several years ago,³ holds the promise of remedying some of the problems inherent with thermal alloying such as incomplete wetting between contact metals and GaAs and in-diffusion of contact constituents. With this novel technique only a selected localized region of the semiconductor undergoes a significant transient temperature excursion. Contacts can, therefore, be produced while exercising considerable control over the size of the heated surface region, the penetration depth of the heat pulse, and the peak temperature reached.

In this study we have explored the experimental conditions and potential advantages of laser processing for ohmic contact formation for GaAs microwave devices by systematically varying material and laser parameters and investigating their influence on contact quality.

*This work was supported in part by Office of Naval Research Contract N00014-78-C-0337 under Defense Advanced Research Projects Agency Order 3564.

ISSN:0094-243X/79/500641-06\$1.50 Copyright 1979 American Institute of Physics

EXPERIMENTS

All ohmic contact test patterns used for these experiments were defined by the lift-off technique. After etching mesas to remove unwanted conducting GaAs material between test patterns, photoresist was applied and the ohmic contact pattern areas were opened. A sequence of 1500 Å of Au:Ge, 400 Å of Ni and 500 Å of Au was deposited onto the wafer by thermal evaporation. (The deposition sequence was modified for two wafers, by omitting one layer, Ni, and two layers, Ni and Au, respectively.) Chemical precleaning was employed to insure that all resist residue was removed prior to contact deposition. After removal from vacuum the resist underlying the unwanted metal was dissolved leaving only the desired contact pattern. Seven different samples were fabricated. The characteristics of the GaAs wafers used are shown in Table I. Most of the wafers had test patterns for contact evaluations and some had contacts for FETs. A small part of each wafer was cleaved off and subjected to the standard alloying procedure used for ohmic contact formation at Hughes. This consists of thermal annealing at 450°C for 30 s in a forming-gas atmosphere.

Five different lasers were used for the annealing experiments. Four of them were pulsed lasers and their characteristics are shown in Table II. The ranges of energy densities employed, which are also shown, included levels at which the damage level of GaAs for the particular laser was reached or exceeded. For practical applications it is certainly necessary to be able to produce good ohmic contacts with an energy density which is well below the damage level.

In addition to the pulsed lasers a cw argon scanning laser (0.51 μm) system was employed. The following parameters were chosen for this laser: spot size, 185 μm; power, 2.5-4.0 W; scan velocity, 0.13-0.43 cm/s which correspond to 9-15 kW/cm², 0.4-1.6 kJ/cm² and a dwell time of 43-142 ms.

After laser irradiation ohmic contact formation was checked with a curve tracer and the I-V characteristic obtained was compared with that of a thermally annealed contact from the same wafer. In all cases where laser-annealing produced a lower resistance, the specific contact resistance was determined using the transmission-line method.⁴ SEM photographs were obtained for several contacts as well.

RESULTS

In general, it was found that the surface morphology of laser-annealed ohmic contacts was far superior to that of thermally annealed contacts. Figure 1, which shows SEM pictures of contacts produced in the two different manners, demonstrates this very clearly. We have also been able, in a few cases, to obtain specific contact resistances which were significantly lower than in the thermally annealed counterpart. Our best laser-annealed contact had a specific resistance of $1 \times 10^{-5} \Omega \text{ cm}^2$ which compares very favorably

Table I. Characteristics of GaAs wafers used for contact annealing

SAMPLE	MATERIAL PARAMETERS	THICKNESS OF CONDUCTING LAYER (μm)	DOPANT	DOPANT CONC (cm^{-3})
A	BULK DOPED		Te	10^{17} - 10^{18}
B	SEMI-INSULATING ION IMPLANTED	0.25	Si	2×10^{17}
C	SEMI-INSULATING WITH LEPI LAYER	0.2	Sn	7×10^{16}
D	SEMI-INSULATING ION IMPLANTED	0.25	Si	2×10^{17}
E	SEMI-INSULATING ION IMPLANTED	0.25	Si	2×10^{17}
F	SEMI-INSULATING ION IMPLANTED	0.25	Si	2×10^{17}
G	SEMI-INSULATING ION IMPLANTED	0.25	Si	2×10^{17}

Table II. Parameter range of pulsed lasers employed

TYPE OF LASER	WAVELENGTH (μm)	PULSE DURATION (FWHM) (ns)	EMPLOYED RANGE OF ENERGY DENSITIES (J/cm^2)	DAMAGE LEVEL ON GaAs (J/cm^2)
SINGLE MODE RUBY (TEM_{00})	0.69	20	0.5 - 1.4	0.9
MULTIMODE RUBY	0.69	30	0.2 - 1.2	0.8
MULTIMODE Nd:YAG	1.06	40	0.3 - 0.6	0.6
CO ₂	10.0	1000	0.9 - 3.0	3

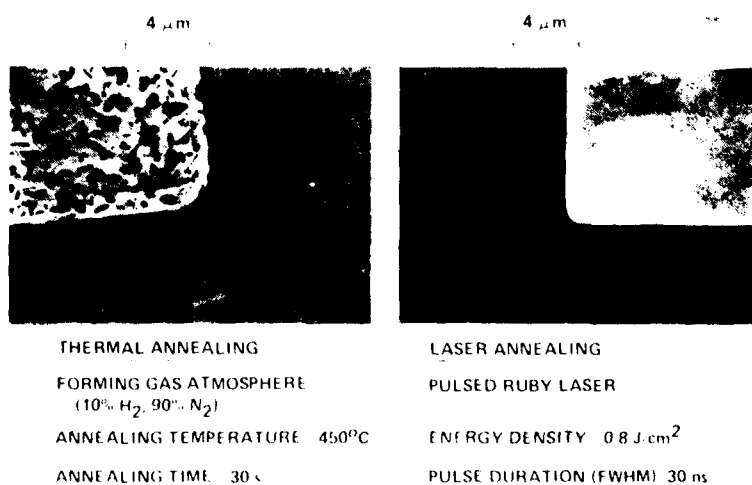


Fig. 1. SEM pictures of AuGe-Ni-Au ohmic contacts on GaAs

with the $5 \times 10^{-5} \Omega \text{ cm}^2$ produced by standard alloying.

Two of the samples received further processing (gate fabrication) after successful laser-annealing of contacts. The dc performance of the resulting FETs was subsequently measured and gave the following results: When the annealing was performed with the Nd:YAG laser, the performance was acceptable. However, when the argon ion laser scanning system was used, the resulting microwave FETs were at least as good as their thermally processed counterparts in terms of dc performance. Figure 2 shows photographs of the contacts and the I-V curves for the differently annealed contacts. Figure 3 displays the dc characteristic of one of the finished devices. Under closer inspection of the FET contacts in Figure 2 one notices on both photographs that one of the edges of the contacts facing the channel is not smooth. This occurred during lift-off and is not associated with annealing. The facing edge of the laser annealed contact is definitely superior to that of the thermally annealed contact. The breakdown voltage (7-8 V) of the channel was measured on many devices of both types and no differences could be detected. A survey of the best results of this study and the conditions under which they were achieved is shown in Table III.

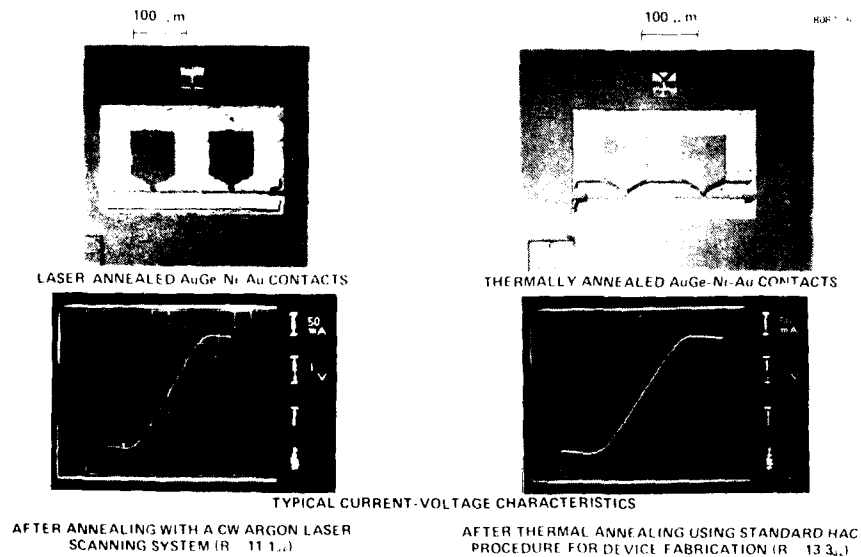


Fig. 2. Ohmic contacts on 1- μm gate microwave FETs.

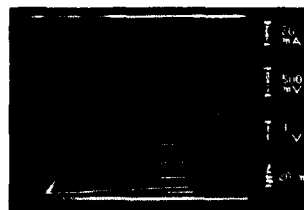


Fig. 3. I-V characteristic as a function of gate bias of a 1- μ m gate microwave FET with laser annealed ohmic contacts.

Table III. Survey of best results on ohmic contact formation.

8087-4

SAMPLE	CONTACT METALS	LASER WAVELENGTH (μ m)	LASER ENERGY DENSITY (J/cm^2)	QUALITATIVE COMPARISON WITH THERMALLY ANNEALED CONTACTS ON PART OF SAME WAFER		
				CONTACT RESISTANCE	SURFACE MORPHOLOGY	ADHESION
A	AuGe-Ni-Au	0.69	0.7	LOWER	IMPROVED	INFERIOR
B	AuGe-Ni-Au	0.69	0.9	LOWER	IMPROVED	INFERIOR
C	AuGe-Ni-Au	0.69	0.8	MUCH HIGHER		INFERIOR
D	AuGe-Ni-Au	0.51	530	COMPARABLE	IMPROVED	COMPARABLE
		0.69	0.6	MUCH HIGHER		INFERIOR
		1.06	0.3	HIGHER	IMPROVED	INFERIOR
		10.0	2.1	HIGHER	IMPROVED	COMPARABLE
E	AuGe-Au	0.69	0.5	HIGHER	INFERIOR	INFERIOR
		1.06	0.6	SLIGHTLY HIGHER	(SLIGHTLY DAMAGED)	INFERIOR
		10.0	1	HIGHER	IMPROVED	COMPARABLE
F	AuGe	0.69	0.7	HIGHER	IMPROVED	INFERIOR
G	AuGe-Ni-Au	0.51	600	SLIGHTLY LOWER	IMPROVED	COMPARABLE
		10.0	2.8	HIGHER	INFERIOR (DAMAGED)	COMPARABLE

DISCUSSION

There have been two earlier papers on ohmic contact formation to III-V compound semiconductors by laser annealing. In the first one by Pounds, et al.³ several pulsed lasers, Q-switched and non-Q-switched were used to make contacts from several different metal compositions to four different compounds. No comparisons with thermally annealed contacts were made and no device fabrication was attempted. The specific contact resistances reported were rather high ($5 \times 10^{-4} \Omega \cdot cm^2$). In the second paper, by Margalit et al.,⁵ Au:Ge ohmic contacts on GaAs were formed with a Q-switched ruby laser. In this case a comparison with a thermally annealed Au:Ge contact was made, which showed superior surface morphology and electrical properties for the laser-alloyed contacts. They reported a specific resistance of $7 \times 10^{-5} \Omega \cdot cm^2$ for the laser-annealed contacts versus $5 \times 10^{-4} \Omega \cdot cm^2$ for the thermally annealed sample. The latter contacts were subjected to considerably longer annealing times than the optimum heating period beyond which the contact resistance is known to increase.⁶ Again, no device fabrication was reported. It is important to note that the photon energy of the

ruby laser is greater than the bandgap energy of GaAs. For this Q-switched laser we found that damage to the substrate frequently occurred at energy densities required for ohmic contact formation. We conclude, therefore, that it is more practical to use either a Q-switched pulsed laser whose photon energy is below the semiconductor bandgap, a long duration pulse, or a cw laser scanning system. During the course of this work we achieved the best results with the cw laser.

CONCLUSION

We have shown in these preliminary experiments that laser annealed ohmic contacts on GaAs can have excellent surface morphology, superior dimensional control, and excellent ohmic contact properties. Further experiments are required to establish the impact of these improvements on device performance and lifetime.

ACKNOWLEDGMENT

The authors are grateful to F. W. Cleary and N. Hirsch for expert technical assistance in sample preparation and device testing and to M. D. Clark and R. A. Jullens for useful discussions.

REFERENCES

1. R. E. Lundgren and G. O. Ladd, 1978 Reliability Physics Symposium Digest, San Diego, CA, April 1978.
2. D. A. Abbott and J. A. Turner, 1975 International Electron Device Symposium Digest, Washington, DC, Dec. 1975.
3. R. S. Pounds, M. A. Saifi, W. C. Hahn, Jr., Solid State Electron. 17, 245 (1974).
4. H. H. Berger, Solid State Electron. 15, 145 (1972).
5. S. Margalit, D. Fekete, D. M. Pepper, C.-P. Lee, A. Yariv, Appl. Phys. L. 33, 346 (1978).
6. K. Heime, U. König, E. Kohn and A. Wortmann, Solid State Electron. 835 (1974).

SECTION 4.B

GaAs MICROWAVE FIELD EFFECT TRANSISTORS WITH LASER ANNEALED OHMIC CONTACTS

(G. Eckhardt, C. L. Anderson, L. D. Hess,
R. A. Jullens, C. F. Krumm)

Because of the success in obtaining high-quality Ohmic contacts on GaAs by laser annealing reported in Section 4.A, we directed attention toward the practical implementation of this technique. These efforts concentrated on the fabrication and testing of 1- μ m gate microwave FETs with source and drain contacts produced by laser annealing. For this attempt at the fabrication of microwave devices using laser annealing, we eliminated three basic processing steps. These steps are not essential to device operation but are required when maximum device performance is desired. Thus, we chose to fabricate two groups of devices that could be compared directly with each other, but not with devices fabricated to optimum performance. The source and drain contacts on one set of devices was annealed with our standard furnace procedure (450°C, 30 sec, forming gas), while another set of devices from the same wafer was fabricated with Ohmic contacts produced by the laser-annealing technique. For these experiments, we used contacts composed of Au:Ge-Ni-Au.

The devices having laser-annealed Ohmic contacts had consistently better dc performance than did those with furnace-annealed contacts. Source-drain resistances were typically 10 to 20% lower for the laser-annealed contacts. Similarly, the FETs having laser-annealed contacts showed improved performance over their furnace-annealed counterparts when tested for noise and gain at 14 GHz. A summary of the microwave performance for this set of devices is given in Table 3. Although the

number of devices was limited, it is encouraging that the average value of device gain is 17% higher for the laser-annealed than for the furnace-annealed contacts. Similarly, the noise figure is 12% lower, and the overall figure of merit (M) is 17% better for the laser-processed devices. However, these characteristics cannot be compared with other devices at this stage since we did not include (1) channel thinning, (2) final gold overlay, or (3) substrate thinning in the fabrication of this first set of microwave FETs with laser-annealed contacts.

Table 3. Microwave FET Performance at 14 GHz; L1-L4 Have Laser-Annealed Ohmic Contacts, T1-T2 Have Furnace-Annealed Contacts

FET	U_G (V)	U_D (V)	I_{DS} (mA)	Gain (dB)	NF (dB)	M (dB)
L1	3.7	3.3	25	5.4	6.6	7.8
L2	3.4	3.6	33	6.0	7.7	8.8
L3	3.7	5.5	20	5.7	6.7	7.8
L4	3.7	4.1	33	6.0	7.9	9.0
T1	6.2	3.0	21	4.2	7.0	8.7
T2	5.9	4.5	35	6.0	8.4	9.5

SECTION 4.C

A COMPARISON OF CHEMICAL AND STRUCTURAL
CHARACTERISTICS OF In-Au:Ge OHMIC CONTACTS
PRODUCED BY BULK HEATING AND LOCALIZED
LASER HEATING

(G. Eckhardt, C. L. Anderson, M. N. Colborn,
L. D. Hess and R. A. Jullens)

Presented at Electrochemical Society Meeting,
Los Angeles, CA, October 1979.

To be published in Proceedings of the
Symposium on Laser and Electron Beam
Processing of Electronic Materials,
Electrochemical Society, 1980.

A COMPARISON OF CHEMICAL AND STRUCTURAL CHARACTERISTICS OF
In-Au:Ge OHMIC CONTACTS ON GaAs PRODUCED BY
BULK HEATING AND LOCALIZED LASER HEATING

G. Eckhardt, C. L. Anderson, M. N. Colborn,
L. D. Hess and R. A. Jullens
Hughes Research Laboratories
3011 Malibu Canyon Road
Malibu, CA 90265

The morphological, chemical and metallurgical properties of as-deposited, laser-annealed and furnace-annealed In-Au:Ge contacts on GaAs have been investigated using scanning electron microscopy and energy-dispersive x-ray analysis. Angle sectioning techniques have been used to study the structural and compositional changes produced by the two annealing procedures throughout annealed layered metal structure samples with identical specific contact resistance.

Introduction

The reliability and efficiency of most GaAs devices depend strongly on the quality of their ohmic contacts. In spite of substantial efforts in many laboratories to understand and improve the properties of metal-semiconductor interfaces, the characteristics of ohmic contacts are not well understood and are unsatisfactory for some applications. An ohmic contact to GaAs generally consists of a composite metal structure which contains a dopant and a "wetting agent" in addition to an inert metal with high electrical conductivity. Conventional processing consists of annealing in a furnace for time periods of a few seconds or minutes. In the time period employed for furnace annealing, extensive inter-diffusion of contact and semiconductor constituents can take place. This causes the most commonly encountered problems in ohmic contact formation, which are poor wetting between contact metals and the semiconductor material, formation of high-resistivity intermetallic compounds, and phase segregation.

The poor surface morphology and the structural nonuniformity of ohmic contacts resulting from furnace annealing are considered acceptable for many photolithographically defined devices. However, with the development of advanced lithographic techniques that permit a substantial reduction of contact dimensions and intra-device spacings, improvements of dimensional accuracy and structural uniformity of ohmic contacts have become necessary. Such improvements appear to be difficult to obtain in contact formation by standard processing techniques.

Recently, it has been found that the problems associated with

furnace annealing can be avoided by laser annealing. Substantial improvements of the specific contact resistance and the surface morphology of ohmic contacts have been achieved when lasers were used for the annealing process (1-4). This novel procedure minimizes interdiffusion of components since the heating periods are limited to much shorter times (typically 10-100 ns for a Q-switched laser and 1-100 ms for a scanning cw laser) than those used in conventional furnace annealing. The emphasis of this study is on an investigation and comparison of the structures produced by the two different annealing procedures in a layered contact metal system on GaAs at various depths below the surface.

Experimental Conditions

Semi-insulating GaAs wafers implanted with $4 \times 10^{12} \text{ cm}^{-2}$, 100 keV Si^+ ions were used ($n \approx 1 \times 10^{17} \text{ cm}^{-3}$ at the wafer surface). The contact test patterns were defined by the lift-off technique. Sequential thermal evaporation of In and Au:Ge eutectic produced a layered structure of 400 Å In followed by 1700 Å Au:Ge. Part of the wafer was cleaved off and annealed in a furnace at 450°C for 30s in a forming-gas atmosphere. A second part was annealed with a cw Ar-ion laser scanning system using a range of scanning velocities and beam powers. The remainder of the wafer was retained unannealed. The specific contact resistances of the annealed contacts were determined by the extended transmission line method (5) and two contacts with identical specific contact resistance values of $1 \times 10^{-6} \Omega \text{ cm}^2$, obtained by the two different annealing procedures, were selected for a study of their morphological and metallurgical properties.

The laser and scanning system used in this study are shown schematically in Fig. 1. The argon ion laser has a maximum output of 20 W in the blue-green spectral region (4880 to 5145 Å). It was limited to single transverse mode operation by an intracavity aperture and had a beam diameter of 1.6 mm. The laser beam was focused with a 30-cm focal length lens onto samples held by vacuum on to a metal plate. The beam was scanned across the samples in a raster pattern, as indicated in Figure 1, by means of orthogonally mounted galvanometer driven mirrors located between the lens and sample holder. In a typical experiment the Y-axis mirror is held fixed while the X-axis mirror is driven by the output from a variable-frequency waveform generator chosen to give the desired scan velocity at the sample. A blanking mirror is activated at the end of a scan and the Y-axis mirror is advanced to a new position during retrace of the beam. For the experiments reported here the focused beam size at the sample was 66 μm , defined as the diameter where the laser intensity was reduced to 1/e of its peak value at the beam center (6). The effective thermal spot size is not precisely known from either calculations or measurements because of the complicated target structures and laser-material interactions involved; it can be larger or smaller than the beam diameter as defined above. Therefore,

the effective dwell time is uncertain as well; as a point of reference, we specify the dwell time as the focused beam diameter ($66\text{ }\mu\text{m}$) divided by the scan velocity v . A laser power of 3.5 W and a scan velocity of 4.3 mm/s were used to produce the contact resistance of $10^{-6}\text{ }\Omega\text{-cm}^2$. Using these parameters and definitions, the peak laser power density I_0 is 102 kW/cm^2 at the beam center and is reduced by the factor $\exp[-r/r_0]^2$ at any radial distance r ; $r_0 = 33\text{ }\mu\text{m}$. The dwell time, $\tau_D = 2 r_0/v$, is 15 ms and the energy density, $0.369 I_0 \tau_D$, is 1.5 kJ/cm^2 .

The two specimens with identical ohmic contacts, together with an as-deposited specimen for comparison, were ion-milled at a shallow angle. A schematic of an ion-milled sample is shown in Figure 2. The ion milling produced a taper whose depth and length were determined with the aid of the as-deposited sample. Using surface profilometer (Dektak) traces and energy-dispersive x-ray (EDX) analysis, the onset of the taper was determined as well as the point at which all metal had been milled off. The distance between these points was measured on SEM photographs. The Dektak stylus traces confirmed the linearity of the slope. Thus, the angle of the taper was established to be about 0.03° . The onset of the taper was not determined very accurately, however, and consequently, the abscissa of the depth profiles discussed in the next section may contain a systematic error.

The ion-milled region on each specimen was investigated at regular intervals along the taper for compositional uniformity (EDX) and for structural characteristics (by scanning electron microscopy). EDX was performed on the total viewed area and on each of the characteristic features revealed by the SEM.

Results and Discussion

Three series of SEM photographs are shown in Figure 3. They represent various regions along the taper on samples that were (a) as deposited, (b) furnace annealed, and (c) laser annealed. The bottom row shows regions close to or on the unmilled metal surfaces, and the top row shows GaAs surfaces after all metal was sputtered off by the ion bombardment process. Each row represents a region at approximately the same depth below the surface.

These photographs demonstrate the existence of structural non-uniformity of the contact metals for all specimens. Each of them, however, has its own distinct appearance and characteristic features. The as-deposited sample shows the most pronounced structure. Globules, a few tenths of a micrometer in size, cover its unmilled surface. These globules are still somewhat evident in the laser-annealed contact layer. Partial melting and fusion of these globules has, however, taken place and has resulted in a finer texture. The furnace-annealed contact exhibits very different characteristics. It is obvious that considerable redistribution must have taken place. Two prominent features can be distinguished, consisting of large, irregular, dark

regions of the order of one micrometer and bright particles of the order of a few tenths of a micrometer in diameter. The appearance of the latter is similar to that of the globules characteristic of the as-deposited sample, but there are much fewer of them on the furnace-annealed specimen.

The photon counts per second, obtained from EDX for Ga, As, and all contact constituents from an area of $(4 \times 5) \mu\text{m}$ were plotted as a function of depth and are shown in Figs. 4 to 6. These depth profiles, although lacking the depth resolution of profiles obtained by Auger analysis, exhibit several very interesting features. It can be deduced from Figure 4 that Ge is not evenly distributed throughout the as-deposited Au layer, although a Au:Ge alloy was used for its deposition. A similar result was obtained by an Auger depth profile of a Au:Ge-Ni-Au contact, where the same metal deposition procedure was used. It is, of course, very undesirable that the Ge is further removed from the GaAs than intended.

The depth profile of the furnace-annealed sample (Fig. 5) demonstrates that very extensive redistribution of the metals has taken place. The In has diffused towards the surface and the Ge towards the GaAs. There is even an indication of a pile-up of Ge at the metal-semiconductor interface. Again, a similar result has been found by Auger spectroscopy of a furnace-annealed In-Au:Ge contact (7). The depth profiles of the laser-annealed specimen (Figure 6) exhibits features that are somewhat similar to those of the furnace-annealed sample except for the distribution profile of Ge which is markedly different. The less pronounced redistribution of Ge caused by laser annealing is attributed to the considerably shorter heating times characteristic of this technique compared to furnace annealing.

EDX analyses of the structural characteristics throughout the contact layers of all specimens showed that, in general, structural uniformity corresponded to compositional uniformity. However, while prominent structural features were frequently manifestations of phase segregations, structural nonuniformity did not necessarily indicate compositional nonuniformity as well. The multilayered contact of the as-deposited sample exhibited good lateral compositional uniformity. This was generally true for the laser-annealed sample as well. However, a strong tendency seems to exist in this type of contact system for Ge to segregate into distinct particles at elevated temperatures. Even after the short time span during which laser annealing takes place, some indications of the formation of particles with higher Ge concentrations were found, while after furnace annealing most of the Ge appears to be concentrated in a precipitate phase (dark areas in photographs of Figure 3b). The bright particles, also a prominent feature of Figure 3b, were identified as Au particles with a small admixture of In.

In order to characterize the lateral compositional uniformity of the three specimens, the maximum variations of the distribution of the ratios of the x-ray count rate of Au/Ge and Au/In were determined.

The results, given in Table I, show a striking difference between the two annealing procedures. The laser heating period was obviously short enough to avoid the strong segregation effects that take place during furnace annealing.

A very comprehensive study has been conducted recently of several multilayer furnace-annealed ohmic contacts to GaAs (7), including the In-Au:Ge contact discussed in the present paper. In that study, micro-segregation and precipitate phases were identified and a correlation between the size of the precipitates and the specific contact resistance was established. It was found that optimum electrical properties occurred when a maximum grain size was obtained. The results of the present paper, where samples with a very low (and identical) specific contact resistance were selected, give strong indications that optimum conditions for ohmic contact formation may be achieved by laser annealing without the establishment of macroscopic precipitate phases that cause undesirable structural nonuniformity.

These findings underline the potential importance of laser annealing for ohmic-contact formation on devices where structural and compositional contact uniformity are important for maximum device performance. In particular, lateral compositional variations can cause substantial variations in specific resistivity and, therefore, may produce strong enhancements of current densities on a microscopic scale. High current densities in ohmic contacts can enhance electromigration which has been shown to deteriorate device performance (9). Thus, problems associated with lifetime and reliability of GaAs microwave devices (8, 9) may be diminished when this novel annealing procedure is applied.

Conclusions

It has been shown by SEM and EDX analysis that laser-annealed In-Au:Ge contacts possess considerably finer texture and far superior compositional uniformity than furnace-annealed contacts from the same wafer, when both types of contacts have identical specific contact resistance. This is expected to have important consequences for the reliability and lifetime of microwave devices, where the small dimensions reduce the tolerances for structural and compositional variations.

REFERENCES

1. S. Margalit, D. Fekete, D. M. Pepper, C. P. Lee and A. Yariv, Appl. Phys. Lett. 33, 346 (1978).
2. R. B. Gold, R. A. Powell and J. F. Gibbons, AIP Conf. Proc. No. 50, Laser-Solid Interactions and Laser Processing, 1978, p. 635.
3. G. Eckhardt, C. L. Anderson, L. D. Hess and C. F. Krumm, AIP Conf. Proc. No. 50, Laser-Solid Interactions and Laser Processing 1978, p. 641.
4. G. Eckhardt, C. L. Anderson, L. D. Hess, N. Hirsch, and C. F. Krumm, "GaAs Microwave Field Effect Transistors with Laser Annealed Ohmic Contacts," presented at Workshop on Compound Semiconductor Microwave Materials and Devices, Atlanta, February 1979.
5. H. H. Berger, Solid-State Electron. 15, 145 (1972).
6. This procedure for specifying the diameter of the focused laser beam is different than used in ref. 3 where the beam size was taken as the diameter of a circle containing 99% of the laser power.
7. A. Christou, Solid-State Electron. 22, 141 (1979).
8. H. M. Macksey, Inst. Phys. Conf. Ser. No. 33b, 254, Gallium Arsenide and Related Compounds, St. Louis, 1976.
9. R. E. Lundgren and G. O. Ladd, 1978 Reliability Physics Symposium Digest, San Diego, CA, April 1978.

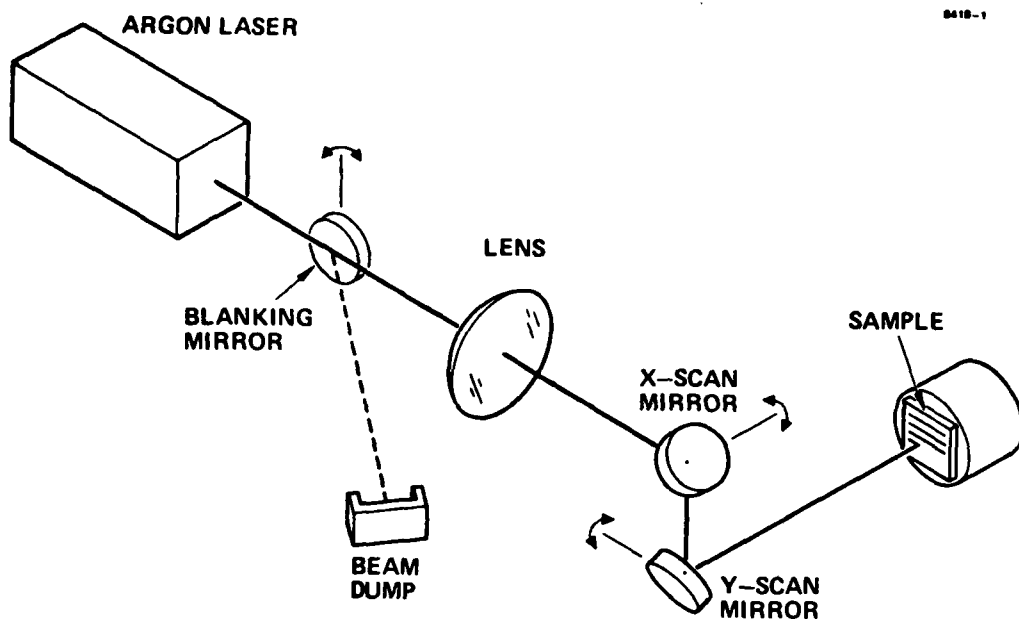


Figure 1. Schematic of cw argon laser annealing apparatus.

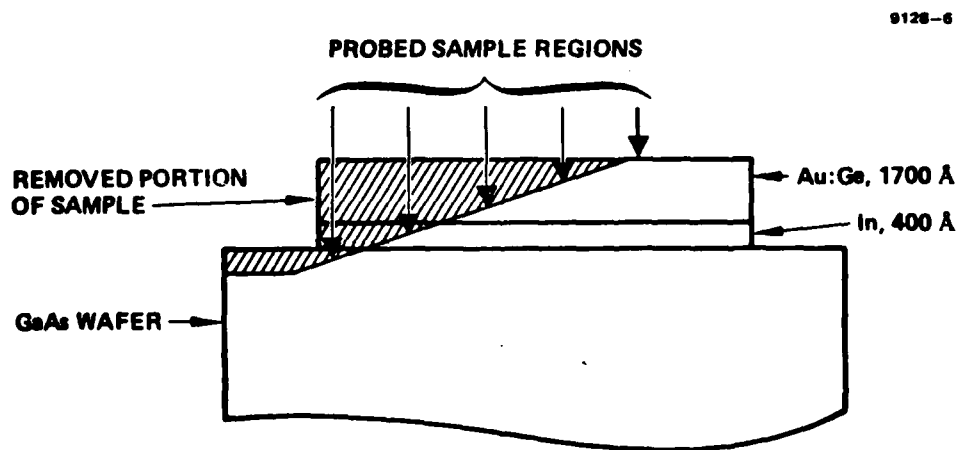


Figure 2. Schematic of ion-milled sample.

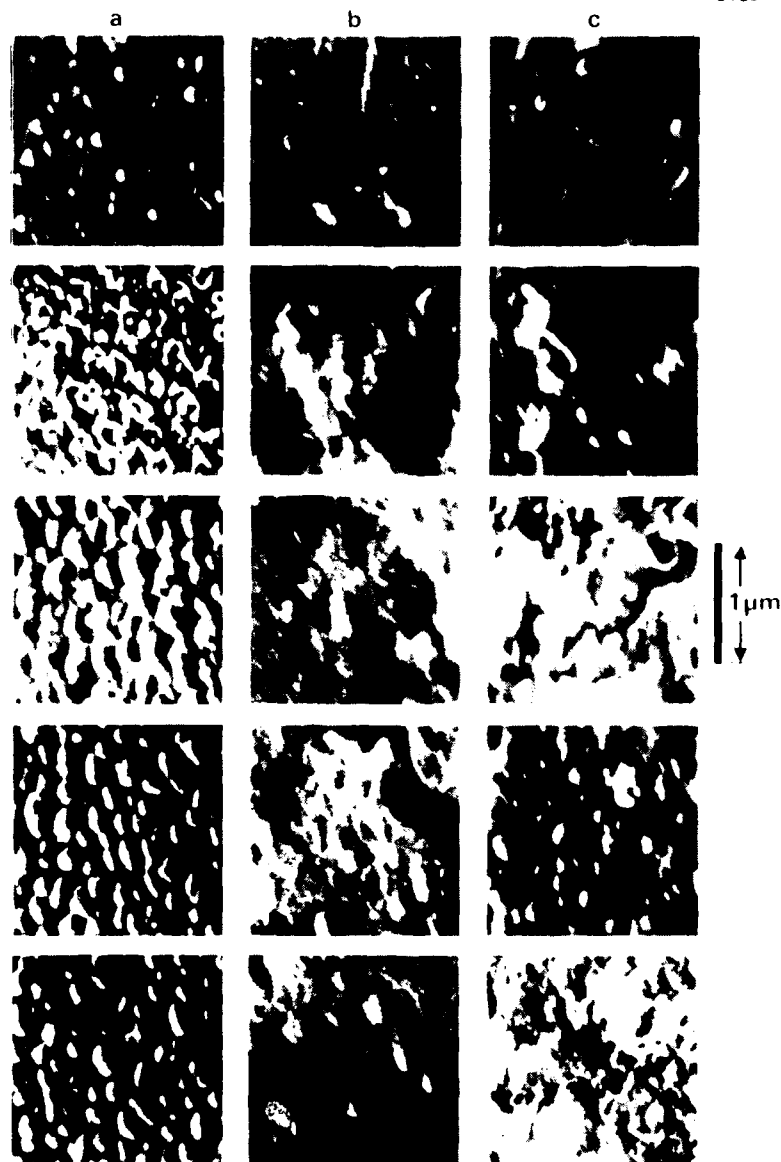


Figure 3. SEM photographs of In-Au:Ge contacts on GaAs, ion-milled at shallow angle. (a) As deposited; (b) furnace annealed; (c) laser annealed.

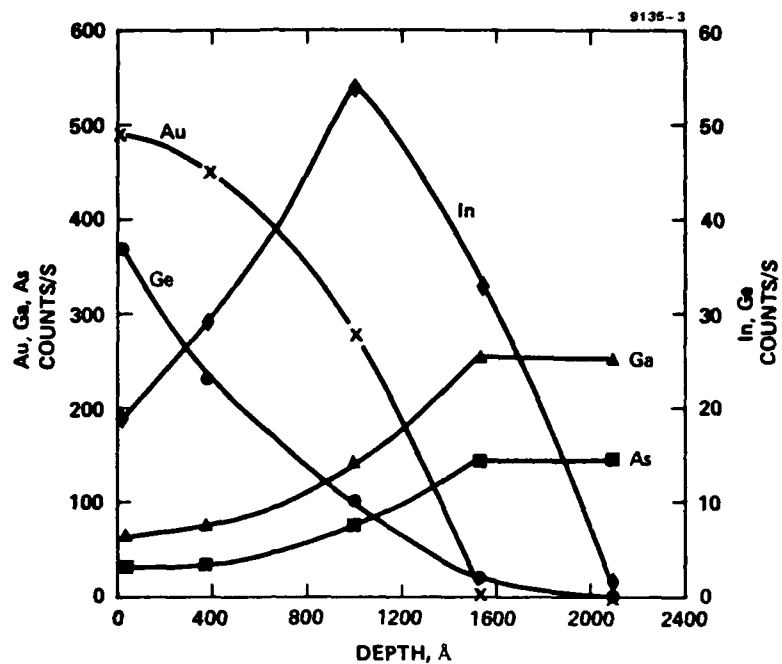


Figure 4. Depth profile of constituents of In-Au:Ge contact, as deposited.

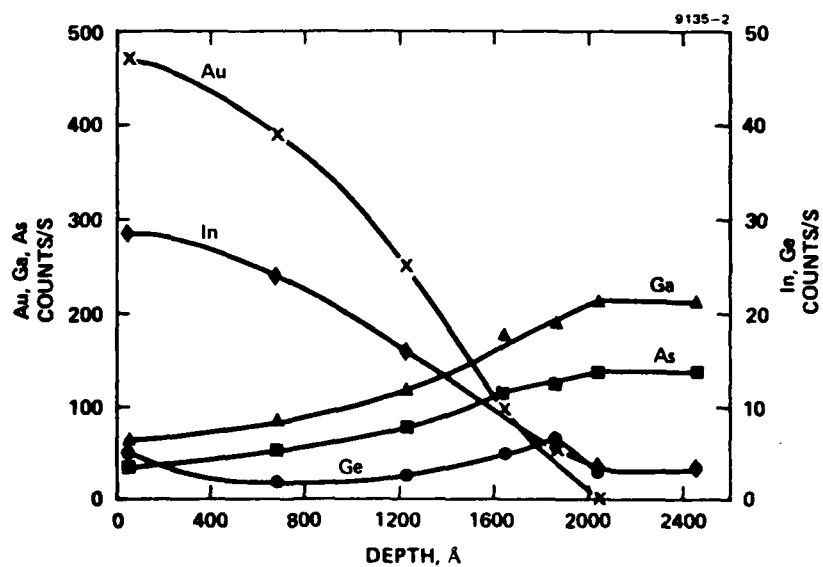


Figure 5. Depth profile of constituents of In-Au:Ge contact, furnace annealed.

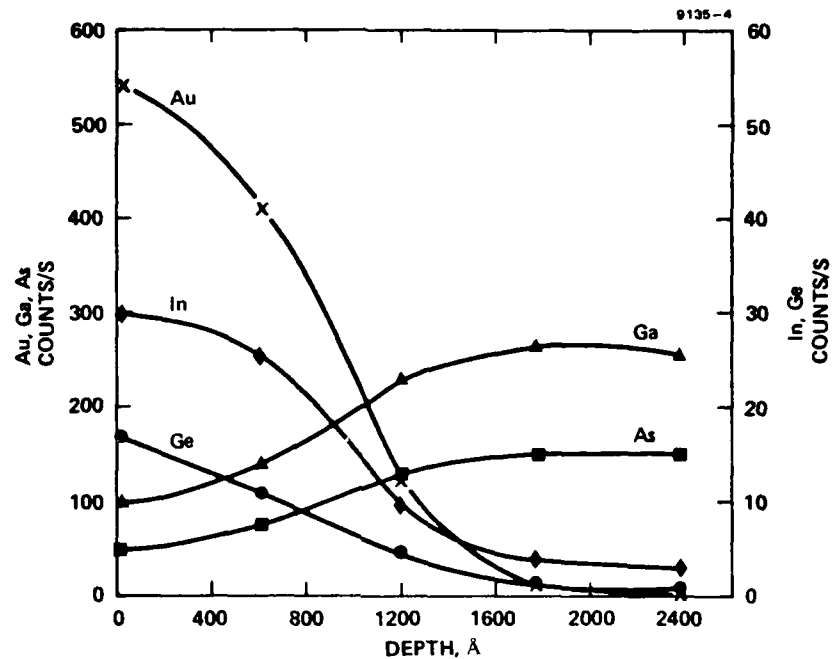


Figure 6. Depth profile of constituents of In-Au:Ge contact, laser annealed.

Table I Maximum Lateral Variation of Ratio of Counts/s for Some of the Contact Constituents

9128-5

	AS-DEPOSITED CONTACT			LASER-ANNEALED CONTACT			FURNACE-ANNEALED CONTACT			
REGION	1	2	3	1	2	3	1	2	3	4
Au/Ge	1.0	1.0	1.2	2.0	2.8	1.6	220	262	—	207
Au/In	1.0	1.6	1.3	1.1	1.1	1.2	1.0	1.0	2.8	2.2

SECTION 4.D

OVERVIEW OF OHMIC-CONTACT FORMATION ON
n-TYPE GaAs BY LASER AND ELECTRON BEAM
ANNEALING

(G. Eckhardt)

Presented at Materials Research Society
Meeting, Cambridge, MA, November 1979

To be published in Laser-Solid Interactions
and Laser Processing - 1979 (American Institute
of Physics, 1980).

OVERVIEW OF OHMIC-CONTACT FORMATION ON N-TYPE GaAs BY LASER AND ELECTRON-BEAM ANNEALING

Gisela Eckhardt
Hughes Research Laboratories
Malibu, California 90265

Researchers of several laboratories have obtained significant results when laser or electron-beam annealing was used for Ohmic-contact formation on n-type GaAs. Two types of contacts have been investigated. For the annealing procedure required by both types during processing, the standard method of furnace annealing has been replaced by laser or electron-beam annealing. The results achieved with the latter two processing techniques are discussed and compared with those obtained by the standard methods.

I. INTRODUCTION

Ohmic contacts between a metal and a semiconductor are defined pragmatically as interfaces that possess current-voltage characteristics with a linear region for both directions of current flow over a large temperature range. This criterion is, however, not sufficient to qualify an interface as a satisfactory Ohmic contact for devices. To be useful, an Ohmic contact not only must have a linear range which is adequate for the particular application, but its resistance must also be sufficiently small so that its effect on device performance is negligible. The latter quality of Ohmic contacts is assessed in terms of their specific contact resistance, which is defined as $\rho_c = \frac{\partial V}{\partial J}$, where J is the current density at the contact and V the applied voltage. The quantity ρ_c is usually determined by the transmission line method (1).

Ohmic contacts to semiconductors have been the subject of a large number of studies and are understood in principle (2-3). However, the formation of Ohmic contacts with low specific contact resistance is still plagued by a multitude of problems. The improvement of Ohmic contacts has become highly desirable with the development of integrated circuits and the application of advanced lithographic techniques that shrink contact dimensions and intra-device spacings. These latest advancements in semiconductor technology have placed more stringent requirements on surface morphology and edge definition because of the higher dimensional accuracy required. Furthermore, these advancements have decreased the tolerance on contact resistance throughout individual wafers for integrated circuits, because uniformity of the electrical parameters (e.g., bias and threshold voltages) is required within a circuit. This necessitates a high structural and compositional uniformity of

This work was supported in part by ONR Contract N00014-78-C-0337 under DARPA Order 3564.

the contact-metal system that is generally not achieved by the standard procedures of Ohmic-contact formation.

In order to produce an Ohmic contact to n-type GaAs one usually attempts to achieve a very high doping level in a thin GaAs layer at the interface. The most widely used procedure for creating such a layer consists of evaporating a multi-component metal structure on the semiconductor surface and then alloying the metal-semiconductor system at elevated temperatures. The evaporated structure typically consists of an inert metal with high electrical conductivity, a dopant, and a "wetting agent." Usually, two of these components are selected such that they form a eutectic with a lower melting point than any single suitable metal would have.

During the alloying step, while one or several contact components are molten, some of the GaAs is dissolved by the melt. When the melt cools down, the GaAs segregates from it, together with some of the dopant from the contact, and regrows on the GaAs crystal, forming a highly doped layer at the interface with the metal. Epitaxial growth, shallow diffusion, shallow ion implantation followed by annealing of the implantation damage, and sintering are other methods for obtaining thin, highly doped layers at the interface (4,5).

Each of these techniques has its specific complications. For example, the occurrence of high-resistivity regions beneath the epitaxial layer may be difficult to avoid, the required diffusion temperatures may be incompatible with other device processing requirements, and adequate electrical activation of the impurities resulting from a high-dose ion implant may not be possible.

Most of the problems encountered in Ohmic-contact formation by furnace annealing arise because of the high temperatures, the melt formation, the bulk heating required, and the long heating times involved. The following phenomena may occur as a consequence of furnace alloying: (1) in-diffusion of surface impurities and/or of some of the contact constituents which are considered undesirable, (2) out-diffusion of semiconductor constituents, (3) poor wetting between contact metals and semiconductor causing non-uniform contacts, (4) formation of high-resistivity intermetallic compounds, and (5) formation of microscopic crystallites of various phases resulting in surface roughness and reduced edge definition.

Recently, it has been demonstrated that many of the problems associated with an annealing step in Ohmic-contact formation can be avoided or greatly diminished if the annealing is performed by laser or electron-beam irradiation. Laser and electron-beam experiments have concentrated on two of the different methods for creating the high impurity concentration at the semiconductor surface required for Ohmic-contact formation: (1) annealing of multi-layered metal structures deposited on the semiconductor surface and (2) annealing of high-dose shallow ion implants of donor atoms into GaAs.

II. LASER AND ELECTRON-BEAM ANNEALING OF SEMICONDUCTOR — METAL SYSTEMS FOR OHMIC-CONTACT FORMATION

The first experiments on Ohmic-contact formation by laser annealing were reported by Pounds, Saifi, and Hahn(6) in 1974. They used several Q-switched

and non-Q-switched lasers to form contacts on GaP, GaAs, GaSb, InAs, and InSb. They achieved specific contact resistances of 10^{-3} to $10^{-4} \Omega \text{cm}^2$. These are several orders of magnitude higher than what can be obtained today by conventional methods. No comparison with furnace-annealed samples was given.

A common observation made during the more recent investigations is the exhibition of superior surface morphology and the retention of pre-anneal accuracy of Ohmic contacts obtained by laser annealing of metal-GaAs systems as compared to furnace-annealed contacts. The first such comparison was made by Margalit et al. (7), who used a Q-switched ruby laser (energy density 1 J/cm^2) to anneal Au:Ge contacts on GaAs, and obtained $\rho_c = 7 \times 10^{-5} \Omega \text{cm}^2$. However, the furnace-annealing times employed (3 min) were considerably longer than the optimum heating period of 30-60s for this type of contact. Beyond this time span the contact resistance is known to increase again (8). This explains the high value of $\rho_c = 5 \times 10^{-4} \Omega \text{cm}^2$ that these workers obtained by the standard annealing method.

Gold and coworkers (9) produced excellent contacts on GaAs with $\rho_c = 2 \times 10^{-6} \Omega \text{cm}^2$ using a cw Ar-ion laser and a non-Q-switched ruby laser (pulse duration $\approx 1 \text{ ms}$, energy densities of the order of 10 J/cm^2). Their material had a doping level of $1 \times 10^{17} \text{ cm}^{-3}$ and they used very thin Au-Ge or Ni-Au-Ge contact layers that were evaporated on GaAs in the sequence Ni(20Å), Au(200Å), Ge(100Å). Their use of Ge as the top layer resulted in an increased photon absorption in the contact without a corresponding absorption increase in the GaAs. To flatten the Gaussian intensity distribution of the laser beam, a lapped quartz rod was inserted into the beam in front of the sample. Both measures assured that contact formation took place at energy density level well below the damage level for GaAs. Gold et al. report, however, a poor reproducibility of their results.

The present author and coworkers (10,11) have investigated the annealing of Au:Ge-based Ohmic contacts to GaAs using pulsed CO_2 ($10.6 \mu\text{m}$), pulsed Nd:YAG ($1.06 \mu\text{m}$), pulsed ruby ($0.69 \mu\text{m}$), and cw Ar-ion ($0.51 \mu\text{m}$) lasers, and compared them with furnace-annealed contacts from parts of the same wafer. Recently, some experiments have been done with a pulsed electron beam as well. Multi-layer metal systems of the type Au:Ge-X-Au or Au:Ge-X, where X stands for the metals Ni, Ag, Pt, Ti, and In, have been studied. Contacts have been made to ion-implanted layers, liquid-phase epitaxial layers, and bulk n-type substrates. The doping level varied from $7 \times 10^{16} \text{ cm}^{-3}$ to 10^{18} cm^{-3} , and three different dopants were used (Se, Si, Te). The contact metal layers were deposited onto the wafer by sequential thermal evaporation of the individual metals, except for Au and Ge which were evaporated jointly from a Au:Ge eutectic alloy. Typical layer thicknesses were 1200-1700 Å for Au:Ge, 400 Å for metal "X," and 500-600 Å for Au. The contact test patterns used were defined by the lift-off technique.

The best results (lowest ρ_c , firmest adhesion between contact and GaAs, and highest reproducibility) were obtained with the single-mode (TEM_{00}) cw Ar-ion laser, and all the recent work was therefore performed with this laser. A summary of some of the results of this work is shown in Table I together with results of pulsed electron-beam annealing (PEBA) experiments that were performed on parts of the same wafer with the SPI-Pulse 6000 system at Spire Corporation.

TABLE I. Best Ohmic Contacts Formed on GaAs by cw Ar-ion Laser and Pulsed Electron-Beam Annealing

CONTACT METAL	LASER ANNEALED CONTACTS				ELECTRON BEAM ANNEALED CONTACTS		
	SPECIFIC CONTACT RESISTANCE (Ωcm^2)	LASER CHARACTERISTICS			SPECIFIC CONTACT RESISTANCE (Ωcm^2)	ELECTRON BEAM CHARACTERISTICS	
		POWER (W)	SCAN VELOCITY (cm/s)	ENERGY DENSITY (kJ/cm^2)		CHARGING VOLTAGE (kV)	ENERGY DENSITY (J/cm^2)
Au-Ge-Ni-Au	4.8×10^{-6}	4.0	0.43	0.64	3.5×10^{-5}	145	0.20
Au-Ge-Pt-Au	1.5×10^{-5}	3.0	0.43	0.61	8.6×10^{-5}	145	0.20
Au-Ge-Ag-Au	2.0×10^{-6}	4.1	0.43	0.66	2.3×10^{-5}	150	0.32
Au-Ge-Ti-Au	1.8×10^{-5}	3.0	0.20	1.35	CONTACT DESTROYED NOT OHMIC	145 140	0.20 0.25
In-Au-Ge	1.3×10^{-6}	3.5	0.43	0.56	CONTACT DESTROYED NOT OHMIC	145 140	0.20 0.25

All samples used for this particular study consisted of semi-insulating GaAs implanted with $4 \times 10^{12} \text{ cm}^{-2}$, 100-keV Si^+ ions ($n \approx 1 \times 10^{17} \text{ cm}^{-3}$ at the wafer surface). The laser beam was always focused onto the sample with a 30-cm focal length lens to a spot size of $66 \mu\text{m}$. Using the spot size, together with laser power and scan velocity given in the table, other pertinent annealing parameters, which are not given, can be computed (11). The electron beam is characterized by the charging voltage on the capacitor. The corresponding values for the approximate energy density of the incident beam were obtained from calibration data furnished by A.C. Greenwald of Spire Corp. The average electron-beam energy was between 10 and 12 keV, the pulse duration 100 ns.

As can be seen from the table, the specific contact-resistance values obtained by laser annealing varied by two orders of magnitude when merely the "wetting agent" Ni of the standard Au:Ge-Ni-Au contact was replaced by other metals — a result which warrants further investigation. The range of ρ_c values obtained with PEBA by variation of metal "X" is much less pronounced, but the results are not nearly as good. Not only were considerably higher ρ_c values obtained, but all contacts whose ρ_c values are given showed slight to severe damage and poor adhesion. This partial or total destruction of the contact pads may be caused by the choice of contact-layer thickness. The thickness was optimized for furnace annealing and may be much too thick for PEBA (12). It is quite probable that an optimization of contact-layer thicknesses will further improve the properties of both electron-beam and laser-annealed contacts.

We have also laser annealed Au:Ge based contacts of a number of 1- μm gate GaAs microwave FETs and compared their microwave performance with that of conventional thermally annealed contacts from the same wafer (13). The laser-annealed contacts were found to be superior or at least as good in every respect. Their contact resistance was lower by 10-20% and the dc characteristics were excellent (10). Average values of gain, noise figure, and noise measure at 14 GHz were somewhat better for the laser-annealed devices. In all

cases, the surface morphology and edge definition of the laser-annealed contacts was far superior to that of their thermally annealed counterparts.

During the furnace annealing of Au:Ge-based contacts the whole device is subjected to temperatures of about 450°C for 30s. This time duration was found to be sufficient for the components of the substrate and the contact metal system to interdiffuse and to form microscopic crystallites of various phases, resulting in surface roughness and reduced edge definition (14,15). In a typical laser-annealing process, on the other hand, the region being annealed experiences a temperature rise for a short period of time only (10-100 ns for a high-power pulsed laser, 1-100 ms for a lower-power cw Ar-ion laser). Because of the shortness of the laser-annealing period, interdiffusion of semiconductor and contact constituents is reduced and microscopic phase separation due to metal flow is prevented.

We have started a study aimed at investigating and comparing the structural and compositional uniformity at laser-annealed and furnace-annealed multi-layered contacts on GaAs. So far, In-Au:Ge (11) and Au:Ge-Ni-Au contacts have been investigated using scanning electron microscope (SEM) photography and energy-dispersive X-ray (EDX) analysis. The samples used for this study again consisted of semi-insulating GaAs implanted with $4 \times 10^{12} \text{ cm}^{-2}$ 100-keV Si⁺ ions ($n \approx 1 \times 10^{17} \text{ cm}^{-3}$ at the wafer surface). They were selected such that the specific contact resistances of furnace and laser-annealed samples were identical or at least very similar: $1 \times 10^{-6} \Omega \text{ cm}^2$ for both In-Au:Ge contacts and $(2 \dots 3) \times 10^{-5} \Omega \text{ cm}^2$ for the two Au:Ge-Ni-Au contacts. All four samples together with two as-deposited specimens for comparison, were ion-milled at a shallow angle. Depth and length of the taper were obtained with the aid of the as-deposited samples. Using EDX analysis and/or surface profilometer traces, the onset of the taper was determined, the linearity of its slope confirmed, and the point determined at which all metal had been milled off. The distance between these points was measured on SEM photographs. The angle of the taper was thus computed to be about 0.03°. The onset of the taper was not determined very accurately, however, and the abscissa of the depth profiles discussed below may contain a systematic error.

A schematic cross section of an ion-milled sample is shown in Fig. 1. Arrows indicate probed sample regions that were investigated along the taper for compositional characteristics by EDX analysis and for structural uniformity by SEM photography. EDX analysis was performed on the total viewed area (typically $4 \mu\text{m} \times 5 \mu\text{m}$) and on each of the characteristic features revealed by the SEM. Three series of SEM photographs are shown for each of the two contact-metal systems in Figs. 2 and 3, representing (a) as-deposited, (b) furnace-annealed, and (c) laser-annealed regions along the taper. Unmilled contact regions are shown in the bottom rows, and the top rows show GaAs surfaces from which all metal was removed by ion milling.

The photographs of the In-Au:Ge contact in Fig. 2 display structural non-uniformity for all specimens. The photographs of the as-deposited contact show the most pronounced structure, those of the laser-annealed contact exhibit evidence of melting and increased uniformity, and those of the furnace-annealed contact show evidence of extensive redistribution of contact

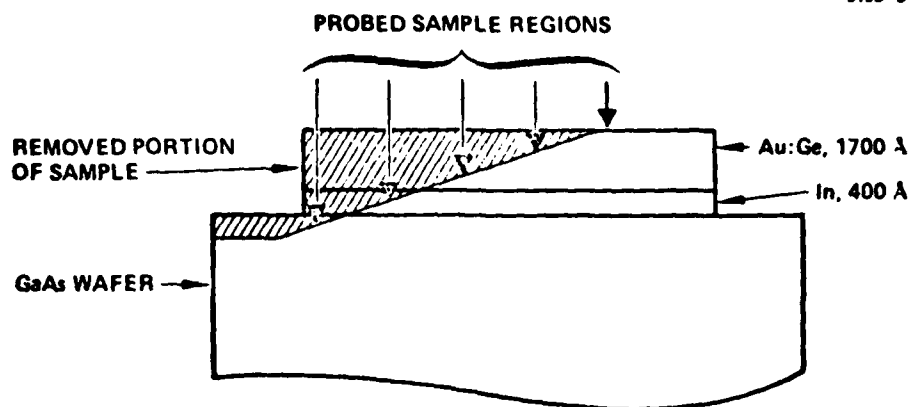


FIGURE 1. Schematic cross section of ion-milled sample.

constituents resulting in precipitate phases (large, dark regions and bright particles). In the case of the Au:Ge-Ni-Au contact the as-deposited layers display excellent structural uniformity, which was largely preserved during laser annealing, but again, the layers underwent massive redistribution and extensive segregation into distinct particles during furnace annealing.

EDX analyses of the structural characteristics of all specimens showed that, although the uniformity of structure generally corresponded to uniformity of composition, structural nonuniformity did not necessarily indicate a nonuniform composition. Only the prominent features displayed by both furnace-annealed contacts were identified as precipitate phases. In the case of the In-Au:Ge contact most of the Ge appears to be concentrated in the dark areas of Fig. 2b, while the bright particles were identified as Au particles with some admixture of In. The particles evident on the photographs of Fig. 3b are mostly composed of Ni, but contain some Ge as well.

The lateral compositional uniformity of the six specimens was characterized by the maximum variations of the ratios of X-ray count rates for Au/Ge, Au/In, and Au/Ni. The results are given in Table II. They prove that the striking differences in surface morphology produced by the two annealing procedures, which have been reported consistently by different researchers, (7,9,10), are indicative of the state of the contact throughout its volume. The laser-heating period that is sufficient to produce excellent Ohmic contacts is obviously too short for sizeable phase segregation to take place.

The photon counts per second obtained from EDX were used to plot depth profiles for Ga, As, and all contact constituents (Figs. 4-9). These curves, although lacking the depth resolution of profiles obtained by Auger analyses, display several interesting features: (1) Ge is not distributed uniformly throughout the as-deposited Au:Ge layers, although a Au:Ge alloy was used for their deposition. The Ge distribution curve peaks at greater distance from the GaAs than intended and desirable. This result was confirmed by Auger analysis; (2) Extensive redistribution of contact constituents

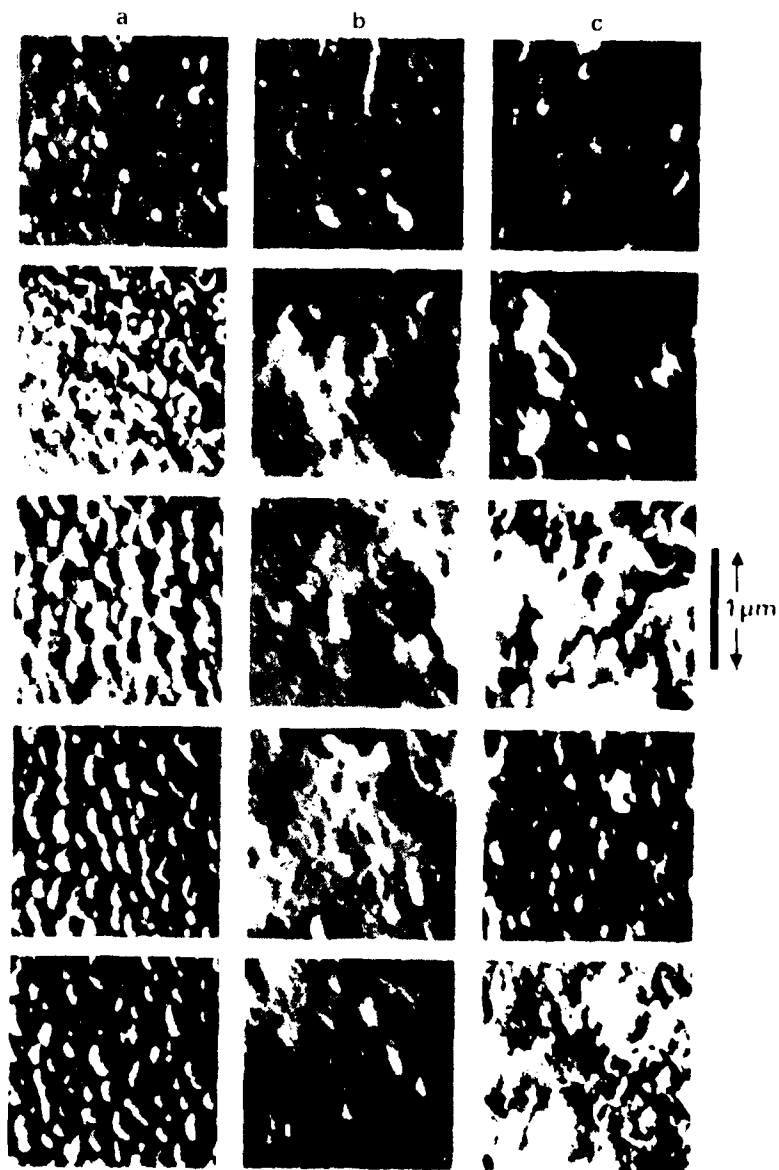


FIGURE 2. SEM photographs of In-Au:Ge contacts on GaAs, ion-milled at shallow angle. (a) As deposited; (b) furnace annealed; (c) laser annealed.

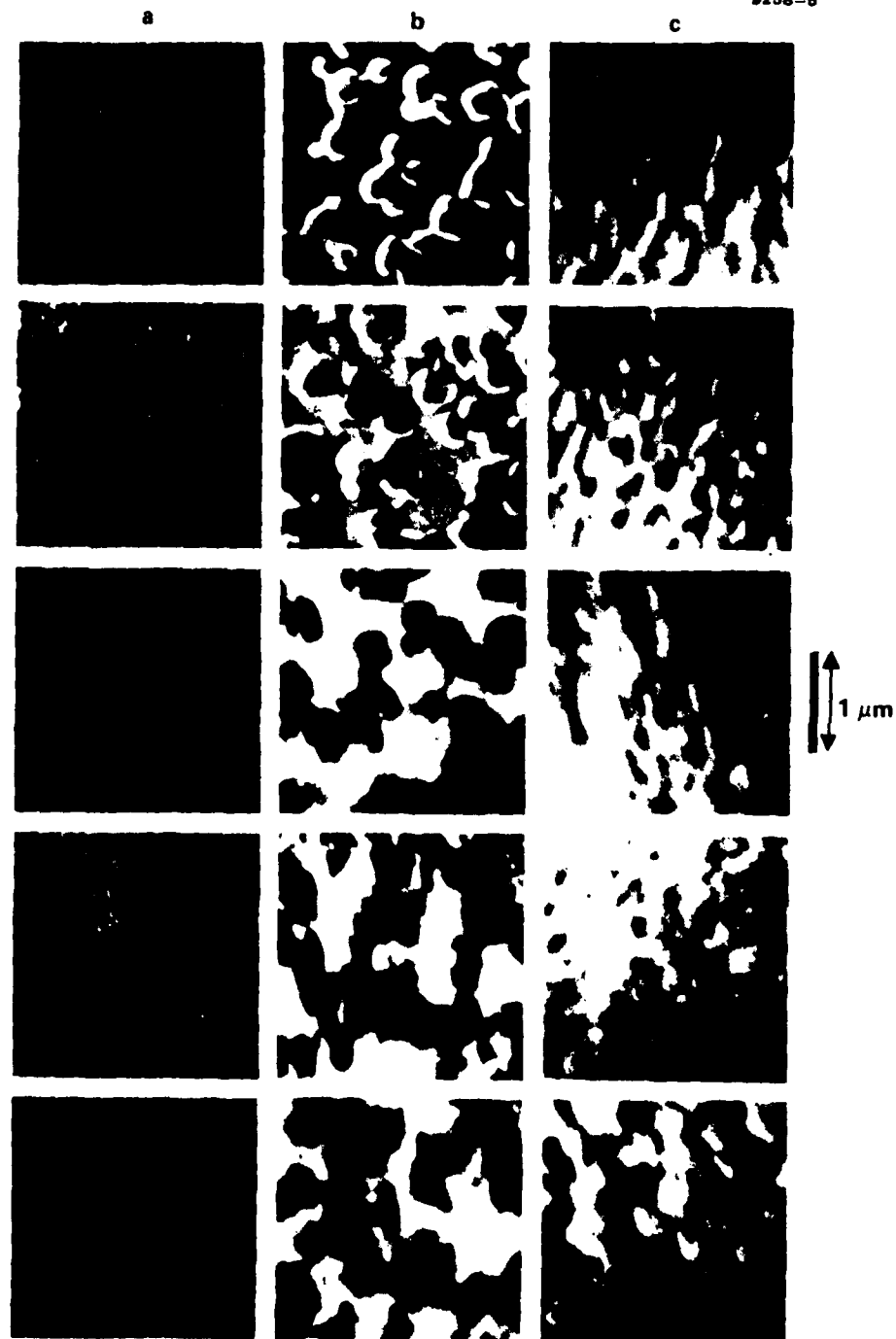


FIGURE 1. SEM photographs of Au-Cu-Ni-Au contacts on GaAs, ion-milled at shadow angle: (a) As deposited; (b) furnace annealed; (c) laser annealed.

TABLE II. Maximum Lateral Variation of Ratio of Counts per Sec for some of the Contact Constituents from EDX Analysis

9288-1

Au:Ge-Ni-Au CONTACT								
SAMPLE TYPE	AS-DEPOSITED				LASER-ANNEALED		FURNACE-ANNEALED	
DEPTH (Å)	0-2400				0-2400		0	480 1090 1890
Au/Ge	1.0				1.0		5.6	10 13 3.1
Au/Ni	1.0				1.0		16	95 42 4.2

In-Au: Ge CONTACT								
SAMPLE TYPE	AS-DEPOSITED				LASER-ANNEALED		FURNACE-ANNEALED	
DEPTH (Å)	0	380	1000	1530	0	620 1200 1770	0	680 1230 1630
Au/Ge	1.0	1.0	1.2	1.0	2.2	2.8 1.6 2.2	220	262 - 207
Au/In	1.0	1.6	1.3	2.8	1.1	1.1 1.2 1.1	1.0	1.0 2.8 2.2

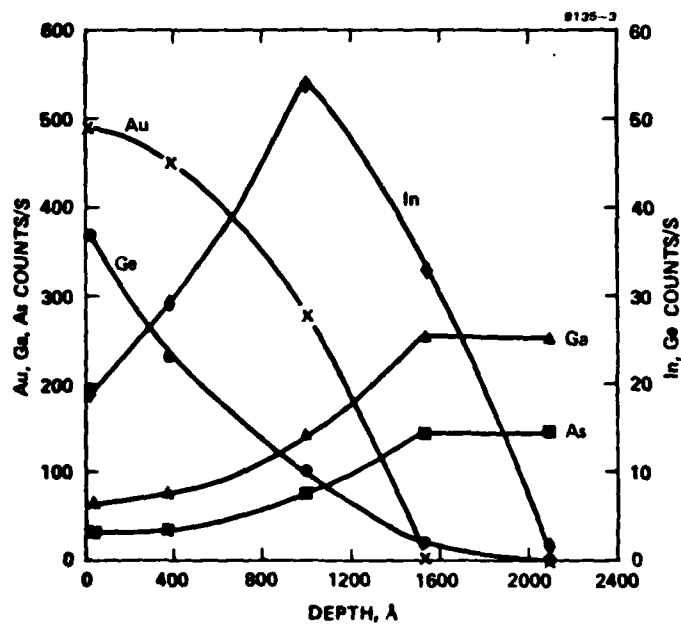


FIGURE 4. Depth profile of constituents of In-Au:Ge contact, as deposited.

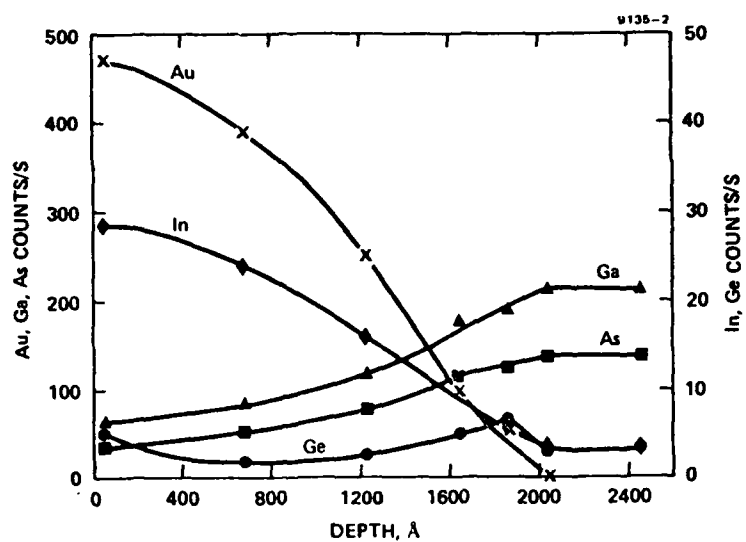


FIGURE 5. Depth profile of constituents of In-Au:Ge contact, furnace annealed.

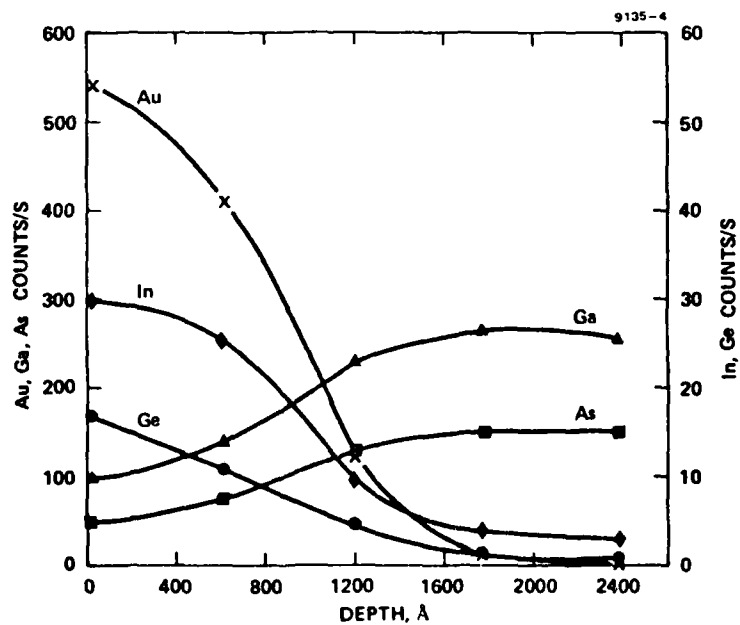


FIGURE 6. Depth profile of constituents of In-Au:Ge contact, laser annealed.

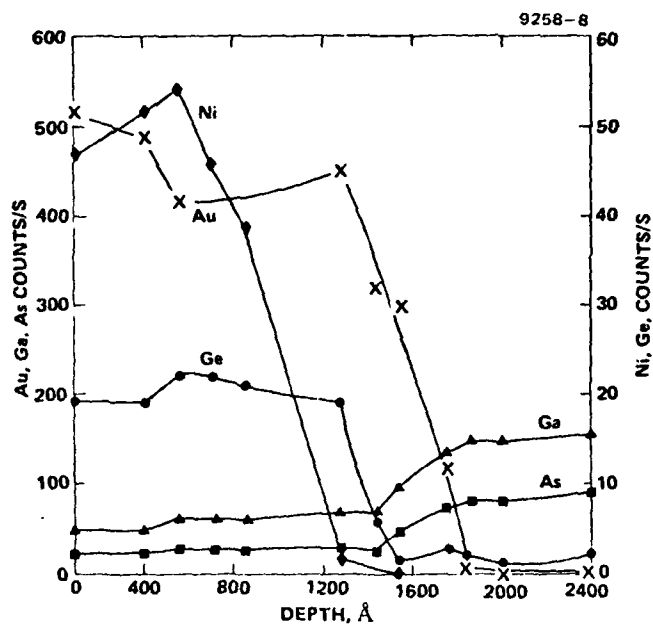


FIGURE 7. Depth profile of constituents of Au:Ge-Ni-Au contact, as deposited.

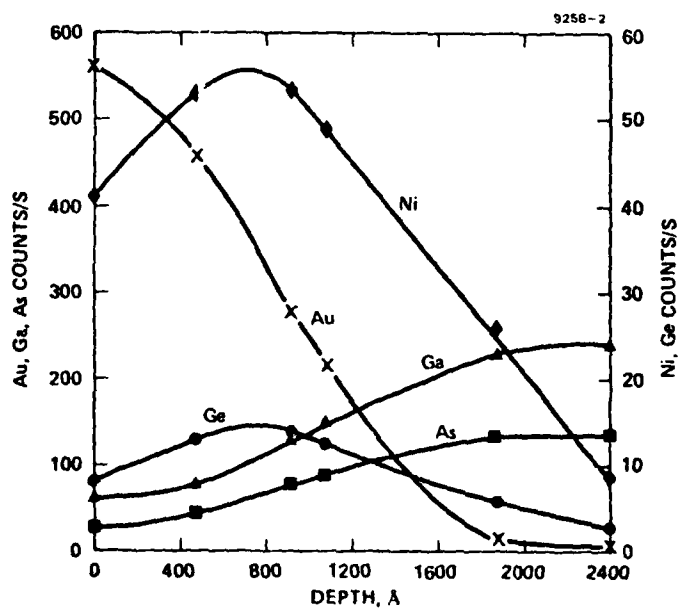


FIGURE 8. Depth profile of constituents of Au:Ge-Ni-Au contact, furnace annealed.

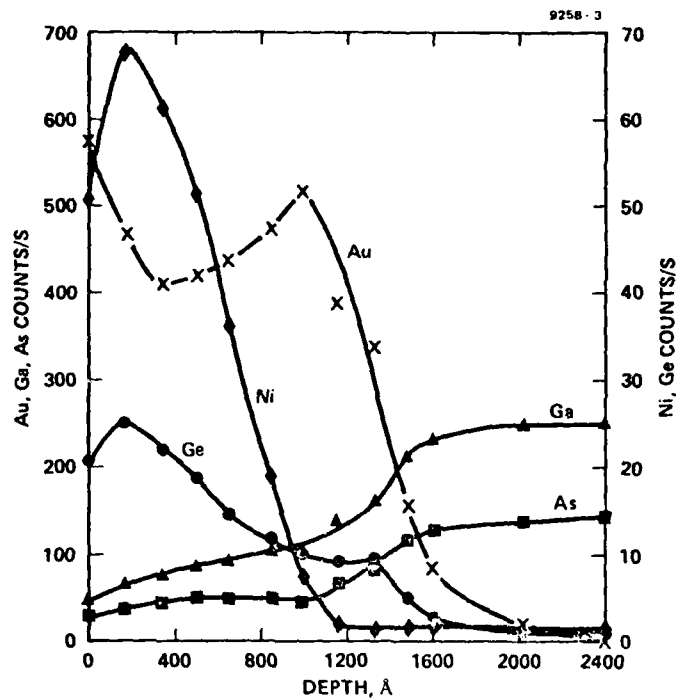


FIGURE 9. Depth profile of constituents of Au:Ge-Ni-Au contact, laser annealed.

has taken place during furnace annealing. In has diffused towards the surface, Ni and Ge have diffused towards the GaAs; (3) Redistribution of metals by laser annealing is much less pronounced in the Au:Ge-Ni-Au contact than it is in the In-Au:Ge contact.

III. LASER AND ELECTRON-BEAM ANNEALING OF ION IMPLANTS FOR OHMIC-CONTACT FORMATION

Laser and electron-beam annealing of high-dose shallow ion implants into n-type GaAs have been used successfully by two groups to create highly doped surface layers for Ohmic-contact formation.

Barnes and coworkers (16,17) used Si doped GaAs wafers ($n \approx 3 \times 10^{18} \text{ cm}^{-3}$) and implanted them with 10^{16} cm^{-2} , 50-keV Te^+ ions. They applied pulses from a Q-switched Nd:YAG laser (pulse duration 125 ns, power densities 12-40 MW/cm^2) to anneal the damaged implanted layers. The lowest reproducible specific contact resistance of $2 \times 10^{-5} \Omega \text{ cm}^2$ was obtained with a laser power density of 20 MW/cm^2 . This ρ_c value corresponds to a donor concentration of $\approx 2 \times 10^{19} \text{ cm}^{-3}$ rather than of $\approx 10^{21} \text{ cm}^{-3}$ as expected from the

ion-implant dose. The observed precipitation of Te at the GaAs surface is assumed to be at least partially responsible for the substantial reduction of ionizable impurities.

Mozzi and coworkers (18) have formed Ohmic contacts by pulsed electron-beam annealing of ion-implanted GaAs followed by deposition of TiPtAu layers. They used a semi-insulating substrate upon which two layers were grown: a buffer layer (thickness 4 μm , carrier concentration $\approx 10^{14} \text{ cm}^{-3}$) followed by a thin Si-doped surface layer (thickness 3300 Å, carrier concentration $9 \times 10^{16} \text{ cm}^{-3}$). The wafers are implanted with $5 \times 10^{15} \text{ cm}^{-2}$, 120-keV Se^+ ions at room temperature and annealed by 10 to 15-keV electrons (pulse duration 150 ns, energy density 0.71 J/cm²). They obtained a specific contact resistance $\rho_c \lesssim 6 \times 10^{-7} \Omega \text{ cm}^2$, which is the lowest value ever reported for n-type GaAs.

IV. CONCLUSIONS

The results of the studies reviewed have shown the potential importance of laser and electron-beam annealing for Ohmic-contact formation on devices where specific contact resistances need to be reduced, where more stringent requirements need to be placed on edge definition and surface morphology, and where structural and compositional uniformity are essential. However, very few GaAs devices with laser or electron-beam annealed contacts have been made so far, and none were tested for reliability and lifetime. Only such studies will determine the practical applicability of these novel techniques.

ACKNOWLEDGEMENT

The author wishes to thank B.A. Ambriz for assistance with the electrical measurements, M.N. Colborn for the SEM and EDX work, R.A. Jullens for the sample preparation, R.N. Robinson for the ion-milling, and C.L. Anderson and L.D. Hess for fruitful discussions.

REFERENCES

1. H.H. Berger, Solid-State Electron. 15, 145 (1972), J. Electrochem Soc. 119, 507 (1972).
2. F.A. Padovani in Semiconductors and Semimetals, Vol. 7A, R.K. Willardson and A.C. Beer, Ed., Academic Press, N.Y. 1971.
3. C.Y. Chang, Y.K. Fang, and S.M. Sze, Solid-State Electron. 14, 541 (1971).
4. V.L. Rideout, Solid-State Electron. 18, 541 (1975).
5. A.K. Sinha, T.E. Smith, and H.J. Levinstein, IEEE Trans. Electron. Devices, ED-22, 218 (1975).
6. R.S. Pounds, M.A. Saifi, W.C. Hahn, Jr., Solid-State Electron. 17, 245 (1974).
7. S. Margalit, D. Fekete, D.M. Pepper, C.P. Lee, and A. Yariv, Appl. Phys. Lett. 33, 346 (1978).

8. K. Heime, U. König, E. Kohn, and A. Wortmann, *Solid-State Electron.* 17, 835 (1974).
9. R.B. Gold, R.A. Powell, and J.F. Gibbons, *AIP Conf. Proc. Nr. 50, Laser-Solid Interactions and Laser Processing-1978*, p. 635.
10. G. Eckhardt, C.L. Anderson, L.D. Hess, and C.F. Krumm, *AIP Conf. Proc. Nr. 50, Laser-Solid Interactions and Laser Processing-1978*, p. 641.
11. G. Eckhardt, C.L. Anderson, M.N. Colborn, L.D. Hess, and R.A. Jullens, "A Comparison of Chemical and Structural Characteristics of In-Au:Ge Ohmic Contacts on GaAs produced by Bulk Heating and Localized Laser Heating," *Symposium on Laser and Electron-Beam Processing of Electronic Materials*, Los Angeles, Calif., Oct. 1979, to be published by the Electrochem. Soc.
12. A.C. Greenwald, private communication.
13. G. Eckhardt, C.L. Anderson, L.D. Hess, N. Hirsch and C.F. Krumm, "GaAs Microwave Field-Effect Transistors with Laser-Annealed Ohmic Contacts," presented at Workshop on Compound Semiconductor Microwave Materials and Devices, Atlanta, February 1979.
14. A.K. Sinha and J.M. Poate, in *Thin Films-Interdiffusion and Reactions*, Ed. J.M. Poate, K.N. Tu, J.W. Mayer, John Wiley & Sons, Inc. 1978
15. A. Christou, *Solid-State Electron.* 22, 141 (1979).
16. P.A. Barnes, H.J. Leamy, J.M. Poate, S.D. Ferris, J.S. Williams, G.K. Celler, *Appl. Phys. Lett.* 33, 965 (1978). Also see *AIP Conference Proceedings No. 50, Laser-Solid Interactions and Laser Processing-1978*, p. 647.
17. P.A. Barnes, H.J. Leamy, J.M. Poate, and G.K. Celler, "Laser Annealed Ohmic Contacts to III-V Semiconductors," *Symposium on Laser and Electron-Beam Processing of Electronic Materials*, Los Angeles, Calif., Oct. 1979, to be published by the Electrochem. Soc.
18. R.L. Mozzi, W. Fabian, and F.J. Piekarski, *Appl. Phys. Lett.* 35, 337 (1979).

SECTION 5

FOCUSED-BEAM ION IMPLANTATION

(R.L. Kubena, C.L. Anderson, M.D. Clark, H.L. Dunlap, R.A. Jullens, R.R. Hart*, R.L. Seliger, and V. Wang)

The most elegant use of a focused ion beam in semiconductor microfabrication is for maskless ion-implantation doping. The primary advantage is process simplification resulting from a dramatic reduction in the number of process steps. Figure 15 compares process sequences for creating a doped submicrometer line by a focused ion beam (2 steps) and by E-beam lithography/conventional ion implantation (8 steps).

In spite of the major importance of ion implantation for focused ion beams, process characterization has just begun. Some concern resulted because focused beams of the typical dopants were not yet available. Nevertheless, RBS analysis and Hall measurements were made on focused gallium implants, and meaningful results were obtained.

A. RUTHERFORD BACKSCATTERING (RBS)

RBS is a technique for analyzing ion-implantation depth profiles and lattice damage in crystalline materials such as Si. Using this technique, lattice disorder was investigated with low-energy proton backscattering and channeling analysis. For the RBS experiments, the focused Ga^+ ion beam had a diameter of 1200 \AA , a current density of 10^5 to 10^6 times greater than the current densities of typical ion implantations. Therefore, it was of particular interest to determine whether the high current density might lead to enhanced annealing of lattice disorder as a result of the high effective temperature of the surface region during implantation.

The focused ion beam was programmed to implant a $150 \text{ }\mu\text{m}$ square array of 1000×1000 individual spots. The $1500\text{-}\text{\AA}$ distance between spots resulted in sufficient overlap of the ion beam edge profiles to produce a uniform dose to $\pm 20\%$ over the $150\text{-}\mu\text{m}$ array. The $\langle 111 \rangle$ axis

*Texas A&M University

FOCUSED ION BEAM

1. WRITE WITH FOCUSED DOPANT BEAM
2. LASER ANNEAL

E-BEAM LITHOGRAPHY

1. DEPOSIT IMPLANTATION MASK
2. APPLY AND BAKE RESIST
3. E-BEAM EXPOSE
4. DEVELOP RESIST
5. ETCH IMPLANT MASK FILM
6. ION IMPLANT
7. REMOVE IMPLANT MASK FILM
8. ANNEAL

REMARKS

- ALL VACUUM PROCESS
- DOPING DEPTH AND CONCENTRATION CAN VARY ALONG THE LINE
- AT LEAST TWO "WET" STEPS
- ACHIEVING $0.1 \mu\text{m}$ QUESTIONABLE

Figure 15. Submicrometer line doping — process step comparison.

of the Si wafer was oriented parallel to the incident ion beam (to within 1°). Consequently, substantial channeling of the Ga^+ ions occurred.

The analysis beam of 140-keV protons in the HRL-RBS system was collimated to an area of $150\text{ }\mu\text{m}$ and centered on the implanted area. For channeling analysis, the $\langle 111 \rangle$ axis of the Si crystal was oriented to within 0.1° of the direction of the incident beam. Backscattered protons were detected by a cooled surface-barrier detector located at a 160° angle to the incident beam.

Backscattered energy spectra are shown in Figure 16 following focused ion beam implantations of 59-keV Ga^+ to various doses. A random spectrum and a $\langle 111 \rangle$ spectrum from an unimplanted area are shown for comparison. The increase in the implanted $\langle 111 \rangle$ spectrum as compared to the unimplanted spectrum at backscattered energies greater than 10 keV is caused by lattice disorder (i.e., atoms displaced by more than $0.2\text{ }\text{\AA}$ from lattice sites). The depth scale in Figure 16 shows that, following the $1.5 \times 10^{13}\text{ Ga}^+/\text{cm}^2$ implantation, the disorder peaks at a depth of $500\text{ }\text{\AA}$. This depth is 25% greater than the $400\text{ }\text{\AA}$ projected range of 59-keV Ga^+ incident on amorphous Si. The increased depth is consistent with deeper penetration of Ga^+ due to channeling. The disorder peak then increases to the random level following the $1.5 \times 10^{14}\text{ Ga}^+/\text{cm}^2$ implantation. Thus, a buried amorphous layer is produced. This amorphous layer then moves slightly toward the surface and to a depth of $1000\text{ }\text{\AA}$ after the $1.5 \times 10^{15}\text{ Ga}^+/\text{cm}^2$ implantation.

For comparison with the focused-ion-beam implantations, the same doses of 58-keV Ga^+/cm^2 were implanted in a conventional implantation system at a current density of $0.4\text{ }\mu\text{A}/\text{cm}^2$. The beam was uniform over the implantation areas and aligned to within 0.1° of the $\langle 111 \rangle$ axis. RBS analysis gave comparable spectra, as shown in Figure 16. However, the $1.5 \times 10^{13}\text{ Ga}^+/\text{cm}^2$ implantation at the low dose rate resulted in a $\langle 111 \rangle$ spectrum about 1/2 the level of that presented in Figure 16 for the focused beam implant.

This result indicates that the rate of disorder production is about a factor of two greater in the focused-ion-beam case. A factor of two

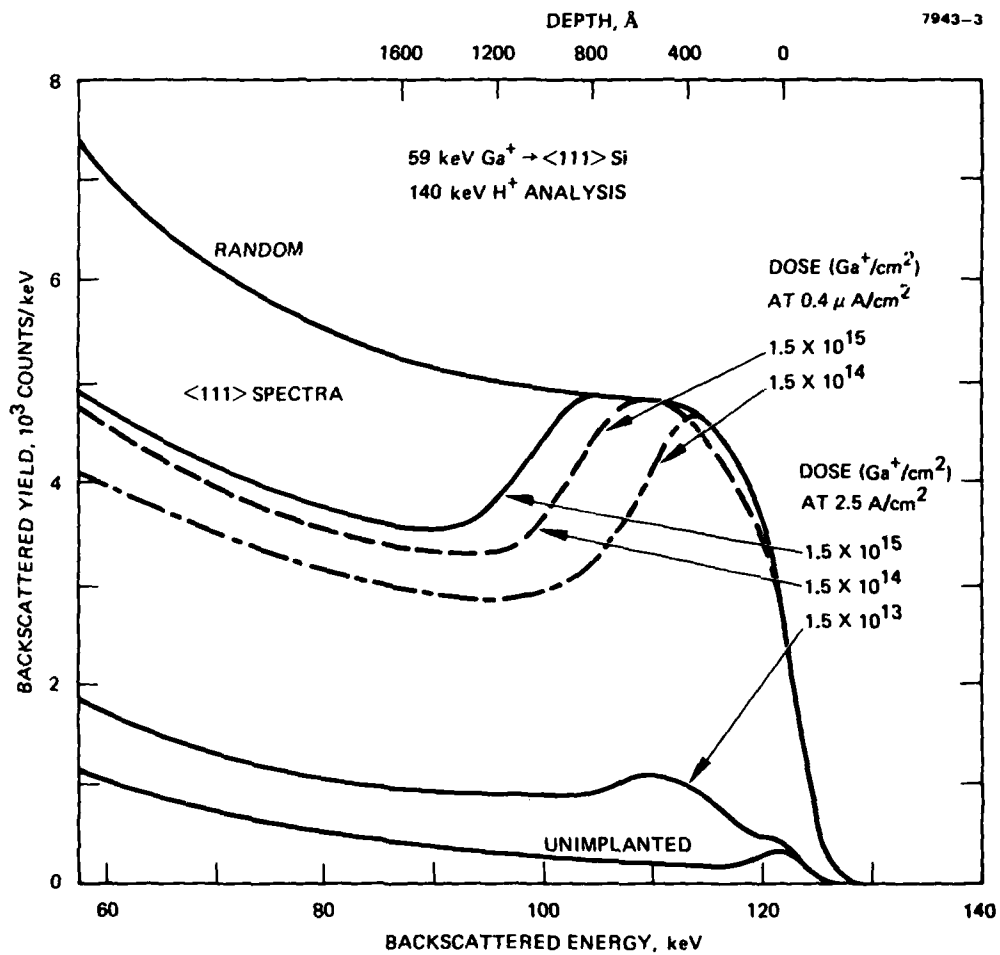


Figure 16. RBS analysis of Ga^+ ion implantation at 59 keV.

increase in the disorder production rate is certainly a small effect when compared to an increase in current density of over six orders of magnitude. In summary, the disorder produced in Si by a focused ion beam of Ga^+ having an extremely large current density is comparable to the disorder produced by an unfocused Ga^+ beam at a current density typical of normal implantations.

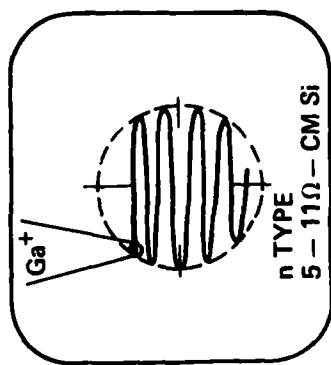
B. HALL MEASUREMENTS

The electrical activity was investigated for regions doped by a focused ion beam at dose rates 10^6 times that of conventional ion implantation. The high dose rates are necessary for the focused beam to have a reasonable writing speed. Measurements of Hall mobility and carrier concentration for a 55-keV Ga^+ focused ion beam implant in $\langle 100 \rangle$ Si demonstrated that no adverse electrical effects occur due to the high current density of Ga^+ .

The process steps used for the Hall measurements are outlined in Figure 17. A $150 \times 150 \mu\text{m}$ square region was implanted by raster scanning the focused Ga^+ beam across the wafer. In addition to implanting the square region, registration marks were cut deeply into the Si by ion sputtering with the focused beam. (These alignment marks provided adequate contrast in a mask aligner even when covered by photoresist.) The wafer was then annealed at 900°C for 30 min in forming gas, and photoresist was applied. A photomask was then aligned by using the ion-milled marks, and the resist was exposed and developed. Si mesas were subsequently etched into the implanted areas, and a glassy dielectric film was deposited on regions outside the mesas. Finally, Al Ohmic contacts were fabricated to access the implanted-mesa regions.

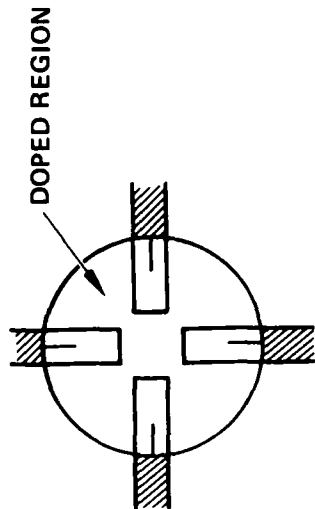
Figures 18 and 19 show an implanted mesa and the Al contacts. The bright areas are the Al contacts. Also visible are the registration lines ion milled by the Ga^+ beam.

Room-temperature electrical activity measurements were made for two implants of Ga^+ in 5 to $11 \Omega\text{-cm}$, n-type $\langle 100 \rangle$ Si. Doping levels were above and below the critical dose of Ga^+ to form an amorphous Si layer

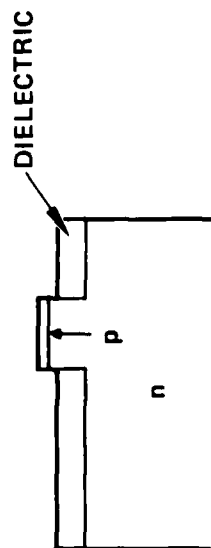


(1) a. DOPE Si WITH 55 KeV FOCUSED Ga^+ BEAM

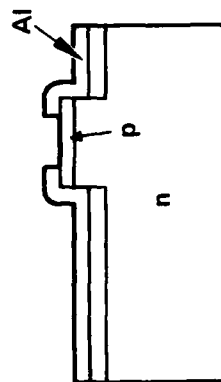
b. ION MACHINE REGISTRATION MARKS



(2) ANNEAL AT 900 °C FOR 30 MINUTES AND ETCH MESAS IN Ga^+ DOPED REGIONS



(3) LAY GLASSY DIELECTRIC OUTSIDE MESAS



(4) DEPOSIT Al: MAKING OHMIC CONTACTS AT CORNERS OF MESAS

Figure 17. Hall processing steps.

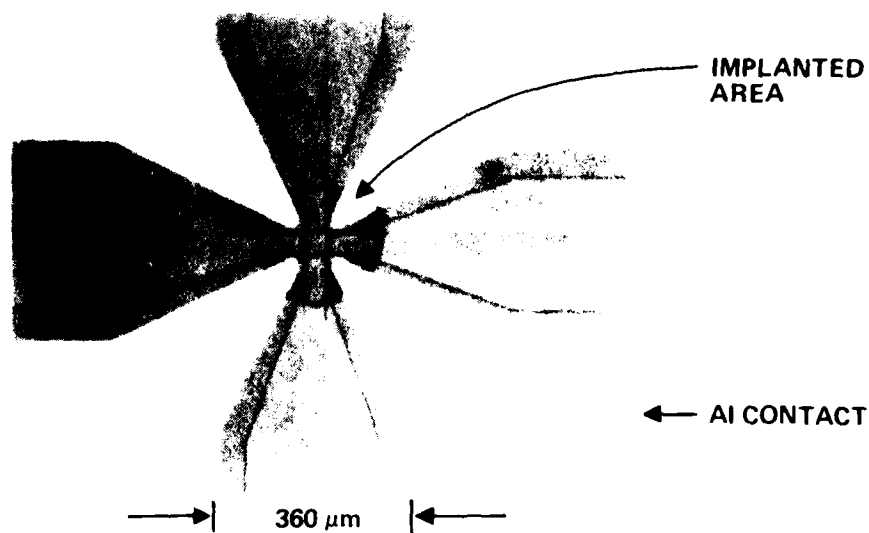


Figure 18. Focused Ga^+ beam implant and Al contacts for Hall measurement.

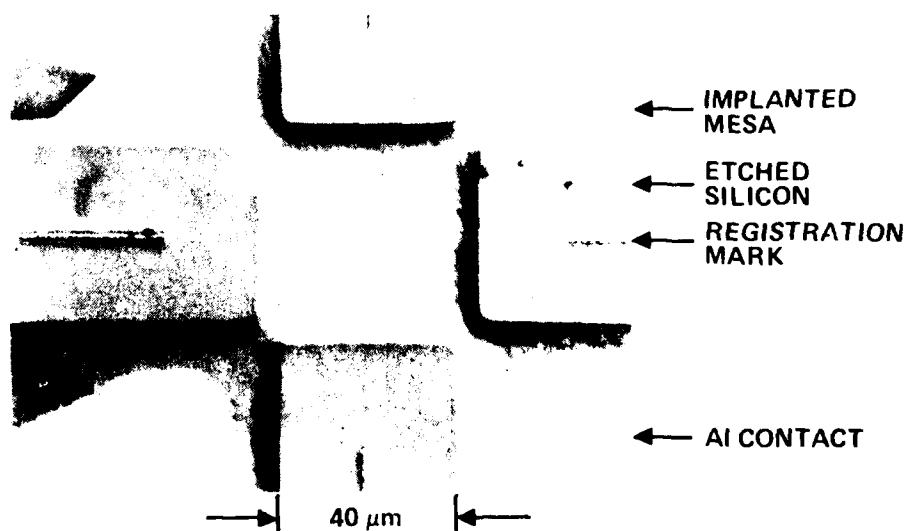


Figure 19. Ga^+ implanted 5 to 10 $\Omega\text{-cm}$, n-type, $\langle 100 \rangle$ Si showing etched mesa, Al contacts, and registration marks. (Enlargement of Figure 18.)

at room temperature. Doses were 7.0×10^{13} and $7.0 \times 10^{14}/\text{cm}^2$. Carrier concentrations of 9.5×10^{12} and $3 \times 10^{13}/\text{cm}^2$ and mobilities of 54 and 64 $\text{cm}^2/\text{V-sec}$, respectively, were obtained by the Van der Pauw Hall method⁸ after the 30-min anneal at 900°C. Since RBS experiments indicated that most of the Ga^+ is deposited within a 500-Å-deep surface layer, the Hall mobilities measured are consistent with normal drift mobilities of holes in Si at room temperature. Thus, no adverse electrical effects have been observed for the high-dose-rate focused-beam implant.

The carrier concentration was only three times larger when a 10 times larger doping level was used. This effect is most likely due to the solid solubility of Ga in Si at 900°C. Further reducing the doping level may increase the percentage of dopant ions that contribute to electrical activity. Moreover, a control experiment is planned in which Ga^+ is implanted in Si using photomasks at the same energy and doses as previously described but at conventional dose rates. A comparison of the activity and mobility of electrical carriers between the conventional and pencil ion beam implants will be made. Thus, a precise evaluation of the effects of the high flux of the focused ion beam on electrical activity should be possible.

DISTRIBUTION LIST - TECHNICAL REPORTS
CONTRACT N00014-78-C-0337

DARPA 1400 Wilson Blvd. Arlington, VA 22209 (Attn: Program Management)	2	Commanding Officer Office of Naval Research Branch Office 1030 East Green Street Pasadena, CA 91101	1
Office of Naval Research Code 427Y 800 North Quincy Street Arlington, VA 22217	4	Dr. M. Malbon/M.S. IC Avantek, Inc. 3175 Bowers Avenue Santa Clara, CA 94304	1
Naval Research Laboratory 4555 Overlook Avenue, S.W. Washington, D.C. 20375 Attn: Code 2627	6	Mr. R. Bierig Raytheon Company 28 Seyon Street Waltham, MA 02154	1
	1		
Office of Naval Research Branch Office 1030 East Green Street Pasadena, CA 91101	1	Dr. R. Bell, K-101 Varian Associates, Inc. 611 Hansen Way Palo Alto, CA 94304	1
TACTEC Battelle Memorial Institute 505 King Avenue Columbus, OH 43201	1	Dr. H. C. Mathanson Westinghouse Research and Development Center Beulah Road Pittsburgh, PA 15235	1
Defense Contract Administration Services Management Area San Francisco 1250 Bayhill Drive San Bruno, CA 94066	1	Dr. F. Blum/Dr. Daniel Chen Rockwell International Science Center P. O. Box 1085 Thousand Oaks, CA 91360	1
Defense Documentation Center Building 5, Cameron Station Alexandria, VA 22314	12	Mr. G. J. Gilbert MSC 100 Schoolhouse Road Somerset, NJ 08873	1
Dr. Y. S. Park AFAL/DHR Building 450 Wright-Patterson AFB Ohio 45433	1	Dr. C. Krumn Hughes Research Laboratory 3011 Malibu Canyon Road Malibu, CA 90265	1
ERADCOM DELET-M Fort Monmouth, NJ 07703	1	Mr. Lothar Wandinger ECOM/AMSEL/TL/IJ Fort Monmouth, NJ 07003	1
Texas Instruments M.S. 105/W. Wiseman P. O. Box 5936 Dallas, TX 75222	1		

Dr. Harry Wieder Naval Ocean Systems Center Code 922 271 Catalina Blvd. San Diego, CA 92152	1	Commander, AFAL AFAL/DHM Mr. Richard L. Remski Wright-Patterson AFB, OH 45433	1
Dr. William Lindley MIT Lincoln Laboratory F124A, P. O. Box 73 Lexington, MA 02173	1	Professor Walter Ku Phillips Hall Cornell University Ithaca, NY 14853	1
Mr. Sven Roosild AFCRL/LQD Hanscom AFB, MA 01731	1	Commander Harry Diamond Laboratories Mr. Horst W. A. Gerlach 2800 Powder Mill Road Adelphia, MD 20783	1
Commander U.S. Army Electronics Command V. Gelnovatch (DRSEL-TL-IC) Fort Monmouth, NJ 07703	1	Advisory Group on Electron Devices 201 Varick Street, 9th floor New York, NY 10014	1
RCA Microwave Technology Center Dr. F. Sterzer Princeton, NJ 08540	1	D. Claxton MS/1414 TRW Systems One Space Park Redondo Beach, CA 90278	1
Hewlett-Packard Corporation Dr. Robert Archer 1501 Page Mill Road Palo Alto, CA 94306	1	Professor L. Eastman Phillips Hall Cornell University Ithaca, NY 14853	1
Watkins-Johnson Company E. J. Crescenzi, Jr./ K. Niclas 3333 Hillview Avenue Stanford Industrial Park Palo Alto, CA 94304	1	AIL TECH 612 N. Mary Avenue Sunnyvale, CA 94086 Attn: D. G. Vendelin	1
Commandant Marine Corps Scientific Advisor (Code AX) Washington, D.C. 20380	1	Professors Hauser and Littlejohn Department of Electrical Engr. North Carolina State University Raleigh, NC 27607	1
Communications Transistor Corp. Dr. W. Weisenberger 301 Industrial Way San Carlos, CA 94070	1		
Microwave Associates Northwest Industrial Park Drs. F. A. Brand/J. Saloom Burlington, MA 01803	1		